

## Editorial corner – a personal view

### Intrinsic fluorescence: an effective means to monitor macromolecular chain motions

*M. Q. Zhang\**

Materials Science Institute, Zhongshan University, Guangzhou 510275, P. R. China

Fluorescence technology belongs to photoluminescence spectroscopy, and has been applied to the investigation of macromolecular chain movements. Although a number of useful information dealing with polymer micro-morphology and microstructure can be obtained accordingly, fluorimetric studies used to be conducted by pre-introducing probes or labels that carry chromophores into the system of interests. In spite of the difficulty of bringing the sensors, either the probes that are physically dispersed in macromolecules or the labels that are covalently attached to macromolecular chains would change microenvironment of the macromolecules and make the macromolecules more hydrophobic. As a result, their complexation ability is enhanced, and the condensed status revealed by fluorescence behaviors differs from the authentic situation.

In fact, macromolecular chain motions of polymers can be monitored by intrinsic fluorescence in case the macromolecular chains contain chromophores. For instance, intrinsic fluorescence of polystyrene has been shown to be highly sensitive to the issues ranging from local polymer conformational populations in solution and phase behavior in solvents and polymer blends to local microenvironments in bulk homopolymers. Relaxations and cold-crystallization processes in polymer (e.g. poly(trimethylene terephthalate)) were thoroughly characterized by intrinsic fluorescence spectroscopy. Compared to conventional approaches, more detailed information about structural variations can be provided, for

example, molecular arrangement in induction stage of cold-crystallization. In addition, by focusing on excimer of intrinsic fluorescence, kinetic process of spinodal decomposition in phase separation of polystyrene/poly(vinyl methyl ether) blends was quantitatively studied.

However, optical physics of inherent chromophores has been less studied so far. The relationship between intrinsic fluorescence and macromolecular microstructure becomes somewhat difficult to be interpreted. This may explain why people prefer probes and labels, as reflected by literature survey. To have objective images of macromolecules movement, intrinsic fluorescence is worth being well explored. Taking its advantages of simplicity and sensitivity, it would be extended for studying oxidation and degradation of polymers. With the help of different inherent chromophores on macromolecular chains, interfacial interaction in polymer blends might be evaluated. By changing temperature, more specific kinetics of the subjects mentioned above would be further understood.



Prof. Dr. Ming Qiu Zhang  
Member of International Advisory Board

\*Corresponding author, e-mail: [ceszmq@mail.sysu.edu.cn](mailto:ceszmq@mail.sysu.edu.cn)  
© BME-PT and GTE

# Effect of extensional cyclic strain on the mechanical and physico-mechanical properties of PVC-NBR/graphite composites

S. A. Mansour\*

Physics Department, Faculty of Science, Suez Canal University, Ismailia, Egypt

Received 13 September 2008; accepted in revised form 27 October 2008

**Abstract.** The variation of electrical resistivity as well as the mechanical properties of PVC (polyvinylchloride)-NBR (acrylonitrile butadiene rubber) based conductive composites filled with different concentrations of graphite were studied. These samples were studied as function of the constant deformation fatigue test. When the specimen was subjected to a large number of rapidly repeating strain cycles, and different strain amplitudes, the conductivity,  $\sigma(T)$ , shows an initial rapid fall followed by dynamic equilibrium. Increasing the number of cycles and strain amplitudes, the conductivity remains almost constant over the temperature range 30–140°C. The equilibrium state between destruction and reconstruction of graphite particles has been detected for all strains of certain values of strain cycles (1000, 2000, 3000, and 4000 cycles for 30% strain amplitude). A preliminary study was done to optimize the possibility to use Conductive Polymer Composites (CPC) as a strain sensor and to evaluate its performance by an intrinsic physico-mechanical modification measurement. The electromechanical characterization was performed to demonstrate the adaptability and the correct functioning of the sensor as a strain gauge on the fabric. The coefficient of strain sensitivity ( $K$ ) was measured for 50 phr graphite/PVC-NBR vulcanized at 3000 number of strain cycles and 30% strain amplitude. There was a broad maximum of  $K$ , with a peak value of 82, which was much higher, compared to conventional wire resistors. A slight hysteresis was observed at unloading due to plasticity of the matrix. A good correlation exists between mechanical and electrical response to the strain sensitivity. Mechanical reinforcement was in accordance with the Quemada equation [1] and Guth model [2] attested to good particle-matrix adhesion. It was found that the viscous component of deformation gradually disappeared and the hardening occurred with increasing strain cycles. The modulus, fracture strength, and elongation at break increased with increasing filler volume fraction up to 40 phr of graphite particles.

**Keywords:** polymer composites, mechanical properties, fracture and fatigue, modeling and simulation

## 1. Introduction

If there is a simple relationship between electrical conductivity and external variables such as temperature [3, 4] and mechanical stretching [5, 6], the composite has potential applications as a sensor. For these reasons, the development of new conductive composites requires an understanding of the changes in conductivity that might occur in service. Conversely, measurement of electrical conductivity under strain can be a probe to understanding

microstructural changes. Carbon black-filled conductive rubbers have wide applications, such as pressure sensitive sensors which can be used for shock proof switches [7], sensors for measurement of vehicle weights to collect toll tax on roads [8], and smart flexible sensors adapted to textile structures, able to measure their strain deformations [9], and tactile sensor that is thin and flexible and able to attach to a curved surface and will make the robot operate in unstructured environments [10,

\*Corresponding author, e-mail: [saidhsa@yahoo.com](mailto:saidhsa@yahoo.com)  
© BME-PT and GTE

11]. For an electronic application of the CPC, the sensor should have a good linear behavior (with the effect of elongation), while the specific electrical resistivity of the system should be in a measurable range ( $<100 \Omega \cdot \text{m}$ ) [12].

Sau *et al.* [13] have reported that the electrical resistivity of strained samples from EPDM, 50/50 NBR/EPDM blend and NBR rubbers, depends on strain amplitude (% elongation), frequency of stress-strain cycle, and also number of stress-strain cycles. Pramanik *et al.* [14] reported the electrical and mechanical properties of Short Carbon Fibres (SCF) and carbon-black-filled nitrile-rubber composites with the variation of filler concentration, filler blend composition, processing parameters, and compressive pressure have a pronounced influence on the conductivity of such composites. In the present work the composite materials composed of different amounts randomly dispersed of graphite particles in an insulating polymer matrix was examined aiming to attain a pronounced change in resistivity with prestrain. The PVC/NBR blend polymer was chosen as the matrix because of its environmental stability and ease in processing, graphite particles were also chosen for their availability and low resistivity, to form strain-sensitive composites.

A preliminary study was done to optimize the possibility to use CPC as a strain sensor and to evaluate its performance by an intrinsic physico-mechanical modification measurement. In this respect three factors are considered: 1 – the strain amplitude, 2 – the number of cycles, and 3 – the optimal filler concentration from the percolation threshold. The results of this initial phase were aiming to have a good compromise between sensor sensitivity and resistivity value.

## 2. Experimental

### 2.1. Materials and preparation of composites

NBR (density  $0.98 \text{ g/cm}^3$  and acrylonitrile content 34%) and suspension polymerized PVC in powder form (density =  $1.38 \text{ g/cm}^3$ ), was supplied by the Transport and Engineering Company (TRENCO), Alexandria, Egypt. Graphite (particle size diameter  $<50 \mu\text{m}$  and density  $1.4 \text{ g/cm}^3$ ) were used as conductive and reinforcing filler. The compound formulations are presented in Table 1. The mixing was

**Table 1.** The formulations of graphite/PVC-NBR composites

NBR	60
PVC	40
Graphite	X
** (DOP)	50
*Zinc oxide	5
*Stearic acid	2
*MBTS	1.5
*TMTD	0.5
*PBN	1.0
*Sulfur	2

\*means all ingredients in (phr) relative to NBR

\*\*means the weight of DOP equals 50% of the weight of PVC

X is the amount of graphite which was varied from 0–70 phr (parts per hundred rubber, by weight) relative to compound

accomplished in a home made two-roll mixing mill (length 0.3 m, radius 0.15 m, speed of slow roll 18 rpm and gear ratio 1.4) was used. The mixing occurred for 40 min at a temperature of  $25^\circ\text{C}$ , with same sequence of mixing of all compounding ingredients to avoid the effect of processing on electrical conductivity. The vulcanization was conducted under a heating press (KARL KOLB, Germany). Compression molded plaques were prepared by sandwiching the polymer between Mylar sheets, heating at  $150 \pm 2^\circ\text{C}$  for 30 min under minimal pressure 0.40 MPa. Plaques were rapidly cooled to ambient temperature. The vulcanized samples were shelf aged for 48 h before testing. The mixing time and vulcanization conditions were fixed for all samples.

### 2.2. Measurement of the initial electrical properties without strain

The electrical resistivities of different composites were measured with linear four point-probe method [15]. Also to diminish the contact resistance between the electrodes and the specimens, the four points were stuck with silver ink. The standard size adopted for each specimen was  $40 \times 10 \times 2 \text{ mm}^3$ . Each resistance measurement was made from the slope of the voltage-current graph over the range of 0.2–10 V. The current flow through the specimen was measured with a sensitive digital electrometer (616 Keithley, USA); the voltage was measured with DC power supply HY 5003. Before taking measurements, each sample was heated at  $70^\circ\text{C}$  for about one hour to remove absorbed moisture.

### 2.3. Application of pre-strain

Some of the composite samples were subjected to a constant number (100) of rapid dynamic flex cycles of constant frequency (5.9 cycles/s), and at different amplitudes in a constant deformation fatigue tester [16]. The number of flex cycles and amplitude of flexing were varied. It was then subjected to different numbers of strain cycles with constant amplitude, which could be changed throughout the experiment. The rectangular specimen of  $10 \times 40 \times 2 \text{ mm}^3$  dimensions was clamped at both ends in a holder attached to the machine. The electrical properties of original (unstrained) and strained (under different conditions) samples were measured using the device described above. A regulated electrical oven was used to control the sample temperature to an accuracy of  $\pm 1^\circ\text{C}$  over a range of temperature from 30 to  $140^\circ\text{C}$ .

### 2.4. Mechanical techniques

True stress and strain at rupture were carried out at room temperature on a tensile testing machine (AMETEK, USA). The test samples were strips of 2 cm working length and of  $\sim 4 \text{ mm}^2$  cross-sectional area. A digital force gauge (Hunter Spring ACCU Force II, 0.01 N resolution, USA) connected to a microprocessor was used to measure extension force ( $F$ ). A home made motor attachment was used to control the strain rate through a gearbox. The strain rate was preset using a variable DC power supply, and was measured using a micro-switch attached to the apparatus wheel. The accuracy of strain measurement was about 0.1 mm. The strain rate  $\dot{\epsilon}$  throughout the experiment was fixed at  $1 \text{ s}^{-1}$ . True stress and strains were calculated as shown by Equations (1) and (2) respectively:

$$\text{True stress} = \frac{F}{A_0}(1+\epsilon) \quad (1)$$

$$\text{True strain} = \ln(1+\epsilon) \quad (2)$$

where  $\epsilon = \Delta l/l_0$  is the tensile strain, and  $A_0$  is the original cross-sectional area.

### 2.5. Electrical properties with strain

The resistivity was measured with a four-terminal technique [16] using a DC power supply model HY

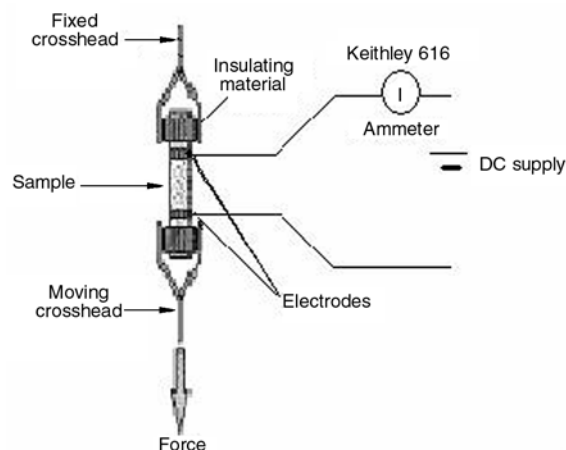


**Figure 1.** Schematics of DC electrical measurements during uniaxial extension

5003 as voltage source and a Keithley model 616 for current measurements. Specimens ( $20 \times 2 \times 2$ ) mm were uniaxially extended at room temperature using an (AMETEK, USA) universal testing machine. A constant crosshead speed was maintained to give a specified deformation rate. All the samples were only extended up to 50% elongation to avoid tensile failure of the specimens. The current and voltage electrodes were located 3 mm apart in the clamp and they were insulated from the machine frame (Figure 1). Conductive silver paint was applied between the sample surface and electrode to ensure a better electrical contact between them. The specimen's extension was measured from the displacement of the machine head. Assuming the sample volume remains constant (i.e.,  $\Delta V = 0$  or  $V = V_0$ ) throughout the experiment. The resistivity could be given by Equation (3):

$$\rho = \frac{RV_0}{l_0^2(1+\epsilon)^2} \quad (3)$$

where  $l_0$  is the initial length of the unstrained sample.

## 3. Results and discussion

### 3.1. Electrical properties

#### 3.1.1. Initial electrical properties without strain

Figure 2 shows the variation of the resistivity with the volume fraction of filler. A dramatic decrease in resistivity, or threshold, is observed for given conductive filler content. This critical concentration corresponds to the percolation volume. At this

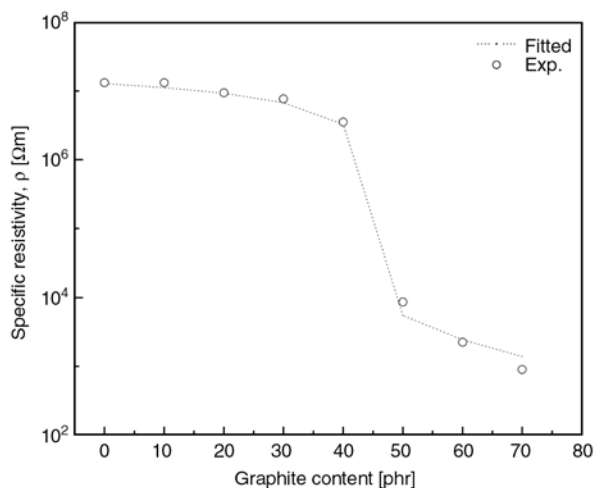


**Figure 2.** Resistivity as a function of graphite content. The dotted line is the statistical percolation fit.

point, the electric charges form electro-conductive channels, and there is a transition of the material from electrically insulating to conductive. This phenomenon is described in the percolation theory [17]. When the conductive particle concentration increases, the number of ohmic conductive paths increases, and the I–V relationship becomes more linear. The model that is most often used to quantify the changes in the transition and conductive regions is the so-called statistical percolation model. Proposed by Kirkpatrick [18] and Zallen [19], this model predicts the electrical resistivity of an insulator-conductor binary mixture by assuming random positions of the filler particles. The result is a power-law variation of the resistivity  $\rho$ , above the percolation threshold, as shown by Equation (4):

$$\rho \propto \left( \frac{\Phi - \Phi_c}{1 - \Phi_c} \right)^{-t} \quad (4)$$

where  $\Phi$  is the volume fraction of filler,  $\Phi_c$  the percolation threshold and  $t$  is a universal exponent that is close to 2 for a 3D dispersion [20]. The two-parameter fit is represented in Figure 2 by the solid line. On the basis of this result, composite with 50 phr filler was used to study the relationships between resistivity and mechanical deformation.

### 3.1.2. Effects of the number of dynamic strain cycles and strain amplitude on conductivity

In this paper, composites are identified by an alphanumeric system. The first letter represents the

conductive graphite used in the 60/40 of an NBR-PVC blend; the number indicates the loading of conductive graphite. For example, G50 represents a 60/40 of an NBR-PVC blend containing 50 phr of conductive graphite.

Figures 3 and 4 illustrate the effect of the number of strain cycles, and different strain amplitudes on the electrical conductivity of PVC-NBR blend system loaded with 30, 50, and 70 phr graphite at room temperature. It is found that the sample with 50 phr is more sensitive to both number of dynamic strain cycles and strain amplitude. The rapid change in conductivity here is presumably because it is very near to the critical percolation limit. Even small changes in the network structure would have the greatest effect on conductivity in the percolation region. Materials in this region are much more sensitive to strain than are more conductive com-

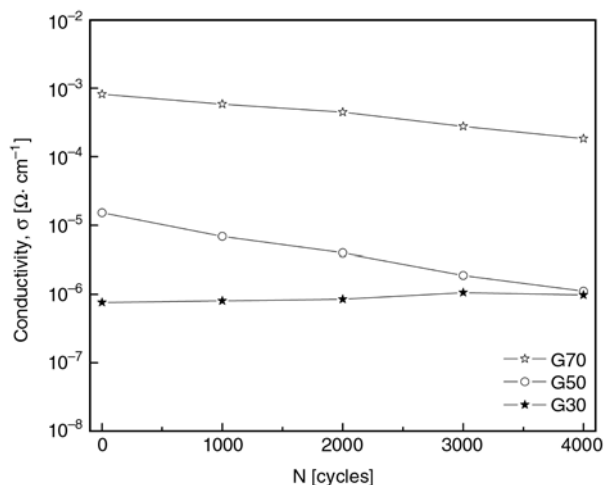


**Figure 3.** Dependence of the electrical conductivity ( $\sigma$ ) on the number of strain cycles ( $N$ ) at constant amplitude of 30%

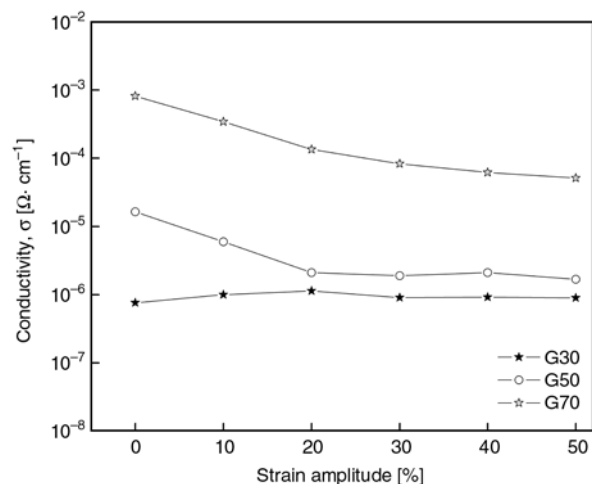


**Figure 4.** Dependence of the electrical conductivity ( $\sigma$ ) on strain amplitude after 100 strain cycles

pounds and then this is the reason behind the choice to study the effect of dynamic strain on the electrical properties of 50 phr graphite/PVC-NBR vulcanized.

High structure graphite manifests a natural tendency towards breakdown. Destruction and reconstruction processes may also occur by mechanical deformation and by thermal expansion and contraction processes. It is conventional to distinguish between low strain and high strain amplitudes and their influence on the properties of rubber composites. Strains below 30% are considered low, while those above 30% are considered high [21]. At low strain amplitudes (< 20%) for G30 sample, the formation of graphite aggregates predominates over their destruction, which in turn slightly increase the initial conductivity of the sample. But for both samples (G50, and G70) the initial conductivity decreases with increasing amplitude of cyclic strain. It could be explained as follows: during the initial strain amplitude, the breakdown of the conductive network becomes more predominant, and at higher frequency level (at strain amplitudes >20%, for all samples), the rate of formation of conductive network becomes faster and the formation and breakdown processes balance each other, leading to a plateau in the plots of conductivity.

### 3.1.3. Effects of the number of dynamic strain cycles and cyclic strain amplitude on the electrical conductivity $\sigma(T)$ filled with 50 phr of graphite

In principle, composites whose resistivities sharply vary near a critical percolation threshold may show a notable change in the resistivity with the temperature. Consequently, it is only possible to find one composite from the PVC-NBR/graphite series for examining the dependence of conductivity on temperature with the effect of repeated cyclic strains at constant amplitude (30%), and strain amplitude (at constant number of cycles 100) for 50 graphite/PVC-NBR blend.

Figures 5 and 6 present plots of conductivity against the temperature, which can be explained as follows:

- (i) The number of strain cycles (0, 1000 and 2000) leads to the initial breakage of the existing continuous conducting network. The increase in temperature leads to an increase in the gap

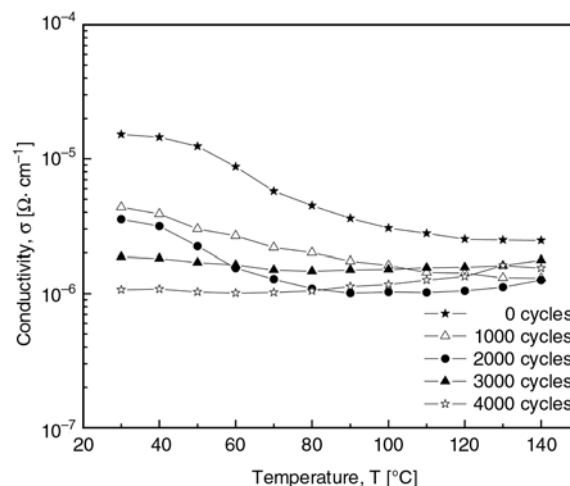


**Figure 5.** Temperature dependence of the electrical conductivity ( $\sigma$ ) of 50 graphite/PVC-NBR on different numbers of strain cycles (at constant strain amplitude 30%)

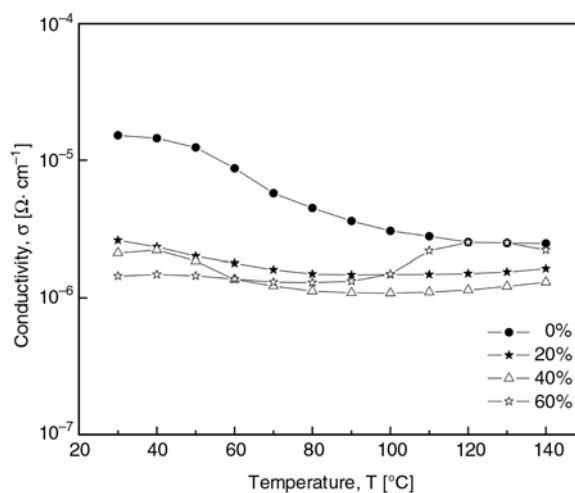


**Figure 6.** Temperature dependence of the electrical conductivity ( $\sigma$ ) of 50 graphite/PVC-NBR sample at different strain amplitude (at constant number of cycles 100)

- between graphite structure and the masking of graphite particles by insulating rubber layers, that results in a slight decrease in conductivity.
- (ii) After this breakdown process, the blend shows a greater tendency for alignment of graphite during the application of cyclic dynamic strain.
- (iii) At high numbers of strain cycles (3000 and 4000) and high degree strain amplitude (20, 40 and 60%) the almost temperature independent behaviour of the electrical conductivity of the blend could be due to a balance between the two mechanisms of conduction mentioned above and to direct contact between graphite aggregates; i.e. the high degree of orientation

of graphite aggregates may nullify the effect of chain breakage and thus a plateau effect is observed. So that it is interesting to study the effect of frequency of stress-strain cycling on electrical resistivity of G50 at strain amplitude of 30% and after 3000 cycles.

### 3.2. Mechanical properties

The mechanical performance of the PVC-NBR/graphite composites was studied in terms of Young’s modulus, tensile strength and elongation at break. It is well known that the increase in modulus is due to strong interactions between polymer chains and particles and/or between particles and particles. Figure 7 illustrates the dependence of elastic modulus ( $E$ ) on graphite volume fraction. It is shown that the elastic modulus ( $E$ ) increases with increasing graphite content. For composites filled with low amounts of weakly interacting spherical particles, the behavior of the change of the elastic modulus depends on the volume fraction of fillers ( $\Phi$ ), and may be predicted by Quemada Equation (5) [1]:

$$E = \frac{E_m}{(1 - 0.5N\Phi)^2} \tag{5}$$

where  $E_m$  is the modulus of the elastomer matrix,  $N$  is variable coefficient (usually  $N = 2.5$ ). The theoretical curve corresponding to Equation (5) shows good accordance with the experimental data as shown in Figure 7.

The results were also compared with Guth reinforcement model [2]. The model for reinforcing particles has the form as given by Equation (6):

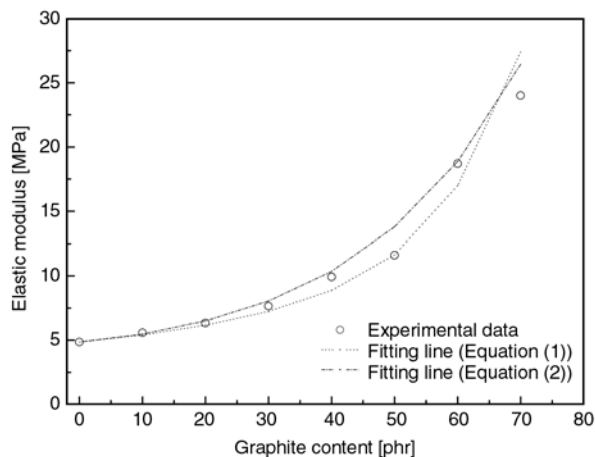


Figure 7. Elastic modulus ( $E$ ) plotted against graphite content [phr]

$$E = E_m (1 + 2.5\Phi + 14.1\Phi^2) \tag{6}$$

Where the linear term accounts for the reinforcing effect of individual particles and the second power term is the contribution of particle pair interactions. This model significantly underestimates the observed reinforcement, as shown in Figure 7. The difference between experimental data and Equation (6) was even observed for a graphite content 40 phr, where the model is most applicable.

The variation of tensile strength is shown in Figure 8. It is observed that the tensile strength increases with increase in filler loading. This can be explained by the following mechanisms: tensile strength is related to the energy required to deform and fracture the polymer chains. The effective crosslink density of the composites increases with increase in filler loading attributed to the increase of polymer-filler interaction with the addition of filler. Thus, at low filler loading, the energy required to deform and fracture the polymer chains is less because of lower crosslink density, whereas at high filler loading, attributed to the higher crosslink density, the energy required to deform and fracture the polymer chains is high. The ability of polymer to stretch several times its original length is one of its chief characteristics. The variation of elongation at break with filler loading is presented in Figure 9.

It can be seen that elongation at break increases with increase in filler loading to a maximum and then shows a decrease with further loading of the filler. This is because at very low filler content, when the matrix is not sufficiently reinforced, it

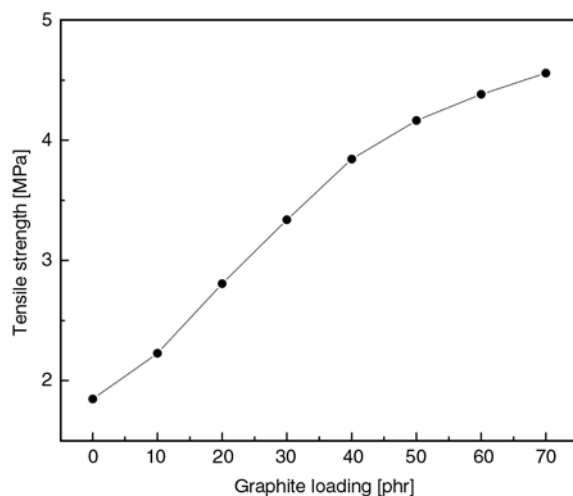
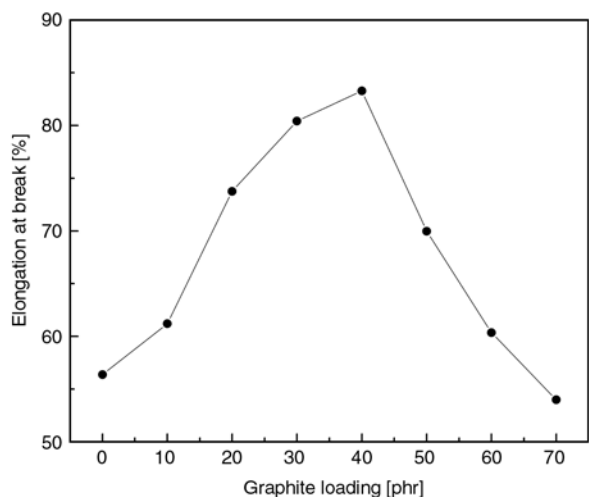


Figure 8. Effect of filler loading on tensile strength of PVC-NBR composites



**Figure 9.** Effect of filler loading on elongation at break of PVC-NBR composites

cannot sustain the load and so failure occurs at lower elongation. However, with increase in filler loading, the matrix is progressively reinforced and a higher elongation at breaking point is observed. With further loading, the molecular segmental motion is restricted because of physical interaction between the filler aggregates and polymer chains. Consequently, the elongation at breaking point decreases with increasing filler loading.

The composites containing 50 phr (G50-0 cycle, and G50-3000 cycles) at constant amplitude 30%, display appreciable irreversibility in the stress-strain plots with applied strain during the extension-retraction cycle. The materials studied here have shown small tensile set as observed from Fig-

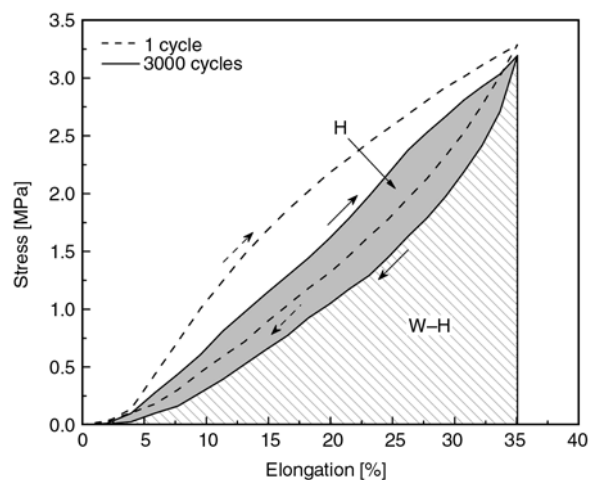


**Figure 10.** Stress-strain plots for the extension-retraction cycle of (G50-0 cycle, and G50-3000 cycles) composites. Hysteresis lost work ( $H$ ), and the work per one cycle ( $W$ ).

ure 10. However, the presence of graphite particles in the composites reduces the set property which in turn reflects a better interaction between graphite and rubber matrix. The reduction in the hysteresis of G50-3000 cycles compared to G50-0 cycle was attributed to viscoelastic relaxation of the matrix. The fact that the stress-strain characteristic of this rubber causes a hysteresis effect was experimentally clarified by Shimojo *et al.* [22]. The index for showing the degree of hysteresis is the ratio  $H/W$ , where  $H$  is the work lost due to hysteresis and  $W$  is the work per cycle, as shown in Figure 10. The ratio ( $H/W$ ) was measured experimentally (0.296 for G50-0, and 0.301 for G50-3000 cycles). The results confirm that the ratio of ( $H/W$ ) does not change up to about 3000 cycles in frequency. As a result, it was confirmed that the form of the hysteresis loop for each cycle did not change, even as cycles were repeated.

The equilibrium stress-strain relation and number of cycles to failure for fatigue life of (3000 cycles) were illustrated in Figure 11. From this figure, the equilibrium stress-strain relation for the first strain cycle exhibits the significant nonlinear deformation and low maximum stress, and then this nonlinearity of deformation decreases and the maximum equilibrium stress increases with an increase in strain cycles. This means that the viscoplastic component of deformation gradually disappears and the hardening occurs during fatigue.

To characterize the variation of equilibrium stress-strain relation during fatigue, the Young's modulus  $E_N$ , and accumulated strain by fatigue ratcheting  $\epsilon_N$

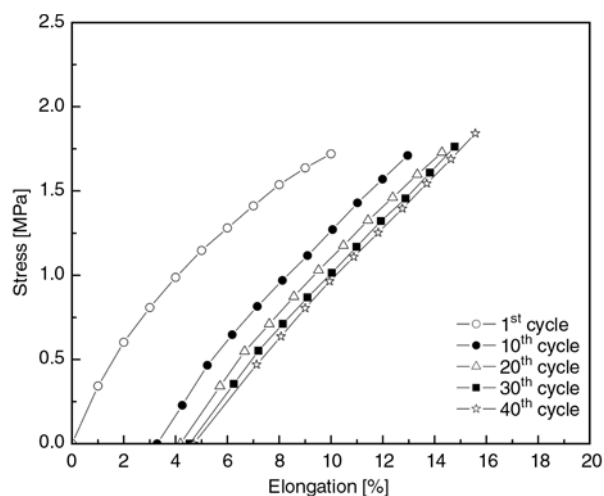


**Figure 11.** Variation of equilibrium stress-strain relation with fatigue (strain cycles for G50-3000 cycles)

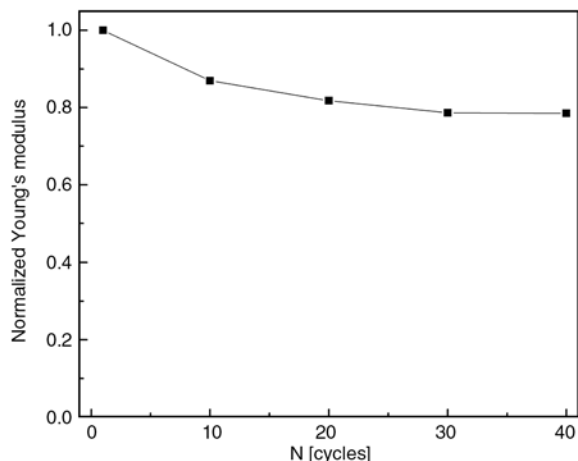


**Figure 12.** Variation of Young’s modulus with the number of cycles for G50-3000 cycles

are determined from the equilibrium stress-strain relation for the  $N^{\text{th}}$  strain cycle as shown in Figure 11. Then normalized Young’s modulus  $E_N/E_1$ , and accumulated strain  $\epsilon_N$  is shown as functions of the number of strain cycles in Figure 12. The stiffness reduces significantly at the early 10 strain cycles and then becomes constant.

### 3.3. Electromechanical properties

Depending on the application, strain gauges can be either metal or semiconductor strain gauges. The latter ones are made of semiconductor materials, but have advantages and disadvantages. On the one hand, semiconductor strain gauges are very small and have large gauge factors. In fact, resistance changes here are much bigger than those obtained with metal strain gauges.

When the sample deforms, the fraction of electrical resistance change ( $\Delta R/R$ ) is expressed by Equation (7) [23]:

$$\frac{\Delta R}{R} = K\epsilon \quad (7)$$

where,  $K$  is a gauge factor. The longitudinal extension of the sensor leads to a shrinking in the cross-section area  $A$ , and according to Equation (1), the resistance  $R$  will increase. Moreover, an extension of the sensor length will cause a decrease in the number of electrical connections between the conductive particles in the CPC, and the resistance will thus increase. The combination of these two phenomena will therefore lead to an important increase

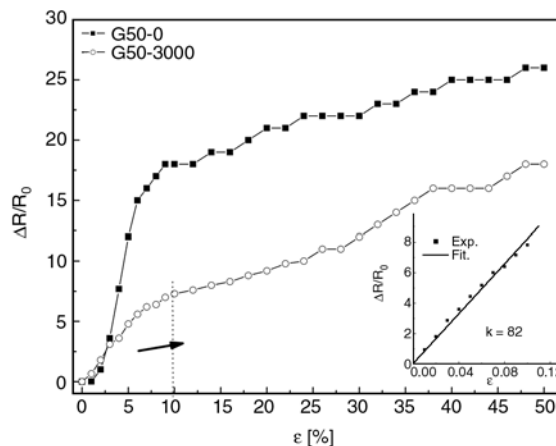


**Figure 13.** Dependence of relative change of resistance vs. strain of the sensor

of the resistance for a small strain deformation. Although the gauge factor varies depending on materials, the value is approximately around 2~4 for most of metallic materials and 80~170 or –95 to –110 for semiconductor strain gauges, depending on the doping level and the design [24, 25]. For classical metallic conductors (copper, nickel), this factor is 2.1 at the maximum. However, the strain range covered by a classical metal gauge is between 0.1 and 0.5% [26]. Figure 13 shows the dependence of relative change of resistance on strain over the range of elongation. The curve obtained on Figure 13 can be divided in two regions for the two samples G50-0 cycle, and G50-3000 cycles: the first one corresponds to a strain below 10%, where the sensor response is practically linear. It is interesting that the strain sensitivity coefficient  $K = \Delta R/R_0\epsilon$  (G50-0 cycles) can be very high, up to 203, which is more than a decade higher compared to commercial wire strain gauges, while the values of  $K$  is 82, which is in agreement with semiconductor strain gauges [25, 26]. In the second region, for strain values greater than 10%,  $K$  was found to be most similar, and equal to 20 for two samples. A study demonstrated that the composite exhibited Ohmic behavior before and after stretching to 10% strain.

The normalized resistivity curves for G50-0, and G50-3000 with deformation to 5% strain illustrated in Figure 14. The resistivity exhibited a small hysteresis loops. The decrease in resistivity upon unloading up to 2% strain was due to relaxation of the stretched polymer, which allowed the particles to reform the network.

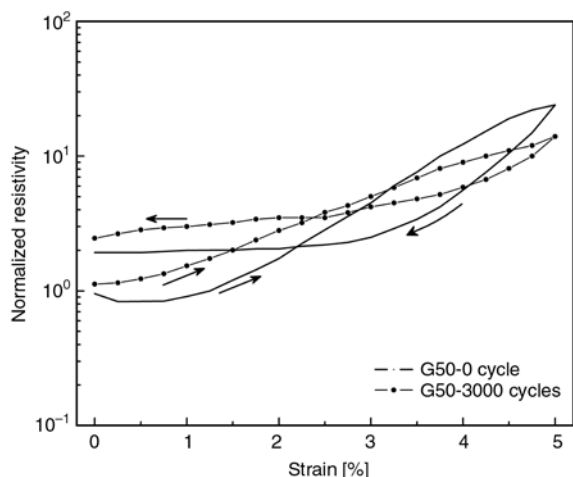


**Figure 14.** Effect of extension-retraction cycle to 5% strain on the normalized resistivity of a composite with graphite 50 phr. G50-0 cycle (solid lines), and G50-3000 cycles (circles)

This complex behavior demonstrates the dynamic and time-dependent nature of microstructural changes in the region of low strain. This region is generally attributed to network breakage; the composite exhibited no permanent strain or irreversible electrical properties during mechanical cycling. The disadvantage of these types of composites is the hysteretic behavior of the sample resistivity when extension-retraction is applied. Composites (G50 at strain amplitude of 30% and after 3000 number of cycles) have a flatter temperature response but unfortunately are not suitable for sensor application. Improvement of particle-polymer chemical interaction and choice of matrix may be able to overcome this problem in the future.

#### 4. Conclusions

The percolation thresholds detected for composites were achieved through the applicability between the electrical as well as the mechanical properties. The composites demonstrated modulus reinforcement in accordance with the Guth model for good particle-matrix adhesion. Typically, reinforcement even with high-structure graphite is accompanied by a decrease in elongation to break. The disadvantage of composites with graphite did not maintain good mechanical properties, generally exhibited an increase in resistivity with strain, and exhibited irreversible changes in both mechanical and electrical properties after extension to even low strains. Cyclic strain markedly affects the value and behav-

our of conductivity with temperature, also is greatly changed by both strain amplitude and the number of strain cycles. The conductivity of 50 phr graphite/PVC-NBR at amplitude of 30% and after 3000 cycles becomes temperature independent. From the variation of the equilibrium stress-strain relations with strain cycles, it is found that the viscous component of deformation gradually disappears and the hardening occurs with increasing strain cycles. The filler loading in the composite which gave the best compromise between sensor sensitivity and measurable resistance values was found to be much higher than the concentration at the percolation threshold.

The electromechanical characterization showed that the sensor presented a classical ohmic linear behaviour for the lower strain levels 10%, the average gauge factor  $K$  in this range is 82.

#### References

- [1] Rusu M., Sofian N., Rusu D.: Mechanical and thermal properties of zinc powder filled high density polyethylene composites. *Polymer Testing*, **20**, 409 (2001).
- [2] Guth E.: Theory of filler reinforcement. *Journal of Applied Physics*, **16**, 20–25 (1945).
- [3] Flandin L., Hiltner A., Baer E.: Interrelationships between electrical and mechanical properties of a carbon black-filled ethylene-octene elastomer. *Polymer*, **42**, 827–38 (2001).
- [4] Shevchenko V. G., Ponomarenko A. T., Klason C.: Strain sensitive polymer composite material. *Smart Material Structures*, **4**, 31–35 (1995).
- [5] Flandin L., Chang A., Nazarenko S., Hiltner A., Baer E.: Effect of strain on the properties of an ethylene-octene elastomer with conductive carbon fillers. *Journal of Applied Polymer Science*, **76**, 894–905 (2000).
- [6] Feller J-F., Linossier I., Levesque G.: Conductive polymers composites (CPCs): Comparison of electrical properties of poly (ethylene-co-ethyl acrylate)-carbon black with poly(butylene terephthalate)/poly(ethylene-co-ethylacrylate)-carbon black. *Polymer Advanced Technology*, **13**, 714–724 (2002).
- [7] Krupa I., Novak I., Chodak I.: Electrically and thermally conductive polyethylene/graphite composites and their mechanical properties. *Synthetic Metals*, **145**, 245–252 (2004).
- [8] Norman R. H.: *Conductive rubber and plastics*. Elsevier, London (1970).
- [9] Cochrane C., Koncar V., Lewandowski M., Dufour C.: Design and development of a flexible strain sensor for textile structures based on a conductive polymer composite. *Sensors*, **7**, 473–492 (2007).

- [10] Shimojo M., Namiki A., Ishikawa M., Makino R., Mabuchi K.: A tactile sensor sheet using pressure conductive rubber with electrical-wires stitched method. *IEEE Sensors Journal*, **4**, 589–596 (2004).
- [11] Inaba M., Hoshino Y., Nagasaka K., Ninomiya T., Kagami S., Inoue H.: A full-body tactile sensor suit using electrically conductive fabric and strings. in 'Proceedings of the IEEE/RSJ International Conference of Intelligent Robots and Systems, Dayton, USA' vol 2, 450–457 (1996).
- [12] Flandin L., Brechet Y., Cavaille J-Y.: Electrically conductive polymer nanocomposites as deformation sensors. *Composites Science and Technology*, **61**, 895–901 (2001).
- [13] Sau K. P., Chaki T. K., Khastgir D.: The change in conductivity of a rubber-carbon black composite subjected to different modes of pre-strain. *Composites Part A: Applied Science and Manufacturing*, **29**, 363–370 (1998).
- [14] Pramanik P. K., Khastagir D., Saha T. N.: Effect of extensional strain on the resistivity of electrically conductive nitrile-rubber composites filled with carbon filler. *Journal of Materials Science*, **28**, 3539–3546 (1993).
- [15] Smits F. M.: Measurement of sheet resistivities with the four-point probe. *Bell System Technical Journal*, **37**, 711–718 (1958).
- [16] Amin M., Nasr G. M., Hassan H. H., El-Guiziri S., Abu-Abdeen M.: Investigation on the dependence of the electrical conductivity of FEF/SBR vulcanizates on the cyclic strain. *Polymer Bulletin*, **22**, 413–420 (1989).
- [17] Roldughin V. I., Vysotskii V. V.: Percolation properties of metal-filled polymer films, structure and mechanisms of conductivity. *Progress in Organic Coating*, **39**, 81–100 (2000).
- [18] Kirkpatrick S.: Percolation and conduction. *Review Modern Physics*, **45**, 574–588 (1973).
- [19] Zallen R.: *The physics of amorphous solids*. Wiley, New York (1983).
- [20] Derrida B., Stauffer D., Herrmann H. J., Vannemius J.: Transfer matrix calculation of conductivity in three-dimensional random resistor networks at percolation threshold. *Journal de Physique-Letters*, **44**, 701–706 (1983).
- [21] Norman R. H.: *Conductive rubbers and plastics*. Elsevier, London (1970).
- [22] Shimojo M., Ishikawa M., Kanaya K.: A flexible high resolution tactile imager with video signal output. in 'IEEE International Conference of Robotics and Automation, Sacramento, USA' vol 1, 384–391 (1991).
- [23] Todoroki A., Yoshida J.: Electrical resistance change of unidirectional CFRP due to applied load. *JSME International Journal, Series A*, **47**, 357–364 (2004).
- [24] Shankland E. P.: Piezoresistive silicon pressure sensors. *Sensors Magazine*, **22**, 22–26 (1991).
- [25] Frank R.: *Understanding smart sensors*. Artech House, Norwood, USA (2000).
- [26] Asch G.: *Les capteurs en instrumentation industrielle*. Dunod, Paris (2000).

# Influence of Engage<sup>®</sup> copolymer type on the properties of Engage<sup>®</sup>/silicone rubber-based thermoplastic dynamic vulcanizates

U. Basuli, T. K. Chaki, K. Naskar\*

Rubber Technology Center, Indian Institute of Technology, Kharagpur 721302, India

Received 22 August 2008; accepted in revised form 30 October 2008

**Abstract.** Thermoplastic vulcanizates (TPVs) are a special class of thermoplastic elastomers, which are produced by simultaneously mixing and crosslinking a rubber with a thermoplastic polymer at an elevated temperature. Peroxide-cured TPVs based on blends of silicone rubber and thermoplastic Engage of two different types, mainly ethylene-octene and ethylene-butene copolymers at different blend ratios have been developed. A detailed comparative study of ethylene-octene vs. ethylene-butene based TPVs are mainly focused in this paper. These TPVs exhibit very good overall mechanical and electrical properties. With increasing amount of Engage in the blends at a fixed concentration of peroxide and coagent, tensile strength, modulus and hardness of the TPVs were found to increase considerably. Ageing characteristics and recyclability of silicone rubber based TPVs are also found excellent. Rheological studies confirm the pseudoplastic nature of these TPVs.

**Keywords:** *polymer blends and alloys, silicone rubber, ethylene-octene, ethylene-butene and peroxide*

## 1. Introduction

Thermoplastic elastomers (TPEs) based on rubber-plastic blends are relatively new class of polymeric materials, where properties can be more easily tailored by simply changing the ratio of the rubber to plastic in the blends. These TPEs are normally phase separated systems, in which one phase is soft and rubbery at room temperature while the other is hard and solid. They possess the elasticity of a rubber and the thermoplasticity of a plastic; yet retain unique features of its components such as good ultraviolet and ozone resistance, solvent resistance and high deformation temperature. Furthermore, they can be processed very easily by extrusion, injection moulding, and blow moulding etc. to provide commercially attractive products that show the softness, extensibility and resilience of conven-

tional thermoset rubbers. The most important feature of this class of materials is that the scrap can be recycled several times without significant deterioration of properties [1–3]. As a result, many commercial TPEs have been developed for various applications particularly in the automotive, electrical, medical and construction industries etc.

The first TPE was introduced to the market in 1972 by Fisher [4]. Significant improvements in the properties of these blends were achieved in 1978 by Coran, Das and Patel by fully vulcanizing the rubber phase under dynamic shear, while maintaining the thermoplasticity of the blends [5, 6]. These blends were further improved by Sabet Abdou-Sabet and Fath [7] in 1982 by the use of phenolic resins as curatives. A series of extensive studies on dynamically vulcanized TPEs or TPVs were car-

\*Corresponding author, e-mail: [knaskar@rtc.iitkgp.ernet.in](mailto:knaskar@rtc.iitkgp.ernet.in)  
© BME-PT and GTE

ried out by Coran and Patel in 1980s [8–15]. Generally, it is easy to combine a rubber and plastic of similar polarities and solubility parameters to produce a useful thermoplastic elastomer, such as polypropylene (PP)/ethylene-propylene-diene copolymer (EPDM), epoxidized natural rubber (ENR) and poly (vinyl chloride) (PVC), acrylonitrile-butadiene rubber (NBR) and nylon etc. However, it is difficult to produce a TPE using a plastic and an elastomer having different polarities and solubility parameters. This is due to the existence of a high interfacial tension between the two polymers. Bhowmick *et al.* [16–24] also reported various TPEs and TPVs. Recently Naskar *et al.* [25–30] extensively studied the effect of various peroxides including multifunctional peroxides as crosslinking agents in PP/EPDM TPVs. They are typically characterized by finely dispersed (micron-sized) crosslinked rubber particles distributed in a continuous thermoplastic matrix. Generally the rubber particle size varies in the range of 0.5–2  $\mu\text{m}$ . A literature survey indicates that there is enough opportunity to generate new materials by blending the existing polymers, especially to improve properties, to cover up the deficiency of one polymer by another and also to reduce cost. This survey also reveals that there is a growing interest of the use of thermoplastic vulcanizates (TPVs) in the last couple of decades. Currently TPVs comprise of the fastest growing elastomer market with an annual growth rate of about 15%.

Only limited researches have been pursued so far in the field of silicone rubber. A few research works in related field have been patented by Dow Corning Corporation [31–33]. Very recently Basuli *et al.* [34, 35] studied the properties of TPVs based on

silicone rubber at a fixed blend ratio of the blend constituents. Potential areas of application of silicone based TPVs could be in wire and cable industries and soft-touch appliances.

The main objective of the present work is basically to study the influence of the type of Engage on the properties of silicone rubber and Engage-based TPVs at varied blend ratios. Two different types of Engage, namely, ethylene-octene and ethylene-butene were taken for this study.

## 2. Experimental

### 2.1. Materials

Silicone rubber (polydimethyl siloxane, PDMS) was supplied by GE Silicones, India having a specific gravity of 0.9  $\text{g}/\text{cm}^3$  and a Mooney viscosity  $\text{ML}_{1+4}$  at 100°C of 45. Engage-8440 (Ethylene-octene grade) and Engage-7256 (Ethylene-butene grade) were supplied by DuPont Dow elastomers, USA. Table 1 [36] shows various properties of Engage-8440 and Engage-7256, which have crystallinity of 27 and 23% respectively. Dicumyl peroxide (DCP) (98%) and triallyl cyanurate (TAC) (50%) were obtained from Akzo Nobel Polymer Chemicals, The Netherlands. DCP was used as the crosslinking agent and TAC was used as the co-agent (booster for peroxide).

### 2.2. Preparation of TPVs

The TPV compositions employed for the present work is shown in Table 2. The experimental variable is the ratio of blend constituents. All TPVs were prepared by a batch process in a Brabender Plasti-Corder PLE 330, Germany having a mixing

**Table 1.** Various properties of Engage-8440 (ethylene-octene grade) and Engage-7256 (ethylene-butene grade)

Type of Engage	Density [ $\text{g}/\text{cm}^3$ ]	Melt index [ $\text{dg}/\text{min}$ ] (190°C, 2.16 kg)	Mooney viscosity $\text{ML}_{1+4}$ at 121°C	Total crystallinity [%]	Hardness [Shore A]	DSC melting peak [°C] (rate 10°C/min)
Engage-8440	0.897	1.6	16	27	92	94
Engage-7256	0.885	2.0	16	23	79	73

**Table 2.** TPV compositions in phr (parts per hundred rubber) at varied PDMS/Engage blend ratios at a fixed DCP/TAC concentration

Components	E <sub>1</sub>	E <sub>2</sub>	E <sub>3</sub>	E <sub>4</sub>	E <sub>5</sub>	E <sub>6</sub>	E <sub>7</sub>	E <sub>8</sub>	E <sub>9</sub>	E <sub>10</sub>
PDMS	100	100	100	100	100	100	100	100	100	100
Engage-8440	25	50	75	100	125	–	–	–	–	–
Engage-7256	–	–	–	–	–	25	50	75	100	125
DCP (98%)	2.5	2.5	2.5	2.5	2.5	2.5	2.5	2.5	2.5	2.5
TAC (50%)	2.0	2.0	2.0	2.0	2.0	2.0	2.0	2.0	2.0	2.0

chamber volume of 70 cm<sup>3</sup>. The mixer temperature was kept at 120–130°C with a constant rotor (cam type) speed of 80 rpm. Engage and silicone rubber (PDMS) were first mechanically melt-mixed. After 6 min of mixing, the co-agent (TAC) was added, followed by the addition of DCP. The mixing was continued for another 4 min to complete the dynamic vulcanization process in the Brabender. Immediately after mixing, the molten mass was passed through a cold two-roll mill to achieve a sheet of about 2 mm thickness. The sheet was cut and pressed (2 mm thick) for 4 min in a compression molding machine (Moore Press) at 130°C. Teflon sheets were placed between the molded sheet and the press plates. The sheet was then cooled down at room temperature under pressure. Test specimens were then die-cut from the compression molded sheet and used for testing after 24 hrs of maturation at room temperature.

### 2.3. Testing procedures

#### 2.3.1. Curing characteristics

Curing characteristics of only silicone rubber (without any Engage) containing cross-linking agents, DCP/TAC were carried out by using Monsanto Rheometer R100S (an oscillating disc rheometer, ODR) at 130°C for 30 minutes.

#### 2.3.2. Mechanical properties

Tensile tests were carried out according to ASTM D 412-98 on dumb-bell shaped specimens using a Zwick tensile testing machine, Zwick 1445, Germany at a constant cross-head speed of 500 mm/min. Three specimens were tried for each condition and average value (having a very little standard deviation in all samples) was reported. Hardness of the samples was measured with a Durometer (Shore A and Shore D, as per ASTM D2240). Tension set test was carried out at room temperature after stretching the samples for 10 min at 100% elongation according to ASTM D 412-98.

#### 2.3.3. Rheological characteristics

Processing and rheological characteristics of the samples were carried out using a Monsanto Processability Tester (MPT), USA at 120°C at varied shear rates (0.05, 0.10, 0.25 and 0.40 in/min).

#### 2.3.4. Ageing test

Ageing test was carried out keeping the samples in the ageing oven at 70°C for 72 hrs to get a preliminary idea about the ageing characteristics of the samples.

#### 2.3.5. Recyclability study

Recyclability tests were carried out by putting the residual molded TPV samples again in the Brabender Plasticorder at 110–120°C, followed by molding the samples at 130°C and subsequently testing them.

## 3. Results and discussion

Peroxide crosslinking chemistry has been known for many years. The mechanism of peroxide crosslinking of rubber is less complicated as compared to sulfur vulcanization. The crosslinking process of high polymers like silicone rubber by organic peroxides (DCP) can be divided into three successive steps [35]. The first step is the homolytic decomposition of DCP and generation of cumyloxy free radicals. This step is the rate-determining step of the overall reactions. These cumyloxy radicals can further undergo  $\beta$  chain scission to produce highly reactive methyl radicals and acetophenone. The second step is the abstraction of hydrogen atoms from the silicone polymer, resulting in stable peroxide silicone polymeric radicals. The final step consists of the combination of two such decomposition products such as methane, acetophenone, and 2-phenyl propanol-2 and silicone polymeric radicals to produce a stable C–C crosslink, which has very high bond strength. Increases in the tensile strength, modulus, and hardness of TPVs can be explained by the higher extent of crosslinking in the PDMS phase. It should be noted, however, that there is a possibility that DCP could also take part in crosslinking the Engage phase to some extent because of its chemical structure. However, crosslinking in the PDMS phase is predominating here and is mainly controlling the final phase morphology and consequently the properties of the blends. In addition, during the process of dynamic vulcanization of silicone rubber and ethylene-octene or ethylene-butene copolymer in the presence of DCP/TAC, there is a possibility of generation of in situ graft links of silicone rubber

**Table 3.** Formulations of the samples used for the ODR experiments (phr) at 130°C and corresponding data

Sample	PDMS	DCP (98%)	TAC (50%)	Minimum ML [dN m]	Maximum MH [dN m]	Max – Min torque [dN m]	T <sub>90</sub> [min]
R-1	100	1.0	2.0	4.50	73.00	68.50	17
R-2	100	2.0	2.0	5.00	77.00	72.00	21
R-3	100	2.5	2.0	7.50	83.00	75.50	20
R-4	100	3.0	2.0	7.50	88.00	80.50	13

and ethylene-octene or ethylene-butene copolymer at the interface (which is very difficult to prove by any analytical technique because of the extremely small amount of grafts being generated), which can in turn enhance the compatibility between the two phases and also can improve the final mechanical properties of the TPVs.

Table 3 shows formulations of the samples for rheograms containing only PDMS, DCP, and TAC and corresponding results. In order to achieve a better in-sight into chemistry involved with dynamic vulcanization in PDMS/Engage blends in presence of DCP, vulcanization characteristics of PDMS gum compounds at different DCP concentrations for ODR study. The delta torque (maximum torque–minimum torques) values, as obtained from the ODR generally correlate with the crosslinking efficiency of the peroxide, which is defined as the number of moles of chemical crosslinks formed per mole of peroxide. It should be noted, however, that the latter could be measured by static vulcanization only in the absence of Engage; which is not exactly a one-to-one comparison to dynamic vulcanization, because of the lack of a high shear rate and the longer timescales.

### 3.1. Physical and mechanical properties

Table 4 illustrates various physical properties of the TPVs at varied PDMS/Engage blend ratios at a

fixed peroxide concentration of 2.5 phr. Table 4 shows that the tensile strength, modulus at 100% (M100), at 200% (M200) and at 300% (M300) of PDMS/Engage-8440 and PDMS/Engage-7256 based TPVs as a function of the amount of Engage. With increasing amount of Engage-8440 from 25 to 125 phr, the tensile strength increases from 3.3 to 11.0 MPa, M100 from 1.1 to 3.2 MPa and M300 from 2.0 to 4.2 MPa respectively. Table 3 also shows the Shore A hardness values of the TPVs as a function of the concentration of Engage-8440. An increase in hardness (40–68 Shore A) is seen with increasing amount of Engage.

In case of Engage-7256, tensile strength increases from 3.3 to 6.4 MPa, M100 from 1.0 to 2.0 MPa and M300 from 1.6 to 2.8 MPa respectively. Table 4 also shows the Shore A hardness values of the TPVs as a function of the concentration of Engage. An increase in hardness (40–58 Shore A) takes place with increasing amount of Engage. The general reason for the increased tensile strength, modulus, hardness, and tension set of TPVs with increasing amount of Engage in PDMS/Engage blend, as seen in Table 4, can be explained by the incorporation of higher amount of thermoplastic hard component in the blends. At low concentration of thermoplastic Engage, both types of TPVs shows more or less similar physico-mechanical properties up to 50 phr of Engage; however beyond 50 phr ethylene-octene grade shows better improvement in

**Table 4.** Physical properties of PDMS-Engage TPVs at varied blend ratios

Sample No.	Tensile strength [MPa]	Elongation at break [%]	Modulus [MPa]			Hardness [Shore A]	Hardness [Shore D]	Tension set [%]
			M100	M200	M300			
E <sub>1</sub>	3.3	350	1.1	1.5	2.0	40	8	4
E <sub>2</sub>	4.5	570	1.9	2.2	2.7	52	11	7
E <sub>3</sub>	6.4	641	2.4	2.8	3.4	56	13	11
E <sub>4</sub>	8.8	755	2.8	3.2	3.8	61	16	15
E <sub>5</sub>	11.0	854	3.2	3.6	4.2	68	19	19
E <sub>6</sub>	3.3	900	1.0	1.3	1.6	40	8	4
E <sub>7</sub>	3.6	950	1.3	1.7	1.9	50	11	8
E <sub>8</sub>	4.9	1025	1.6	1.9	2.2	53	13	12
E <sub>9</sub>	5.8	1100	1.9	2.2	2.5	56	14	16
E <sub>10</sub>	6.4	1200	2.0	2.5	2.8	58	15	20

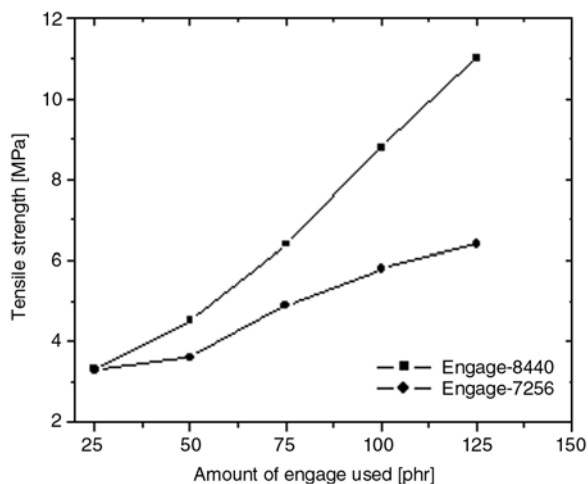


**Figure 1.** Tensile strength of TPVs as a function of amount of Engage

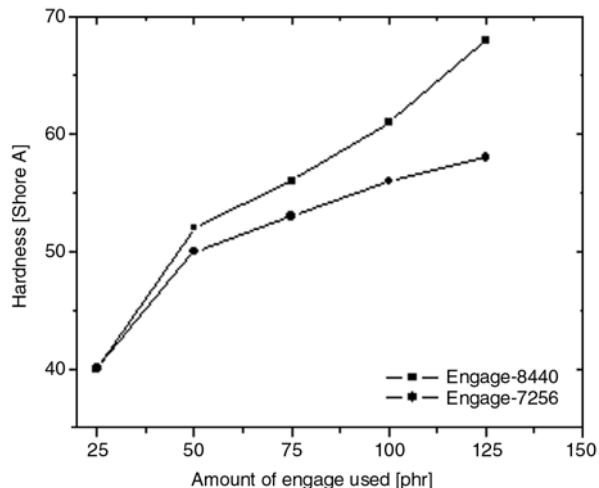


**Figure 4.** Hardness of TPVs as a function of amount of Engage

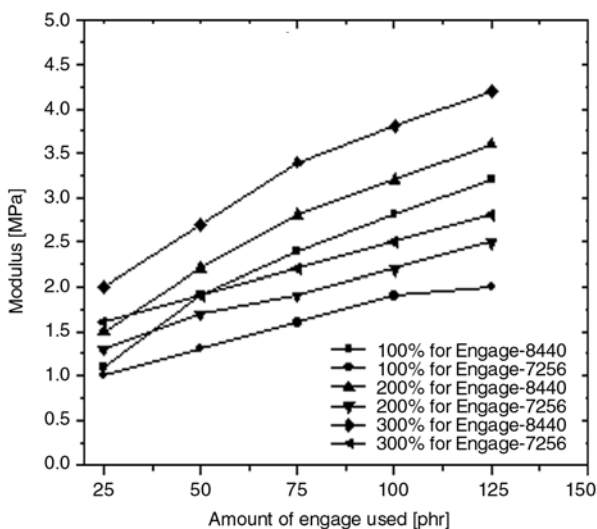


**Figure 2.** Modulus at different elongation of TPVs as a function of amount of Engage

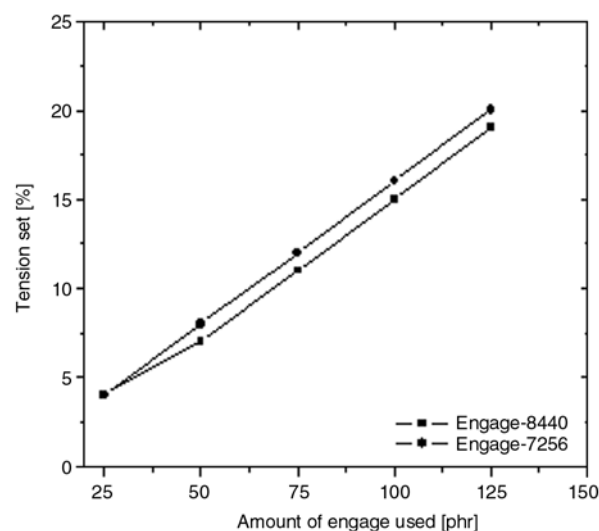


**Figure 5.** Tension set of TPVs as a function of amount of Engage

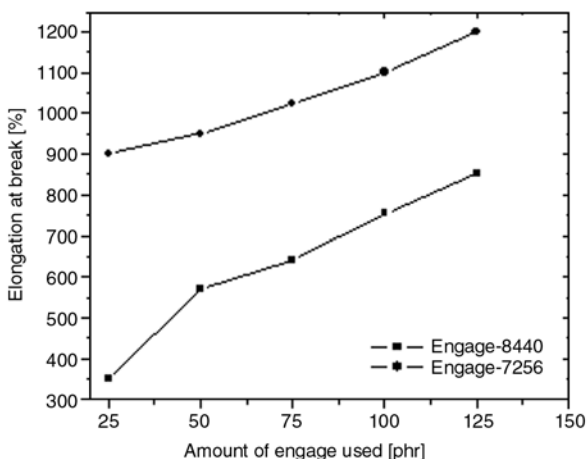


**Figure 3.** Elongation at break of TPVs as a function of amount of Engage

properties than ethylene-butene grade. Hardness of these TPVs are found to be almost same, only little

difference is observed of two different TPVs of same amount of two different Engage grades. This is due to the slight difference in their crystallinity values. Engage-8440 with PDMS always shows better properties; however, Engage-8440 i.e. ethylene-octene co-polymer is more expensive material because of the presence of octene monomer as compared to ethylene butene.

Figures 1–5 show various mechanical properties of Engage-8440 and Engage-7256 based TPVs at varied amounts of Engage.

### 3.2. Rheological study

Figures 6 and 7 show the plot of apparent shear stress vs. apparent shear rate and apparent viscosity vs. apparent shear rate respectively for Engage-

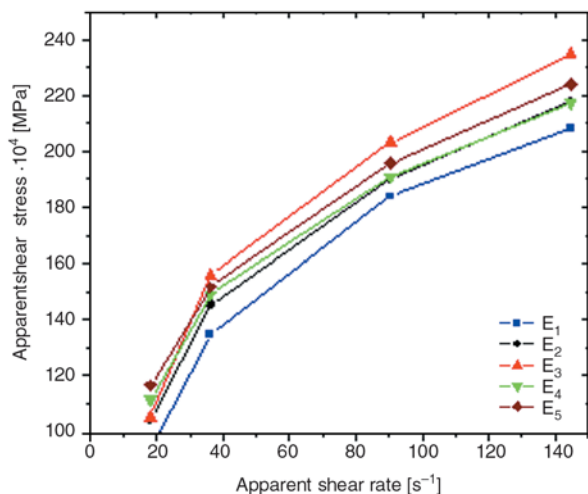


**Figure 6.** Relation between apparent shear stress and apparent shear rate for PDMS/Engage-8440 TPVs

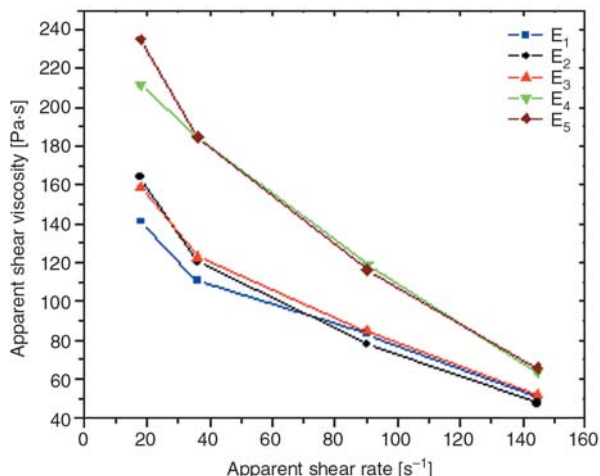


**Figure 9.** Relation between apparent viscosity and apparent shear rate for PDMS/Engage-7256 TPVs

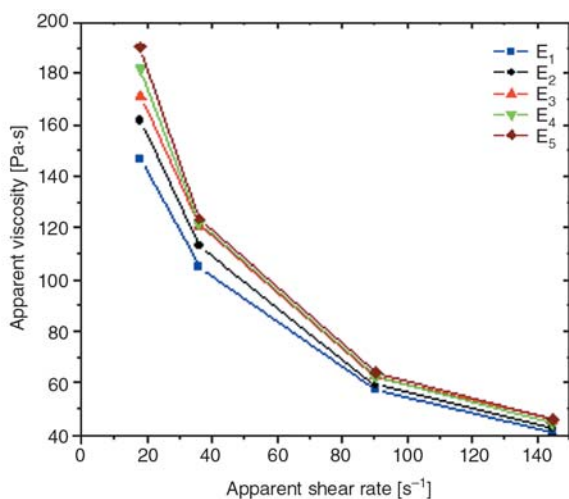


**Figure 7.** Relation between apparent viscosity and apparent shear rate for PDMS/Engage-8440 TPVs

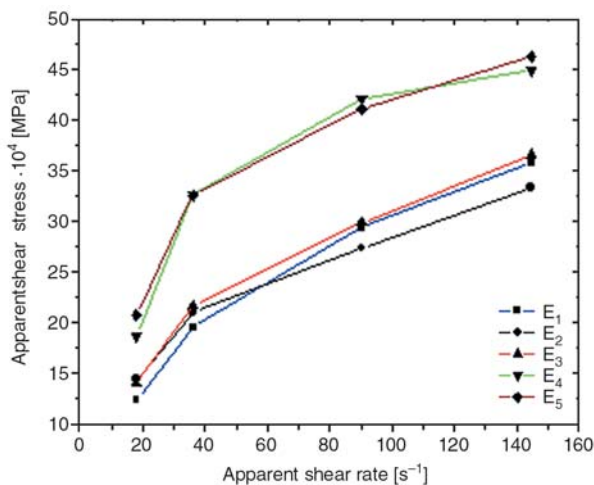


**Figure 8.** Relation between apparent shear stress and apparent shear rate for PDMS/Engage-7256 TPVs

8440. Apparent shear stress of the TPVs increases with increasing apparent shear rate and apparent viscosity decreases with increasing shear rate. However, at a particular shear rate, TPV containing higher level of Engage-8440 exhibits higher shear stress as compared to a TPV containing lower amount of Engage-8440. On the other hand, Figures 8 and 9 show the plot of apparent shear stress vs. apparent shear rate and apparent viscosity vs. apparent shear rate respectively for Engage-7256. Apparent viscosity of the TPVs decreases with increasing shear rate indicating pseudoplastic behaviour. From the MPT experiment, it is also observed that viscosity increases with increasing amount of Engage.

### 3.3. Ageing study

Table 5 shows the ageing result of PDMS/Engage TPVs. It can be seen that even after ageing at 70°C for 72 hrs., the PDMS/Engage TPV still keeps a relatively high tensile strength and elongation at break. Only the M100 of the PDMS/Engage-7256 TPVs slightly changes with ageing. However, no linear behavior for the parameters has been observed in a comparison of the influence of Engage before and after aging. Most of the TPVs show very good retention of properties even after aging, and this indicates good resistance to heat. Peroxide curing provides strong C–C linkages as crosslinks, and this is reflected in the better aging behavior. More or less similar results were observed for PDMS/Engage-8440 and PDMS/Engage-7256 TPVs.

**Table 5.** Change of tensile strength, elongation at break, modulus of the TPVs due to ageing (72 hrs at 70°C)

Sample No.	Tensile strength [MPa]			Elongation at break [%]			M100 [MPa]			M300 [MPa]		
	Before ageing	After ageing	Change [%]	Before ageing	After ageing	Change [%]	Before ageing	After ageing	Change [%]	Before ageing	After ageing	Change [%]
E <sub>1</sub>	3.3	2.9	-8.3	350	325	-3.9	1.1	0.8	-27.3	2.0	2.0	0
E <sub>2</sub>	4.5	3.0	-33.3	570	360	-36.8	1.9	2.2	+15.8	2.7	2.7	0
E <sub>3</sub>	6.4	5.3	-21.8	641	605	-5.6	2.4	2.7	+12.5	3.4	3.7	+8.8
E <sub>4</sub>	8.8	7.3	-17.0	755	630	-16.6	2.8	3.1	+10.7	3.8	3.9	+2.6
E <sub>5</sub>	11.0	9.0	-18.2	854	708	-17.1	3.2	3.3	+3.1	4.2	4.3	+2.4
E <sub>6</sub>	3.3	1.3	-60.0	900	550	-39.0	1.0	1.3	+30.0	1.6	2.0	+25.0
E <sub>7</sub>	3.6	2.5	-31.0	950	700	-26.0	1.3	1.6	+30.0	1.9	2.8	+47.0
E <sub>8</sub>	4.9	2.8	-43.0	1025	950	-7.0	1.6	2.0	+25.0	2.2	2.5	+14.0
E <sub>9</sub>	5.8	3.5	-40.0	1100	1025	-7.0	1.9	2.0	+5.0	2.5	2.5	0
E <sub>10</sub>	6.4	3.8	-41.0	1200	1060	-12.0	2.0	2.1	+5.0	2.8	2.6	-7.1

**Table 6.** Change of tensile strength, elongation at break, modulus of the TPVs after recycling

Sample No.	Tensile strength [MPa]			Elongation at break [%]			M100 [MPa]			M300 [MPa]		
	Before	After	Change [%]	Before	After	Change [%]	Before	After	Change [%]	Before	After	Change [%]
E <sub>1</sub>	3.3	2.9	-12.1	350	400	+14.3	1.1	1.8	+64	2.0	3.0	+50
E <sub>2</sub>	4.5	4.5	0.0	570	450	-21.0	1.9	2.8	+58	2.7	4.4	+63
E <sub>3</sub>	6.4	8.0	+25.0	641	640	0.0	2.4	3.0	+25	3.4	4.4	+29
E <sub>4</sub>	8.8	8.8	0.0	755	700	-7.3	2.8	3.0	+7	3.8	4.1	+8
E <sub>5</sub>	11.0	13.0	+18.2	854	785	-8.2	3.2	3.8	+19	4.2	5.2	+24
E <sub>6</sub>	3.3	2.0	-39.0	900	310	-65.0	1.0	1.3	+30	1.6	2.0	+25
E <sub>7</sub>	3.6	4.2	+17.0	950	670	-29.0	1.3	1.6	+23	1.9	2.8	+47
E <sub>8</sub>	4.9	3.5	-26.0	1025	650	-37.0	1.6	1.7	+6	2.2	2.5	+14
E <sub>9</sub>	5.8	5.0	-14.0	1100	1100	0.0	1.9	1.8	-5	2.5	2.5	0
E <sub>10</sub>	6.4	5.1	-20.0	1200	1130	-6.0	2.0	2.0	0	2.8	2.9	+4

### 3.4. Recyclability study

One of the most important criteria of TPEs is its recyclability. Table 6 shows the data of recycling test, which shows very good recyclability of both types of TPV samples. Table 6 also illustrates tensile strength, M100 and M300 and elongation at break values for various systems before and after recycling. All the systems show a slight decrease in tensile strength and modulus after recycling. More or less similar results were observed for PDMS/Engage-8440 and PDMS/Engage-7256 TPVs.

## 4. Conclusions

Thermoplastic vulcanizates based on blends of silicone rubber and thermoplastic Engage have been developed. These TPVs exhibit very good overall mechanical properties with respect to two different types of Engage (Engage-8440 and Engage-7256). With increasing amount of Engage in the blends at a fixed DCP concentration of 2.5 phr, tensile

strength, elongation at break, modulus and hardness of the TPVs were found to increase considerably. This can be explained by the incorporation of more thermoplastic hard component in TPVs. Ageing characteristics and recyclability of these TPVs are also found very good. Peroxide cured Silicone rubber/Engage TPVs exhibit very good overall performance towards heat ageing resistance, processability and recyclability. PDMS/Engage-8440 system was compared with PDMS/Engage-7256 system for physical properties, heat aging, processability, and morphology studies. PDMS/Engage-8440 system was found to exhibit better behavior in all respect. However, Engage-8440 i.e. ethylene-octene co-polymer is more expensive because of the presence of octene monomer, as compared to ethylene-butene grade. MPT shows good correlation with shear stress vs. shear rate and shear viscosity vs. shear rate. Rheological studies also confirm the pseudoplastic nature of these TPVs.

## References

- [1] Legge N. R., Holden G., Schroeders H. E.: Thermoplastic elastomer: A comprehensive review. Hanser, Munich (1987).
- [2] Bhowmick A. K., Stephens H. L.: Handbook of elastomers: New developments and technology. Marcel Dekker, New York (1988).
- [3] De S. K., Bhowmick A. K.: Thermoplastic elastomers from rubber plastic blends. Horwood, London (1990).
- [4] Fisher W. K.: Thermoplastic blend of partially cured monoolefin copolymer rubber and polyolefin plastic. US Patent 3862106, USA (1973).
- [5] Coran A. Y., Patel R.: Rubber-thermoplastic compositions. Part IV. Thermoplastic vulcanizates from various rubber-plastic combinations. *Rubber Chemistry and Technology*, **54**, 892–903 (1981).
- [6] Coran A. Y., Das B., Patel R. P.: Thermoplastic vulcanizates of olefin rubber and polyolefin resin. U.S. Patent 4130535, USA (1978).
- [7] Abdou-Sabet S., Fath M. A.: Thermoplastic elastomeric blends of olefin rubber and polyolefin resin. U.S. Patent 4311628, USA (1982).
- [8] Coran A. Y., Patel R.: Rubber-thermoplastic compositions. Part I. EPDM-polypropylene thermoplastic vulcanizates. *Rubber Chemistry and Technology*, **53**, 141–150 (1980).
- [9] Coran A. Y., Patel R.: Rubber-thermoplastic compositions. Part II. NBR-nylon thermoplastic elastomeric compositions. *Rubber Chemistry and Technology*, **53**, 781–794 (1980).
- [10] Coran A. Y., Patel R.: Rubber-thermoplastic compositions. Part III. Predicting elastic moduli of melt mixed rubber-plastic blends. *Rubber Chemistry and Technology*, **54**, 91–100 (1981).
- [11] Coran A. Y., Patel R.: Rubber-thermoplastic compositions. Part IV. Thermoplastic vulcanizates from various rubber-plastic combinations. *Rubber Chemistry and Technology*, **54**, 892–903 (1981).
- [12] Coran A. Y., Patel R., William D.: Rubber-thermoplastic compositions. Part V. Selecting polymers for thermoplastic vulcanizates. *Rubber Chemistry and Technology*, **55**, 116–136 (1982).
- [13] Coran A. Y., Patel R.: Rubber-thermoplastic compositions. Part VII. Chlorinated polyethylene rubber nylon compositions. *Rubber Chemistry and Technology*, **56**, 210–225 (1983).
- [14] Coran A. Y., Patel R.: Rubber-thermoplastic compositions. Part VIII. Nitrile rubber polyolefin blends with technological compatibilization. *Rubber Chemistry and Technology*, **56**, 1045–1060 (1983).
- [15] Coran A. Y.: Vulcanization: Conventional and dynamic. *Rubber Chemistry and Technology*, **68**, 351–375 (1995).
- [16] Jha A., Bhowmick A. K.: Thermoplastic elastomeric blends of nylon-6/acrylate rubber: Influence of interaction on mechanical and dynamic mechanical thermal properties. *Rubber Chemistry and Technology*, **70**, 798–814 (1997).
- [17] Jha A., Bhowmick A. K.: Crystallization and thermal properties of thermoplastic elastomeric reactive blends of polyamide-6 and acrylate rubber. *Polymer and Polymer Composites*, **6**, 505–511 (1998).
- [18] De Sarker M., De P. P., Bhowmick A. K.: Effect of casting solvents on physical properties of hydrogenated styrene-butadiene copolymer. *Polymer*, **40**, 1201–1208 (1999).
- [19] Naskar A. K., Bhowmick A. K., De S. K.: Thermoplastic elastomeric composition based on ground rubber tire. *Polymer Engineering and Science*, **41**, 1087–1098 (2004).
- [20] Chattopadhyay S., Chaki T. K., Bhowmick A. K.: Development of new thermoplastic elastomers from blends of polyethylene and ethylene-vinyl acetate copolymer by electron-beam technology. *Journal of Applied Polymer Science*, **79**, 1877–1889 (2001).
- [21] Kader A., Bhowmick A. K.: Novel thermoplastic elastomers from fluorocarbon elastomer, acrylate rubber and acrylate plastics. *Rubber Chemistry and Technology*, **74**, 662–676 (2001).
- [22] Anandhan S., De P. P., De S. K., Bandyopadhyay S., Bhowmick A. K.: Novel thermoplastic elastomers based on acrylonitrile-butadiene-styrene terpolymer [ABS] waste computer equipment and nitrile rubber. *Rubber Chemistry and Technology*, **76**, 1145–1163 (2003).
- [23] Roychoudhury N., Bhowmick A. K.: Compatibilization of natural rubber-polyolefin thermoplastic elastomeric blends by phase modification. *Journal of Applied Polymer Science*, **38**, 1091–1109 (1989).
- [24] Jha A., Dutta B., Bhowmick A. K.: Effect of fillers and plasticizers on the performance of novel heat and oil-resistant thermoplastic elastomers from nylon-6 and acrylate rubber blends. *Journal of Applied Polymer Science*, **74**, 1490–1501 (1999).
- [25] Naskar K., Noordermeer J. W. M.: Dynamically vulcanized PP/EPDM blends: Effects of different types of peroxides on the properties. *Rubber Chemistry and Technology*, **76**, 1001–1018 (2003).
- [26] Naskar K., Noordermeer J. W. M.: Multifunctional peroxides as a means to improve properties of dynamically vulcanized PP/EPDM blends. *Kautschuk, Gummi, Kunststoffe*, **57**, 235–239 (2004).
- [27] Chatterjee K., Naskar K.: Development of thermoplastic elastomers based on maleated ethylene propylene rubber (m-EPM) and polypropylene (PP) by dynamic vulcanization. *Express Polymer Letters*, **1**, 527–534 (2007).
- [28] Naskar K., Noordermeer J. W. M.: Dynamically vulcanized PP/EPDM blends: effects of multifunctional peroxides as crosslinking agents. *Rubber Chemistry and Technology*, **77**, 955–971 (2004).
- [29] Babu R. R., Singha N. K., Naskar K.: Studies on the influence of structurally different peroxides in polypropylene/ethylene alpha olefin thermoplastic vulcanizates (TPVs). *Express Polymer Letters*, **2**, 226–236 (2008).

- [30] Datta S., Naskar K., Jelenic J., Noordermeer J. W. M.: Dynamically vulcanized PP/EPDM blends by multi-functional peroxides: Characterization with various analytical techniques. *Journal of Applied Polymer Science*, **98**, 1393–1403 (2005).
- [31] Gornowicz G. A., Lupton K. E., Romenesko D. J., Struble K., Zhang H.: Thermoplastic silicone elastomers. U.S. Patent 6013715, USA (2000).
- [32] Gornowicz G. A.: Thermoplastic silicone elastomers based on fluorocarbon resin. U.S. Patent 6015858, USA (2000).
- [33] Gornowicz G. A., Zhang H.: Thermoplastic silicone vulcanizates prepared by condensation cure. U.S. Patent 6153691, USA (2000).
- [34] Basuli U., Chaki T. K., Naskar K.: Thermoplastic vulcanizates based on silicone rubber and ethylene butene copolymer: Study at a fixed blend ratio. *Progress in Rubber Plastics, and Recycling Technology*, **23**, 223–240 (2007).
- [35] Basuli U., Chaki T. K., Naskar K.: Mechanical properties of thermoplastic elastomers based on silicone rubber and an ethylene-octene copolymer by dynamic vulcanization. *Journal of Applied Polymer Science*, **108**, 1079–1085 (2008).
- [36] The Dow Chemical Company: Technical brochure: Engage polyolefin elastomers. <http://www.dow.com/footwear/products/engage.htm> (2005).

# Physico-mechanical and electrical properties of conductive carbon black reinforced chlorosulfonated polyethylene vulcanizates

M. Nanda, D. K. Tripathy\*

Rubber Technology Center, Indian Institute of Technology, Kharagpur 721302, India

Received 14 September 2008; accepted in revised form 31 October 2008

**Abstract.** The present work deals with the effect of conductive carbon black (Ensaco 350G) on the physico-mechanical and electrical properties of chlorosulfonated polyethylene (CSM) rubber vulcanizates. The physico-mechanical properties like tensile strength, tear strength, elongation at break, compression set, hardness and abrasion resistance have been studied before and after heat ageing. Up to 30 parts per hundred rubber (phr) filler loading both tensile and tear strength increases beyond which it shows a decreasing trend whereas modulus gradually increases with the filler loading. Incorporation of carbon black increases the hysteresis loss of filled vulcanizates compared to gum vulcanizates. Unlike gum vulcanizate, in filled vulcanizates the rate of relaxation shows increasing trend. The bound rubber content is found to increase with increase in filler loading. Dielectric relaxation spectra were used to study the relaxation behavior as a function of frequency (100 to 10<sup>6</sup> Hz) at room temperature. Variation in real and imaginary parts of electric modulus has been explained on the basis of interfacial polarization of fillers in the polymer medium. The percolation limit of the conductive black as studied by ac conductivity measurements has also been reported.

**Keywords:** rubber, dielectric properties, fillers, crosslink density, reinforcement

## 1. Introduction

Electrically conductive CSM composites are widely used in electronic sectors in power distribution, audio, and telephone application, as packaging and semi conductive polymeric materials due to their good weather resistance, good electrical properties and good ageing resistance. The systematic study of the CSM rubber particularly filled with highly conductive carbon black has not received much attention till today. Literature study reveals that very few research works dealing with CSM rubber have been reported [1–4]. The preparation of electrically conductive polymer composites filled with conductive fillers has already been reported by several researchers [5–7]. The relation between electrical and mechanical properties of conductive

polymer composites [8] has also been subject of recent research. Very recently electrical relaxation dynamics in polymer matrix-ceramic composites has been reported by Psarras *et al.* [9, 10].

The incorporation of filler in to a rubber for instance CSM, not only enhances the mechanical properties of the final product but also decreases the cost of the end product. The reinforcement of an elastomer by filler is associated with a strong interaction between a rigid phase and a soft solid phase, which may be of physical or chemical type. However the nature of interaction and the significance of carbon black surface chemistry for reinforcement of polar rubbers have not been reported in the literature. It is widely accepted that the surface area and the concentration of functional groups present

\*Corresponding author, e-mail: [dkt@rtc.iitkgp.ernet.in](mailto:dkt@rtc.iitkgp.ernet.in)  
© BME-PT and GTE

on the surface of filler plays an important role towards the degree of reinforcement. It has been reported earlier that CSM has a great affinity towards polar sites on carbon black surface [11, 12]. The crosslink density is also influenced by the structure and surface chemistry of carbon black [13, 14]. Present study uses a newly generated highly conductive carbon black (Ensaco 350G) having very high surface area and exhibiting very high conductivity. In this work the cure characteristics, physico-mechanical properties, bound rubber measurement and electrical properties of conductive black reinforced rubber compound having an accelerated sulfur cure system have been studied.

The elastomer filler interactions are often characterized by the content of apparent ‘bound rubber’ which is determined as the amount of insoluble part of rubber matrix adhering to the dispersed carbon black aggregates before vulcanization. The bound rubber depends upon characteristics such as surface area, structure, morphology and surface activity of filler. With respect to the polymer, the chemical structure (saturated or unsaturated and polar or non polar) also affects the bound rubber content. Though the bound rubber is a parameter that is simple to measure but the factors that influence test results are complicated. The polymer filler interaction leading to formation of bound rubber involves physical adsorption, chemisorptions and mechanical interaction. In the present work the variation of bound rubber content with variation of filler loading has been studied taking three different solvents such as toluene, tetrahydrofuran (THF) and chloroform. The relaxation behavior of CSM vulcanizates has been studied as a function of frequency (100 to  $10^6$  Hz). Electric modulus formalism has been used to study the dielectric characteristics of the rubber vulcanizates. Percolation limit of the filler as obtained from the ac conductivity study has also been reported.

## 2. Experimental

### 2.1. Materials

Details of the compositions of the mixes are given in Table 1. CSM rubber ((Hypalon-40), 35% chlorine content, Mooney viscosity  $ML_{1+4}$  at  $100^\circ\text{C} = 56$ ) manufactured by DuPont Limited, Delaware, USA, was used. The conductive filler used in this study was highly conductive carbon black, Ensaco

**Table 1.** Compositions of unfilled and Ensaco 350G filled CSM vulcanizates in phr (parts per hundred rubber)

Mix designation	G <sub>0</sub>	HB <sub>1</sub>	HB <sub>2</sub>	HB <sub>3</sub>	HB <sub>4</sub>
CSM	100	1 00	100	100	100
MgO	4	4	4	4	4
Ensaco 350G	0	10	20	30	40
DOP	0	1	2	3	4
MBTS	0.5	0.5	0.5	0.5	0.5
DPG	0.5	0.5	0.5	0.5	0.5
Tetrone-A	0.75	0.75	0.75	0.75	0.75
Sulfur	1	1	1	1	1

350G having a Brunauer-Emmett-Teller (BET) nitrogen surface area,  $770\text{ m}^2/\text{g}$ , pH-8, manufactured by Timcal Corporation, Belgium. The plasticizer used was dioctyl phthalate (DOP), pharmaceutical grade processing oil with B.P  $340^\circ\text{C}$ , supplied by C.D. Pharmaceuticals, Calcutta, India. Magnesium oxide was of analytical grade, with a specific gravity of  $3.8\text{ g/cm}^3$ , which was supplied by E. Merck Limited, Bombay, India. Sulfur of chemically pure grade, with a specific gravity of  $1.9\text{ g/cm}^3$  was supplied by M/S Nice chemicals Private limited Cochin, India. Dibenzothiazyl disulfide (MBTS), diphenyl-guanidine (DPG) and dipentamethylenethiuram tetrasulfide (Tetrone-A) were supplied by M/S ICI limited, Hoogly, India which were used as curatives. Other compounding ingredients used were procured locally.

### 2.2. Sample preparation

The mixing was carried out in a two roll mixing mill ( $325\text{ mm}\times 150\text{ mm}$ ) at a friction ratio of 1: 1.19 according to ASTM D 3182 standards with careful control of temperature, nip gap, mixing time and uniform cutting operation. The curing characteristics of the compounds were determined by Monsanto Rheometer (R-100) according to ASTM D 2084 and ASTM D 5289 procedures. After mixing, moulding was done in an electrically heated hydraulic press having ( $300\text{ mm}\times 300\text{ mm}$ ) platens at  $150^\circ\text{C}$  at a pressure of 4.0 MPa. Vulcanization was done to optimum cure (90% of the maximum cure) using different molding conditions determined from torque data obtained from Monsanto Rheometer. The test specimens were punched out from test sheets.

### 3. Characterization and testing

#### 3.1. Physical test method

Curing characteristics of the compounded stocks were determined by using an oscillating disc Rheometer with an arc of oscillation of 3°. Tensile strength, modulus at 100% (M100), 200% (M200), and 300% (M300) extension and elongation at break were determined according to ASTM D-412 using dumbbell specimen in a Hounsfield 1145 universal testing machine. Tear strength was also determined by using Hounsfield 1145 according to ASTM method D-624 using a die C specimen. Measurement of hysteresis is also carried out in the same machine. The hardness of the vulcanizates was measured using a Shore-A durometer as per ASTM D 676-59T. Molded sheets were heat aged at 100°C for 72 hours in an electrically heated air oven for ageing study. Compression set was carried out by compressing the specimen to 25% of its original thickness for 22 hours at 70°C according to ASTM D395-85. Abrasion loss in cubic centimeter per hour [cm<sup>3</sup>/h] was measured by Dupont abrader according to BS-903.

#### 3.2. Chemical test methods

The resistance to solvent was obtained by swelling test. The volume fraction of rubber ( $V_r$ ) in the vulcanizate was determined by equilibrium swelling in toluene, using the method reported by Ellis and Welding [15]. The relationship used for calculating  $V_r$  is represented by Equation (1):

$$V_r = \frac{(D-FT)\rho_r^{-1}}{(D-FT)\rho_r^{-1} + A_0\rho_s^{-1}} \quad (1)$$

where  $T$  is the weight of the test specimen,  $F$  is the weight fraction of the insoluble components in the sample,  $D$  is the de-swollen weight of the test specimen,  $A_0$  is the weight of absorbed solvent, corrected for swelling increment,  $\rho_r$  is the density of the rubber. The number of effective network chains per unit volume of rubber is denoted as  $\nu$  which was calculated using Flory-Rehner equation (Equation (2)) [16, 17]:

$$\nu = \frac{-1}{V_s} \cdot \frac{\ln(1-V_r) + V_r + \mu V_r^2}{V_r^{1/3} - \frac{V_r}{2}} \quad (2)$$

where  $\nu$  is the number of effective network chains per unit volume of rubber,  $V_s$  is the molar volume of the solvent and  $\mu$  is the polymer-solvent interaction parameter (Flory-Huggins's interaction parameter), which was found to be 0.401 [18].

#### 3.3. Bound rubber measurement

The contents of bound rubber (BdR) were determined by extracting the unbound materials such as the ingredients and free rubber with three different solvents for seven days followed by drying for two days at room temperature. The weights of the samples before and after extraction were measured, and the BdR contents were calculated using the Equation (3):

$$\text{BdR}[\%] = 100 \cdot \frac{w_{fg} - w_i \left( \frac{m_f}{m_f + m_r} \right)}{w_i \left( \frac{m_r}{m_f + m_r} \right)} \quad (3)$$

where BdR is the bound rubber content;  $w_{fg}$  the weight of filler and gel,  $w_i$  the weight of the sample,  $m_f$  the weight fraction of the filler in the compound and  $m_r$  the weight fraction of the rubber in the compound.

#### 3.4. Dielectric relaxation spectra

The dielectric and electrical properties of the conductive black reinforced CSM vulcanizates were obtained using a computer-controlled impedance analyzer (PSM 1735) on application of an alternating electric field across the sample cell with a blocking electrode (aluminum foil) in the frequency range of 10<sup>2</sup>–10<sup>6</sup> Hz at room temperatures. The test cell comprises of two electrodes and a voltage of 30 mV ( $V_{rms}$ ) was applied across the cell. The parameters like dielectric permittivity ( $\epsilon'$ ) and dielectric loss tangent ( $\tan\delta$ ) were obtained as a function of frequency. The ac conductivity ( $\sigma_{ac}$ ) was calculated from the dielectric data using the relation given in Equation (4):

$$\sigma_{ac} = \omega\epsilon_0\epsilon'\tan\delta \quad (4)$$

where  $\omega$  is equal to  $2\pi f$  ( $f$  is the frequency) and  $\epsilon_0$  is vacuum permittivity and  $\epsilon'$  dielectric permittivity which is determined according to Equation (5):

$$\epsilon' = \frac{C_p}{C_0} \quad (5)$$

where  $C_p$  is the observed capacitance of the sample (in parallel mode) and  $C_0$  is the capacitance of the cell. The value of  $C_0$  is calculated using the expression  $(\epsilon_0 A)/d$ , where  $A$  and  $d$  are the area and thickness of the sample respectively.

## 4. Results and discussion

### 4.1. Rheometric characteristics

The Rheometric characteristics of the unfilled and conductive carbon black filled CSM vulcanizates are given in Table 2. The respective Monsanto rheographs are shown in Figure 1. From the table it is observed that with increase in filler loading both minimum and maximum torque increases. This may be due to increase in crosslink density with increase in filler loading [19]. With incorporation of filler cure rate (slope of cure curve) gradually increases and scorch safety (time to scorch) decreases [20, 21]. The optimum cure time decreases with increase in filler loading.

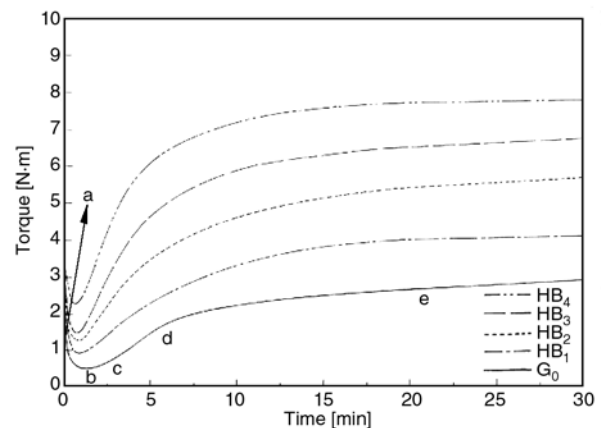


**Figure 1.** Representative rheographs of unfilled and Ensaco 350G filled CSM vulcanizates: effect of filler loading. a – initial viscosity, b – minimum torque, c – scorch time, d – cure rate (slope of cure curve), e – maximum torque

### 4.2. Physico-mechanical properties

The Physico-Mechanical properties of CSM vulcanizates reinforced with conductive carbon black (Ensaco 350G) at different filler loading have been determined. From Table 3 it can be observed that tensile strength, tear strength and modulus increases up to 30 phr filler loading beyond which tensile strength and tear strength decreases but modulus increases. Since modulus is a function of crosslink density it increases with increase in num-

**Table 2.** Rheometric characteristics of unfilled and Ensaco 350G filled CSM vulcanizates

Mix designation	Initial viscosity [N·m]	Minimum torque [N·m]	Maximum torque [N·m]	Scorch time [min]	Cure rate [min <sup>-1</sup> ]	Optimum cure time [min]
G <sub>0</sub>	1.9	0.525	2.9	3.0	6.89	17.5
HB <sub>1</sub>	2.3	0.85	4.1	2.50	7.40	16.0
HB <sub>2</sub>	2.9	1.3	5.7	1.75	8.16	14.0
HB <sub>3</sub>	3.2	1.5	6.7	1.5	9.09	12.5
HB <sub>4</sub>	4.1	2.2	7.8	1.25	11.40	10.0

**Table 3.** Physico mechanical properties of unfilled and Ensaco 350G filled CSM vulcanizates

Properties	G <sub>0</sub>		HB <sub>1</sub>		HB <sub>2</sub>		HB <sub>3</sub>		HB <sub>4</sub>	
	Before ageing	After ageing	Before ageing	After ageing	Before ageing	After ageing	Before ageing	After ageing	Before ageing	After ageing
Tensile strength [MPa]	27.3	28.6	29.3	31.0	31.4	32.0	33.5	34.0	32.3	32.4
M100% [MPa]	1.7	1.9	3.4	3.6	6.9	7.1	11.4	11.8	15.6	15.7
M200% [MPa]	2.3	2.7	8.1	8.3	16.9	17.0	25.6	25.7	–	–
M300% [MPa]	3.3	3.7	14.1	14.2	22.1	22.1	–	–	–	–
Elongation at break [%]	874.0	770.0	570.0	545.0	390.0	365.1	268.0	250.6	190.2	182.8
Tear strength [N/mm]	28.0	29.1	57.3	58.2	64.0	64.8	67.0	67.8	54.2	54.6
Hardness IRHD	50	51	58	61	67	69	70	72	82	85
Compression set 22 hrs at 100°C [%]	6.8	5.6	5.0	3.9	3.4	3.3	3.0	3.0	1.6	1.5
Abrasion loss [cc/hr]	0.37	0.33	0.25	0.24	0.15	0.14	0.10	0.09	0.13	0.12
Crosslink density ( $\nu \cdot 10^3$ ) [mol/cc]	2.0	2.3	3.0	3.2	3.8	3.9	4.2	4.2	4.8	4.8

ber of crosslinks. Increase in moduli is due to stronger carbon black-rubber rigid interactions which are confirmed by bound rubber measurement. At 30 phr filler loading CSM gives the highest value of tensile strength, which means that at this loading polymer-filler interaction is maximum whereas at higher filler loading filler-filler interaction predominates. Unlike conventional carbon black conductive carbon black possess high structure and very high surface area and this complex structure of the branched filler aggregates attributes to a strong surface polymer interaction leading to higher bound rubber content. Incorporation of fillers is a major source of energy dissipation there by increasing the tensile strength of carbon black vulcanizates. On addition of filler like conductive carbon black to the vulcanizates, free space between the chains is filled up thus depriving the chains to straighten thereby reducing elongation. The higher the filler loading the more is the reinforcement and the more crosslinks are formed during vulcanization, thereby trapping the free ends of polymer chains. As the degree of crosslinking increases, the hardness progressively increases. The more compact the networks, the shorter are the molecular segments between the crosslinks and hence the tighter is the network, which causes increase in hardness [22]. Very high value of hardness is due to highly reinforcing conductive black having very high surface area. Compression set property is also a function of crosslink density, which increases with increase in crosslink density. Very good abrasion resistance may be due to chemically bound flexible chains with the carbon black, which provide a coupling action between carbon black surface and rubber molecules thus retarding the polymer to be abraded out from the surface. With increase in filler loading the bound rubber value increases which decreases the abrasion loss gradually. Above 30 phr filler loading decrease in tensile strength and tear strength is observed which may be due to agglomeration of filler particles at the highest filler loading. At lower filler loading cross-linking density decreases which may also cause increase in elongation at break whereas at higher filler loading cross linking density and viscosity both increases which causes decrease in elongation at break. Like tensile strength, tear strength also increases up to 30 phr but at 40 phr it decreases. This may be due to increase in crosslink-

**Table 4.** Hysteresis loss in  $J/m^2$  of unfilled and Ensaco 350G filled CSM vulcanizates at 100% elongation

Mix designation	1 <sup>st</sup> cycle	2 <sup>nd</sup> cycle
G <sub>0</sub>	0.107	0.049
HB <sub>1</sub>	0.152	0.061
HB <sub>2</sub>	0.390	0.146
HB <sub>3</sub>	0.645	0.226
HB <sub>4</sub>	1.610	0.606

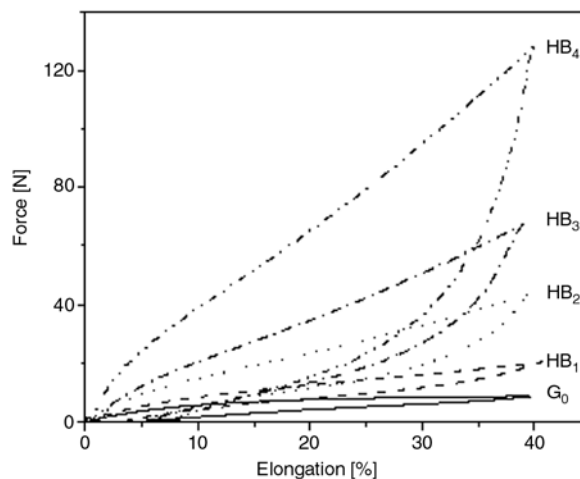


**Figure 2.** Hysteresis loss plots of unfilled and Ensaco 350G filled CSM vulcanizates

ing density at higher filler loading. It may be concluded that around 30 phr of Ensaco 350G is optimum filler loading for hypalon 40. The hysteresis loss values of different vulcanization at 100% elongation are given in Table 4. Figure 2 shows the plot of hysteresis loss of unfilled and filled vulcanizates. The result exhibits that the incorporation of Ensaco 350G filler causes an increase in the hysteresis loss. The low hysteresis loss of gum vulcanizates can be attributed to low energy absorption characteristics of the rubber matrix, which can act as an elastic body and is incapable of dissipating energy. The stress relaxation behavior of CSM vulcanizates is determined by stretching the samples at constant strain level of 100%. Figure 3 shows the decay of stress with time of unfilled and Ensaco 350G filled vulcanizates. The nature of decay is almost same for gum and filled vulcanizates. The stress relaxation phenomenon in the unfilled vulcanizate may be associated with a number of elementary processes like rearrangement of broken chains, crosslinks and entanglements. Unlike gum vulcanizate, in filled vulcanizates the rate of relaxation increases due to breaking-up of carbon black structure and distorted broken carbon elastomer linkage

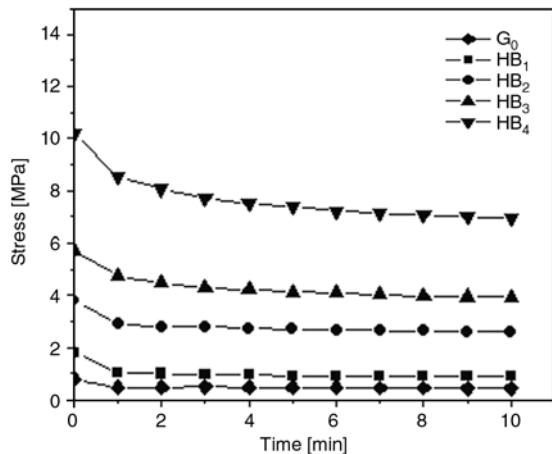


**Figure 3.** Stress relaxation behavior of unfilled and Ensaco 350G filled CSM vulcanizates

[23]. CSM rubber having no unsaturation sites possesses excellent resistance to heat, weather, ozone and chemicals. Enhancement of tensile strength after ageing in all cases may be due to post vulcanization. It can be clearly observed that crosslink density gradually increases on ageing for 72 hrs. Since CSM rubber has no reactive sites prone to oxygen attack it shows very good resistance to heat ageing. It has been observed that as the cure progresses tensile strength, hardness increases while compression set, elongation at break decrease. The significant increase in tear strength after ageing for 72 hrs is expected to be related to the formation of excessive cross-linked structure, which may be due to post curing effect. Increase in hardness value after aging may be due to increase in crosslink density, which agreed well with the increase in 100, 200, and 300% modulus after thermo-oxidative ageing process. Compared to gum vulcanizate in filled vulcanizates the increase in tensile strength after ageing is not so much pronounced which may be due to increase in inelastic nature of the rubber matrix. In case of higher filler loading the tensile strength after ageing remains almost same.

#### 4.3. Bound rubber

Bound rubber can be defined as the rubber portion of uncured compound, which cannot be extracted by a good solvent due to adsorption of rubber molecules on to the filler surface. Bound rubber measurement plays an important role in determination of surface activity of the filler and the degree of reinforcement. It is widely accepted that the formation

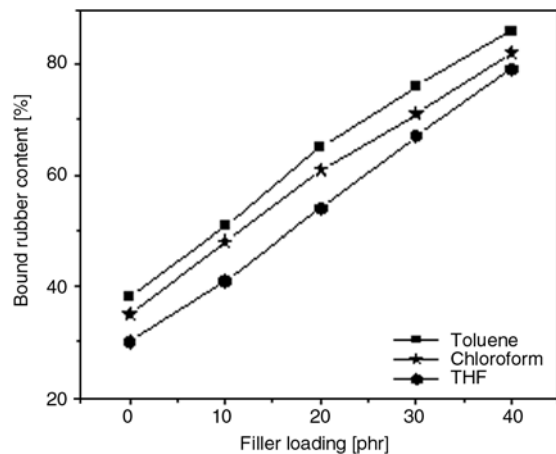


**Figure 4.** The variation of the bound rubber content for different solvents as a function of filler loading in CSM vulcanizates

of bound rubber in a compound involves physical adsorption, chemisorption and mechanical interaction of which chemisorption is considered as the crucial one. The adsorption of polymer molecules onto the filler surface leads to two phenomena, which are: the formation of bound rubber and a rubber shell on the filler surface. Many studies have been carried out on the mechanisms and factors affecting the formation of bound rubber [24–30]. The physico-chemical characteristics of the filler surface and filler morphology has a profound effect on the bound rubber content in a compound. The variation of bound rubber content with filler loading has been studied with three different solvents like toluene, tetrahydrofuran (THF), and chloroform. Figure 4 shows the variation of the bound rubber content with the filler loading for CSM vulcanizates. Irrespective of the nature of solvent bound rubber content increased with filler loading which may be due to increase in degree of reinforcement. The high percentage of BdR content is attributed to high surface area, high structure and high concentration of oxygen containing surface functional groups. With increase in the structure of conductive carbon black the breakdown of the aggregates during mixing is greater which results in an increase in filler-polymer interface. High bound rubber values in sulfur added compounds have been reported earlier by Gessler [31]. During mixing of rubber and carbon black, free radicals are generated which results in instantaneous interactions between carbon black and the rubber chain end. Gessler explained the phenomenon of forma-

tion of bound rubber as a two step theory: the reaction of sulfur with black and the reaction of this sulfur modified black with the polymer. The functional groups on carbon black surface react with sulfur and cure accelerators as a result  $\equiv\text{CS}\cdot$ radicals or  $\equiv\text{CX}$  (X is SH or residues of a cure accelerator) are formed [32]. The surface activity, which can be related to different chemical groups on the black surface such as carboxyl, quinonic, phenol, and lactonic groups, dominates polymer-filler interactions, filler aggregate interactions, as well as filler-ingredient interactions. The surface of conductive carbon black (Ensaco 350G) has a number of hydroxyl groups, which results in strong filler-filler interactions. High bound rubber content in case of CSM vulcanizates does not necessarily mean a large amount of polymer-filler interaction. The strong polar groups present in filler surface may lead to both polymer-filler interaction as well as filler-filler interaction.

#### 4.4. Effect of solvents

The nature of the extracting solvent is important in bound rubber formation. For bound rubber measurement the uncured rubber compound is exposed to a solvent capable of totally extracting the polymer in the absence of any polymer-filler bonding. These solvents for polymers may or may not interact with conductive carbon black. The solvents, which are poorly interacting with conductive carbon black, cannot disrupt the filler network to release the trapped polymer chain [33]. In regard to interaction with black, tetrahydrofuran (THF) is found to be the best solvent, followed by chloroform and toluene. Bound rubber content decreases with increasing solvation of carbon black. Solvents with more interaction with the polymer tend to show lower bound rubber value.

#### 4.5. Dielectric relaxation spectra

One of the most valuable tools for characterizing the relaxation behavior of polymer composites is dielectric relaxation spectroscopy (DRS). Dielectric spectroscopy is a useful complement to the most customary mechanical methods of probing the viscoelastic properties of polymers. Though there have been many studies on the dielectric relaxation behavior of conductive black reinforced rubber vul-

canizates [34] but it has never been reported in CSM rubber vulcanizates. Dielectric spectroscopy offers advantages to study the high frequency dynamics of polymers. Dielectric spectra reflect the same chain motions as the mechanical modulus; however it has reduced interference due to symmetry from shorter time process making it more accurate than the traditional dynamic mechanical analysis [35]. The ‘electric modulus’ formalism first introduced by McCrum *et al.* [36] and extensively used for the investigation of relaxation phenomena in polymer composites by Tsangaris *et al.* [37, 38] can be defined as the inverse quantity of complex permittivity and is given by the following expression (Equation (6)):

$$M^* = \frac{1}{\epsilon^*} = \frac{\epsilon'}{\epsilon'^2 + \epsilon''^2} + j \frac{\epsilon''}{\epsilon'^2 + \epsilon''^2} = M' + jM'' \quad (6)$$

where  $M^*$  is the complex electric modulus,  $M'$  is the real and  $M''$  is the imaginary part of electric modulus,  $\epsilon'$  and  $\epsilon''$  are the real and imaginary parts of permittivity.

$M^*$  characterizes the dynamic aspects of the charge motion in conductors in terms of relaxation in an electric field [39]. Figure 5 shows the variation of the real part of the electric modulus as a function of frequency in conductive carbon black loaded CSM vulcanizates. From the figure it can be observed that irrespective of the amount of filler in the composite, the value of  $M'$  is nearly zero at low frequencies indicating that the electrode polarization gives a negligibly low contribution to  $M'$  and can be ignored [40]. After this initial low value,  $M'$  increases steeply in the range of  $10^3$ – $10^5$  Hz for all

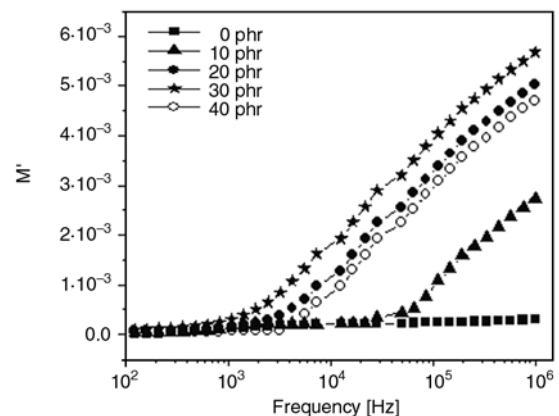


**Figure 5.** The variation of the real part of the electric modulus ( $M'$ ) as a function of frequency in CSM vulcanizates at increasing filler loadings

filler loadings. From the figure it can be observed that with increasing filler loadings there is an increase in modulus values up to 30 phr beyond which it decreases. This may be due to agglomeration of filler particles in the polymer matrix. The increase in real part of the electric modulus with filler loading can be explained on the basis of the viscoelastic properties of cross linked multiphase polymeric materials, which depend upon molecular relaxation processes and the morphology of the composites. Although these relaxations can usually be associated with each component, their appearance depends upon the chemical and physical interactions between the phases (filler and polymer matrix). Conductive carbon black like Ensaco 350G shows high interaction with the polymer matrix, because of their high surface activity, thereby leading to the formation of a weak interphase compared to other carbon blacks. The thickness of the interphase is inversely proportional to the interfacial tension between the polymeric phases. The interphase formed between the filler and the polymer matrix has distinct properties that differ from the bulk. A polymer layer having higher stiffness than the bulk polymer in the vicinity of the dispersed phase surface is created from restricted molecular mobility that is attributable to interactions between phases.

Figure 6 shows the variation of the imaginary parts of the modulus as a function of frequency at increasing filler loadings. It can be observed that with increase in filler loading,  $M''$  peaks in general exhibit increasing peak heights and peak maximum shifts to higher frequencies. It can be explained on

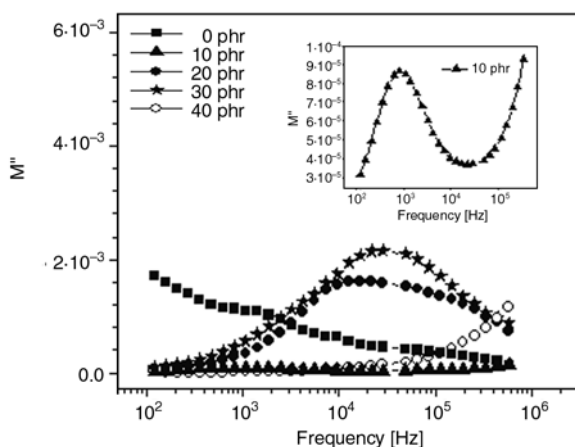


**Figure 6.** The variation of the imaginary part of the electric modulus ( $M''$ ) as a function of frequency in CSM vulcanizates

the basis of Maxwell-Wagner-Sillars polarization. The broad nature of the  $M''$  peaks can be interpreted as being the consequence of distributions of relaxation time. At low filler loadings, the value of  $M''$  reaches a peak in the range of 1000 Hz for 10 phr and around 10 000 Hz in case of 20 phr and 30 phr filler loaded samples. Further increase in filler loading shifts the peak value towards higher frequency region and could not be found due to instrumental limitations.

The Cole-Cole plots plotted as  $M''$  vs.  $M'$  (imaginary part of electric modulus vs real part of electric modulus) for all filler loadings are shown in Figure 7. The advantage of  $M''$  vs.  $M'$  is that it offers better resolution than  $\epsilon''$  vs.  $\epsilon'$  plots (imaginary part of electric permittivity vs. real part of electric permittivity). From the Figure 7 it can be clearly observed that with increasing filler loadings the semicircle nature of the peak is reducing and at higher filler loadings the semi-circle become more skewed which can be explained on the basis of interfacial polarization. The filler particles are electrically charged by fixed or adsorbed ions or polar molecules and are surrounded by small counter-charges (probably of the polymer matrix), forming an electrical double layer. The resulting medium frequency relaxation is caused primarily by interfacial polarization due to the build-up of charges on boundaries and interfaces between materials with very different electrical properties [41]. Imposition of an external AC field causes polarization of large colloidal particles and creates perturbation in a miniature double layer on each particle, which then behaves like a macro-ion [42]. Under the influence

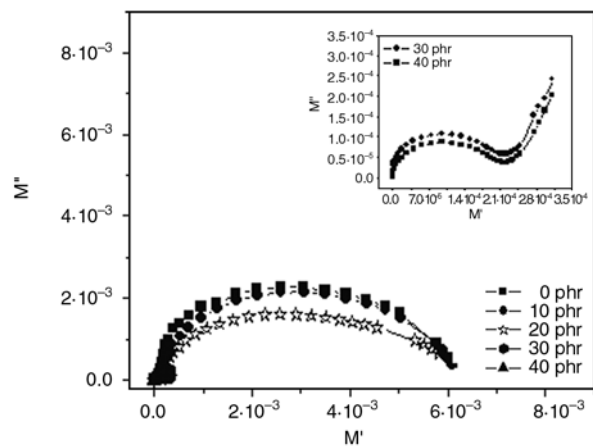


**Figure 7.** Cole-Cole plots of CSM vulcanizates reinforced with Ensaco 350G conductive carbon black

of an external electric field, the counter-ions become redistributed along the surface of a filler particle, and the double layer becomes deformed and polarized, leading to interfacial polarization and the resulting relaxation or dispersion.

### Percolation

Many studies have been done on the percolation phenomenon in carbon black reinforced polymer composites. But no research work related to percolation phenomenon in CSM vulcanizates has been reported so far. Figure 8 shows the effect of filler loading on the conductivity of Ensaco 350G reinforced vulcanizates at  $10^6$  Hz. At low levels of filler loading the conductivity of the composite is slightly higher than that of the base polymer as the filler particles are isolated from each other by the insulating polymer matrix. As the filler loading is increased, mutual contacts between the filler particles are developed and at a critical loading of the filler a sharp increase in conductivity is observed, indicating the ‘percolation limit’. Depending upon the type of filler, the occurrence of percolation varies. In Ensaco 350G reinforced CSM vulcanizates the percolation region is occurring at 30 phr loading of the filler. According to Medalia [43] percolation is due to the tunneling of electrons and the conductivity is controlled by the gaps between the carbon black aggregates. Many questions regarding the actual mechanism of conduction through such heterogeneous materials are still prevalent. Interpretation of dielectric and conductivity performance of such materials has been analyzed through percolation theory [44]. According to Das *et al.*

[45] the variation of conductivity with filler loading can be divided into three regions (Figure 8). In region I the ‘inductive region’, a small increase in conductivity of the composite with increasing filler loading can be attributed to the transportation of the small number of charged particles through the system without having any continuous conductive path. Region II is referred as ‘percolation region’ where conductivity increases sharply due to a continuous conductive path developed in the polymer matrix. In region III, further addition of filler has marginal effect on conductivity. Carbon blacks are widely used as reinforcing agent in elastomers because of their high surface to mass ratio, molecular-scale forces, and their interactions with the polymer matrix. Due to van der Waals forces, flocculation of carbon black particulates in the polymer matrix occurs which results in the formation of secondary structures whereas electrostatic charges or steric effects lead to a stabilization of the dispersion. The percolation phenomenon may be of lattice percolation or continuum percolation. This involves two processes: randomly adding or removing particles from a simple lattice space till an infinite cluster is not formed. It has been recognized that the conductivity of polymer composites not only depends on the geometry of filler particles but also on the processing of the materials [46]. Due to high surface activity of conductive black (Ensaco 350G) and high surface area, agglomeration of the filler particles occurs in the polymer matrix, which results in the formation of clusters.

### 5. Conclusions

Irrespective of the solvent the bound rubber contents increase with increase in the carbon black content. Very high value of bound rubber is due to high reinforcement obtained due to high structure and high surface area of conductive black. Both maximum and minimum Rheometric torque increase with increase in filler loading which may be due to increase in viscosity. Cure rate and scorch rate increase with increase in filler loading. Tensile strength and tear strength increase with filler loading up to 30 phr beyond which it decreases whereas modulus increases at high filler loading. Elongation at break gradually decreases with filler loading. With filler loading hardness also gradually increases which may be due to increase in crosslink

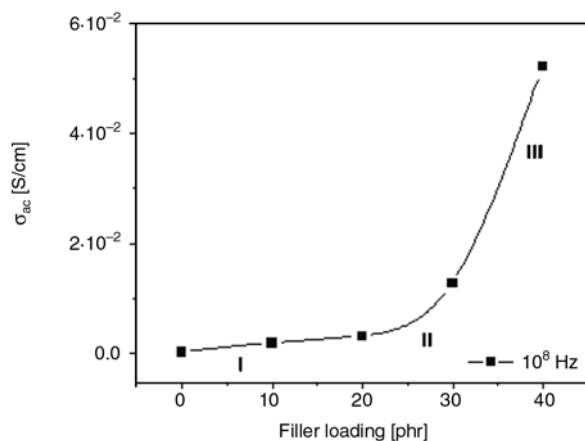


**Figure 8.** Variation in ac conductivity ( $\sigma_{ac}$ ) with filler loading in CSM vulcanizates

density. Compression set property gradually increases with filler loading whereas abrasion loss shows gradual decrease which may be due to increase in stiffening property. The hysteresis loss increases with increase in the filler loading, which may be due to the inelastic behaviour of the rubber matrix. The stress relaxation behavior shown by gum vulcanizates follows nearly the same trend as filled vulcanizates. Increase in tensile strength, hardness, tears strength and decrease in elongation at break, compression set is observed after ageing which may be due to post curing effect. It is concluded that 30 phr Ensaco 350G can be taken as an optimum filler loading, which exhibits better physical and mechanical properties. The dielectric relaxation spectra of the composites showed an additional relaxation in the frequency range of  $10^3$  to  $10^5$  Hz. This has been explained on the concept of formation of interphase layer between the filler and the polymer matrix. From the conductivity studies percolation limit of the conductive carbon black (Ensaco 350G) in the polymer matrix has been found to be 30 phr, which is in good agreement with the physico-mechanical results.

### Acknowledgements

The authors are thankful to Mr. Umesh N. Vyas of Piyu Corporation, Mumbai for providing Ensaco 350G.

### References

- [1] Smith D. A.: Thermal stability of chlorosulfonated polyethylene. *Polymer Letters*, **2**, 665–670 (1964).
- [2] Nersasian A., King K. F., Johnson P. R.: Novel curing systems for chlorosulfonated polyethylene. *Journal of Applied Polymer Science*, **8**, 337–354 (1964).
- [3] Maynard J. T., Johnson P. R.: Ionic crosslinking of chlorosulfonated polyethylenes. *Journal of Applied Polymer Science*, **7**, 1943–1950 (1963).
- [4] Mukhopadhyay S., De S. K.: Miscibility of self-vulcanizable rubber blend based on epoxidized natural rubber and chlorosulphonated polyethylene: Effect of blend composition, epoxy content of epoxidized natural rubber and reinforcing black filler. *Polymer*, **32**, 1223–1229 (1991).
- [5] Jana P. B., De S. K.: Short carbon fiber filled polychloroprene. *Plastics Rubber and Composites Processing and Applications*, **17**, 43–49 (1992).
- [6] Sau K. P., Chaki T. K., Khastgir D.: Electrical and mechanical properties of conducting carbon black filled composites based on rubber and rubber blends. *Journal of Applied Polymer Science*, **71**, 887–895 (1999).
- [7] Pramanik P. K., Khastgir D., Saha T. N.: Electromagnetic interference shielding by conductive nitrile rubber composites containing carbon fillers. *Journal of Elastomers and Plastics*, **23**, 345–361 (1991).
- [8] Micusik M., Omastova M., Prokes J., Krupa I.: Mechanical and electrical properties of composites based on thermoplastic matrices and conductive cellulose fibers. *Journal of Applied Polymer Science*, **101**, 133–142 (2006).
- [9] Patsidis A., Psarras G. C.: Dielectric behaviour and functionality of polymer matrix-ceramic BaTiO<sub>3</sub> composites. *Express Polymer Letters*, **2**, 718–726 (2008).
- [10] Kontos G. A., Soulintzis A. L., Karahaliou P. K., Psarras G. C., Georga S. N., Krontiras C. A., Pisanias M. N.: Electrical relaxation dynamics in TiO<sub>2</sub>-polymer matrix composites. *Express Polymer Letters*, **1**, 781–789 (2007).
- [11] Roychoudhury A., De P. P.: Elastomer-carbon block interaction: Influence of elastomer chemical structure and carbon black surface chemistry on bound rubber formation. *Journal of Applied Polymer Science*, **55**, 9–15 (1995).
- [12] Roychoudhury A., De S. K., De P. P., Ayala J. A., Joyce G. A.: Chemical interaction between carbon black and elastomer: Crosslinking of chlorosulfonated polyethylene by carbon black. *Rubber Chemistry and Technology*, **67**, 662–671 (1994).
- [13] Cotton G. R.: The effect of carbon black surface properties and structure on rheometer cure behavior. *Rubber Chemistry and Technology*, **45**, 129–144 (1972).
- [14] Chen C. H., Koenig J. L., Shelton J. R., Collins E. A.: The influence of carbon black on the reversion process in sulfur-accelerated vulcanization of natural rubber. *Rubber Chemistry and Technology*, **55**, 103–115 (1982).
- [15] Ellis B., Welding G. N.: Estimation, from swelling, of the structural contribution of chemical reactions to the vulcanization of natural rubber Part I. General method. *Rubber Chemistry and Technology*, **37**, 563–570 (1964).
- [16] Flory P. J.: *Principles of polymer chemistry*. Cornell University Press, Ithaca, USA (1953).
- [17] Flory P. J., Rehner J.: Statistical mechanics of cross-linked polymer networks II. Swelling. *Journal of Chemical Physics*, **11**, 521–526 (1943).
- [18] Braton A. F. M.: *Handbook of solubility parameters and other cohesion parameters*. CRC Press, Boca Raton, USA. (1983).
- [19] Basfar A. A., Abdel-Aziz M. M., Mofti S.: Influence of different curing systems on the physico-mechanical properties and stability of SBR and NR rubbers. *Radiation Physics and Chemistry*, **63**, 81–87 (2002).
- [20] Devlin E. F.: The effect of cure variables on cis/trans isomerization in carbon-black-reinforced cis-1, 4-polybutadiene. *Rubber Chemistry and Technology*, **59**, 666–692 (1986).

- [21] Roychoudhury A., De P. P., Dutta N. K., Choudhury N., Roychoudhury N., Haidar B., Vidal A.: FTIR and NMR studies on crosslinking reaction between chlorosulfonated polyethylene and epoxidized natural rubber. *Rubber Chemistry and Technology*, **66**, 230–241 (1993).
- [22] Chakraborty S. K., Bhowmick A. K., De S. K.: Mixed cross-link systems in elastomers. *Polymer Reviews*, **21**, 313–332 (1981).
- [23] Dutta N. K., Tripathy D. K.: Effect of plasticizer concentration on the hysteresis, tear strength and stress-relaxation characteristics of black-loaded rubber vulcanizate. *Colloid and Polymer Science*, **269**, 331–342 (1991).
- [24] Wolff S., Wang M-J.: Carbon black reinforcement of elastomers. in 'Carbon Black: Science and Technology' (eds.: Donnet J. B., Bansal R. C., Wang M. J.) Marcel Dekker, New York, USA, 289–345 (1993).
- [25] Kraus G.: Reinforcement of elastomers. Wiley Interscience, New York (1965).
- [26] Stickney P. B., Falb R. D.: Carbon black-rubber interactions and bound rubber. *Rubber Chemistry and Technology*, **37**, 1299–1340 (1964).
- [27] Sircar A. K., Voet A.: Immobilization of elastomers at the carbon black particle surface. *Rubber Chemistry and Technology*, **43**, 973–980 (1970).
- [28] Wolff S., Wang M. J., Tan E. H.: Filler-elastomer interactions. Part VII. Study on bound rubber. *Rubber Chemistry and Technology*, **66**, 163–177 (1993).
- [29] Kraus G.: Reinforcement of elastomers by carbon black. in 'Advances in Polymer Science' (eds.: Bunde A., Havlin S.) Springer Berlin, Heidelberg, Vol 8, 155–237 (1971).
- [30] Donnet J. B., Rigaut M., Frustenberger R.: Study by electronic paramagnetic carbon black resonance treats by the azodiisobutyronitrile in absence of oxygen. *Carbon*, **11**, 153–162 (1973).
- [31] Gessler A. M.: Evidence for chemical interaction in carbon and polymer associations: Extension of original work on effect of carbon black structure. *Rubber Chemistry and Technology*, **42**, 858–873 (1969).
- [32] Sridhar V., Gupta B. R., Tripathy D. K.: Bound rubber in chlorobutyl compounds: Influence of filler type and storage time. *Journal of Applied Polymer Science*, **102**, 715–720 (2006).
- [33] Roychoudhury A., De P. P., Roychoudhury N., Vidal A.: Chemical interaction between chlorosulfonated polyethylene and silica -Effect of surface modifications of silica. *Rubber Chemistry and Technology*, **68**, 815–823 (1995).
- [34] Mahapatra S. P., Sridhar V., Chaudhary R. N. P., Tripathy D. K.: AC conductivity and positive temperature coefficient effect in microcellular EPDM vulcanizates. *Polymer Composites*, **29**, 1125–1136 (2008).
- [35] Roland C. M., Bero C. M.: Normal mode relaxation in linear and branched polyisoprene. *Macromolecules*, **29**, 7521–7526 (1996).
- [36] McCrum N. G., Read B. E., Williams G.: Anelastic and dielectric effects in polymeric solids. Wiley Interscience, London (1967).
- [37] Tsangaris G. M., Psarras G. C., Kouloumbi N.: Electric modulus and interfacial polarization in composite polymeric systems. *Journal of Materials Science*, **33**, 2027–2037 (1998).
- [38] Psarras G. C., Manolakaki E., Tsangaris G. M.: Electrical relaxations in polymeric particulate composites of epoxy resin and metal particles. *Composites Part A: Applied Science and Manufacturing*, **33**, 375–384 (2002).
- [39] Han M. G., Im S. S.: Dielectric spectroscopy of conductive polyaniline salt films. *Journal of Applied Polymer Science*, **82**, 2760–2769 (2001).
- [40] Lee H-T., Chuang K-R., Chen S-A., Wei P-K., Hsu J-H., Fann W.: Conductivity relaxation of 1-methyl-2-pyrrolidone-plasticized polyaniline film. *Macromolecules*, **28**, 7645–7652 (1995).
- [41] Schwarz G.: Dielectric relaxation of biopolymers in solution. *Advanced Molecular Relaxation Processes*, **3**, 281–295 (1972).
- [42] Grimnes S., Martinsen O. G.: Bioimpedance and bioelectricity basics. Academic Press, New York (2000).
- [43] Medalia A. I.: Electrical conduction in carbon black composites. *Rubber Chemistry and Technology*, **59**, 432–454 (1986).
- [44] Lux F.: Models proposed to explain the electrical conductivity of mixtures made of conductive and insulating materials. *Journal of Materials Science*, **28**, 285–301 (1993).
- [45] Das N. C., Chaki T. K., Khastgir D., Chakraborty A.: Electrical and mechanical properties of conductive carbon black filled EVA, EPDM and their blends. *Kautschuk, Gummi, Kunststoffe*, **55**, 300–306 (2002).
- [46] Halperin B. I., Feng S., Sen P. N.: Differences between lattice and continuum percolation transport exponents. *Physical Review Letters*, **54**, 2391–2394 (1985).

# Electromechanical responses of poly(3-thiopheneacetic acid)/acrylonitrile-butadiene rubbers

P. Thipdech, R. Kunanuruksapong, A. Sirivat\*

Conductive and Electroactive Polymer Research Unit The Petroleum and Petrochemical College,  
Chulalongkorn University, Bangkok, 10330, Thailand

Received 19 September 2008; accepted in revised form 11 November 2008

**Abstract.** Acrylonitrile-butadiene rubber (NBR) and blends of poly(3-thiopheneacetic acid)/ acrylonitrile-butadiene rubber, P3TAA/NBR, were fabricated, and the electrorheological properties, dielectric, and electrical conductivities were investigated. The electrorheological properties were determined under an oscillatory shear mode in a frequency range of 0.1 to 100 rad/s at various electric field strengths, from 0 to 2 kV/mm, at a fixed 27°C to observe the effects of acrylonitrile content (ACN) in the rubber systems and the conductive particle concentration in the blends. For the pure rubber systems, the storage modulus response ( $\Delta G'$ ) is linearly dependent on its dielectric constant ( $\epsilon'$ ), and increases with the ACN content. For the NBR/P3TAA blends, the storage modulus response varies nonlinearly with the dielectric constant. The bending responses of the rubbers and the blends were investigated in a vertical cantilever fixture. For the pure rubber system, the bending angle and the dielectrophoresis force vary linearly with electric field strength. For the blend system, the bending angle and the dielectrophoresis force vary nonlinearly with electric field strength.

**Keywords:** smart polymers, electrorheological properties, dielectric properties, acrylonitrile-butadiene rubber, poly(3-thiopheneacetic acid)

## 1. Introduction

Various materials have been used as artificial muscles: pneumatic actuators, shape memory alloys (SMAs), and electroactive ceramics. However, these materials have several disadvantages. A most recent approach to address these problems is electroactive polymers (EAPs), having attractive characteristics in their ability to emulate the operation of biological muscles with high fracture toughness, large actuation strains, and inherent vibration damping [1]. Dielectric elastomers belong to a type of EAPs capable of producing large strains and quick electromechanical responses, essential properties required in advanced electromechanical and dielectric applications [1, 2]. The principle operation of a dielectric elastomer can be described by the electrostatic model of actuation as put forth by

Pelrine *et al.* [2]. The response of the elastomer is directly proportional to the square of the applied electric field and linearly proportional to the dielectric constant.

Acrylonitrile-butadiene rubber (NBR) is one type of elastomer possessing excellent resistance to petroleum products. With increasing the amount of ACN content, the dielectric properties are expected to change; the molecules become more polar along with an increase in electrical permittivity. Moreover, NBR has been known to possess relatively good miscibility with several conductive polymers [3]. One of these conductive polymers is polythiophene. A substituted poly(thiophene) at 3- and/or 4-position of the thiophene ring not only confers processability to poly(thiophene)s but it can also be used to modify their properties [4].

\*Corresponding author, e-mail: [anuvat.s@chula.ac.th](mailto:anuvat.s@chula.ac.th)  
© BME-PT and GTE

The presence of fillers, such as electrically conductive additives, in elastomers has been observed to change their electrical, dielectric, and mechanical properties, along with their morphology [3, 5, 6]. The incorporation of the conductive materials into dielectric elastomers has been widely studied as both magnetorheological (MR) and electrorheological (ER) fluids. Lokander and Stenberg (2003) studied the MR properties of NBR having different acrylonitrile amount as well as blends of NBR with iron particles [7]. Dynamic mechanical properties, under the influence of an electric field, of doped poly(3-hexylthiophene), P3HT, blended with a silicone elastomer have also been investigated [8]. Shiga (1997) reported the ER effect of polymethacrylic acid cobalt(II) salt (PMAcCo) particles in silicone gel; increase in the elastic modulus induced by an electric field was 4 kPa, with a particle volume fraction of more than 25%. As the particles were incorporated into the rubber matrix, interaction between the particles occurred under an electric field [9].

In our previous work, various matrix systems were used to investigate the electrorheological (ER) properties, with emphasis on the effects of electric field strength, particle concentration, and operating temperature. The systems were poly(dimethyl siloxane) (PDMS) networks containing camphor-sulfonic acid (CSA)-doped polyaniline (PANI) particles [10]. The ER properties of PDMS gel and PPV/PDMS blends were studied for the effect of particle electrical conductivity [11]. The ER properties of pure crosslinked polyisoprene elastomers, polythiophene/polyisoprene blends, and poly(*p*-phenylene) and an acrylic rubber blends were also investigated [12, 13].

In this work, we are interested in the electromechanical properties of elastomeric actuator materials – acrylonitrile-butadiene rubber containing a conductive poly(3-thiopheneacetic acid) – towards artificial muscle applications. Several NBRs having various amounts of ACN were chosen as matrices because of their polarity towards the incorporated poly(3-thiopheneacetic acid). The effects of the acrylonitrile content in acrylonitrile-butadiene rubber, and the conductive polymer particle concentration, on the electrorheological and dielectric properties of the pure rubbers and the blends are reported.

## 2. Experimental

### 2.1. Materials

#### 2.1.1. Synthesis of poly(3-thiopheneacetic acid)

AR grade 3-thiopheneacetic acid, 3TAA (Fluka) was used as the monomer. Anhydrous ferric chloride, FeCl<sub>3</sub> (AR grade, Riedel-de Haën), was used as the oxidant. Chloroform, CHCl<sub>3</sub> (AR grade, BDH), and methanol, CH<sub>3</sub>OH (AR grade, CARLO ERBA) dried over a molecular sieve for 24 hours under a nitrogen atmosphere and then distilled, were used as solvents. Perchloric acid, HClO<sub>4</sub> (AR grade, AnalaR) was used as the dopant. Sulfuric acid, H<sub>2</sub>SO<sub>4</sub>, was used to protect the oxidative decomposition of the monomer. Diethyl ether and deionized water were used to extract materials. Sodium hydroxide, NaOH, was used as the hydrolyzing agent.

#### 2.1.2. Acrylonitrile-butadiene rubbers (NBR)

Several commercial grades of acrylonitrile-butadiene rubber (NBR) (Nipol NBR<sup>®</sup> DN101L, Nipol NBR<sup>®</sup> DN 2850, Nipol NBR<sup>®</sup> DN401L (Zeon Advanced Polymix, Thailand; containing 7% carboxylic group), Krynac<sup>®</sup> 3345 F, and Krynac<sup>®</sup> X7.50 (Lanxess)) having bound acrylonitrile amounts and specific gravities of 42.3%, 1; 28%, 0.97; 18.5%, 0.94; 33%, 0.97; and 26.5%, 0.99 respectively, were used as the elastomeric matrices.

### 2.2. Polymerization procedure

#### 2.2.1. Preparation of 3-thiophene methyl acetate (TMA)

The reaction was by oxidative-coupling polymerization according to the method of Kim *et al.* (1999) [14]. A 10.0 g amount of 3-thiopheneacetic acid was refluxed for 24 hours in 50 ml of dry methanol (with 1 drop of concentrated H<sub>2</sub>SO<sub>4</sub> in order to protect the oxidative decomposition of the carboxylic acid group of monomer during oxidative-coupling polymerization). The methanol was evaporated, and the residue extracted with fresh diethyl ether. The extract was washed with deionized water, dried with anhydrous MgSO<sub>4</sub>, and then filtered. The diethyl ether was evaporated from the filtrate by a rotating evaporator and a TMA product was obtained.

### 2.2.2. Synthesis of poly(3-thiophene methyl acetate) (PTMA)

A solution of 10 mmol of protected monomer in 20 ml of chloroform was added dropwise to a solution of 40 mmol of ferric chloride dissolved in 30 ml of dry chloroform under nitrogen atmosphere. The oxidant-to-monomer molar ratio was 4:1 in all cases. The reaction was carefully maintained at 0°C ( $\pm 0.5^\circ\text{C}$ ) for 24 hours. The reaction mixture was precipitated by pouring it into an excess amount of methanol [11]. The product was repeatedly washed with methanol and deionized water to obtain the PTMA.

### 2.2.3. Synthesis of poly(3-thiopheneacetic acid) (PTAA)

PTMA was hydrolyzed by adding 0.5 g of the PTMA to a 50 ml 2.0 M NaOH solution and was heated for 24 hours at 100°C. The mixture was filtered, neutralized, and precipitated with a dilute HCl solution ( $\sim 0.5$  M) to obtain the polymer product. P3TAA was washed several times with deionized water before vacuum drying at room temperature for 2 days. The final product, PTAA was ground with a mortar and passed through a 38  $\mu\text{m}$  sieve to control the particle size.

### 2.3. Preparation of pure acrylonitrile-butadiene rubber

Crude acrylonitrile-butadiene rubber was purified by dissolving it in  $\text{CHCl}_3$  (AR grade, BDH) and coagulating it in methanol, and was subsequently dried (Vallim *et al.*, 1999) [6]. The purified rubber was dissolved in  $\text{CHCl}_3$  to obtain a rubber solution prior to casting into films with a thickness of around 1 mm. Then the films were left in an air atmosphere at  $27 \pm 1^\circ\text{C}$  overnight, and later placed in a vacuum oven to remove any remaining solvents.

### 2.4. Preparation of the PTAA/acrylonitrile-butadiene rubber blends

The PTAA/acrylonitrile-butadiene rubber mixtures were prepared by the mechanical blending of doped and undoped synthesized polythiophene at various particle volume concentrations (5, 10, 15,

20, and 30% vol/vol) into the acrylonitrile-butadiene rubber. The solutions were magnetically stirred for  $\sim 24$  hr at  $27^\circ\text{C}$ . Bubbles were removed in atmosphere at room temperature,  $27^\circ\text{C}$ , overnight prior to casting the solution into films. Then they were placed in a vacuum at  $27^\circ\text{C}$  to remove any remaining solvent.

### 2.5. Characterization methods

A Fourier transform infrared spectrometer (Thermo Nicolet, Nexus  $\pm 4$  cm), covering a wavenumber range of  $4000\text{--}400\text{ cm}^{-1}$  and using a deuterated triglycine sulfate detector, was used to characterize the conductive polymer. The samples were prepared by grinding the conductive polymer particles with KBr (Carlo Erba Reagent) at a ratio of P3TAA:KBr = 1:20. Then the mixtures were compressed into pellets. The acrylonitrile-butadiene rubber and the polymer blends, were characterized by using a Horizontal Attenuated Total Reflectance accessory (HATR) equipped with ZnSe.

Nuclear Magnetic Resonance,  $^1\text{H-NMR}$  (Varian Unity Inova) data were recorded at  $25 \pm 1^\circ\text{C}$  at a 500 MHz to characterize the synthesized conductive polymer. Deuterated dimethyl sulfoxide was used as the standard solvent.

Particle sizes of the P3TAA powder were determined by using a particle size analyzer (Malvern, Master Sizer X).

A thermogravimetric/differential thermal analyzer (Perkin Elmer, Pyris Diamond), with a temperature scan from 30 to  $800^\circ\text{C}$  at a heating rate of  $10^\circ\text{C}/\text{min}$  under  $\text{N}_2$  atmosphere, was used to investigate the thermal behavior of the synthesized polythiophene, the pure acrylonitrile-butadiene rubber, and the polythiophene/acrylonitrile-butadiene rubber blends.

A scanning electron microscope (JOEL, model JSM-5200-2AE) was used to determine the morphological structure of the conductive polymers and the polymer blend morphology. The samples, in pellet form, were cut into small pieces and adhered to a brass-stub by using adhesive tape. Then they were coated with a thin layer of gold by using a JFC-1100E ion-sputtering device prior to observation.

A custom-built two-point probe electrometer (Keithley, Model 6517A) was used to determine the electrical conductivity of the conductive poly-

mer (25 mm diameter and 0.2 mm thickness prepared by molding with a hydraulic press). The relation  $\sigma = (1/Rt)(1/K) = (I/Vt)(1/K)$  was used to calculate the specific conductivity, where  $t$  is the pellet thickness,  $I$  is current change,  $V$  is applied voltage (voltage drop), and  $K$  is the geometric correction factor, which is equal to the ratio  $w/l$ , where  $w$  and  $l$  are the probe width and the length, respectively. The geometrical correction factor ( $K$ ) was determined by calibrating the two-point probe with semi-conducting silicon sheets of known resistivity values. These two probes were connected to a voltmeter (Keithley, Model 6517A), which supplied a constant voltage and recorded the resultant current. Electrical conductivity values of several samples were first measured at various applied voltages to identify their linear Ohmic regimes.

A resistivity testing fixture (Keithley, Model 8009) connected to a source meter (Keithley, Model 6517A) was also used to determine the electrical conductivity of the matrix materials and the blended films. It is a constant voltage source and the resultant current was read under the atmospheric pressure, 54–60% relative humidity, and at 24 to 25°C. The volume resistivity ( $\rho_v$ ) of matrices was calculated following ASTM standard D257,  $\rho_v = K_v R/t$ , where  $K_v$  is the effective area of the guarded electrode for the particular electrode arrangement employed (22.9 cm<sup>2</sup>),  $t$  is the pellet thickness, and  $R$  is the volume resistance in ohms. The conductivity of the polymer blends and the polymer matrices were calculated by using this relation  $\sigma = 1/\rho_v = (t_c \cdot I)/(22.9 \cdot V)$ , where  $t_c$  is the pellet thickness,  $I$  is the resultant current, and  $V$  is the applied voltage (voltage drop).

Dielectric measurements were carried out in the frequency range of 20 Hz up to 600 kHz under an applied voltage of 1 V at 27±0.5°C by using an LCR meter (HP, 4284A), which was connected to and controlled by a melt rheometer (Rheometric Scientific, ARES) fitted with a custom-built copper parallel plate fixture (diameter of 25 mm). The samples were coated with a silver conductive paint (Electrolube) to prevent air being trapped between the samples and the electrodes.

A melt rheometer (Rheometric Scientific, ARES) was used to measure the electrorheological properties. It was fitted with a custom-built copper parallel plate fixture (diameter of 25 mm). A DC voltage was applied with a DC power supply (Instek, GFG

8216A), which can deliver an electric field up to 4 kV. A digital multimeter (Tektronix, CDM250)) was used to monitor the voltage input. In these experiments, oscillatory shear strain was applied and the dynamic moduli ( $G'$  and  $G''$ ) were measured as functions of frequency (0.1–100 rad/s) and electric field strength (0–2 kV/mm) and at 27±1°C. Strain sweep tests were first carried out to determine the appropriate strain to measure  $G'$  and  $G''$  in the linear viscoelastic regime. The suitable strain was 0.1% for all samples. Before each measurement, each sample was presheared at a low frequency (0.04 rad/s) with and without electric field for 30 min.

Bending measurements were carried out by using a DC power supply (Goldsen, GPS 30035) connected to an amplifier (Gamma High Voltage, UC5-30P) supplying a high DC voltage to copper electrodes (30 mm long, 30 mm wide, and 1.0 mm in thickness; the distance between the electrodes is 10 mm). The apparatus setup is shown in Figure 6. The specimens were immersed in silicone oil, having a viscosity of 100 cP, between the pair of parallel copper electrode plates. The specimen widths were 5 mm, and thicknesses 0.6 mm. All the measurements were carried out at ambient temperature, 27±1°C. The bending responses of the specimens were recorded by a video camera, and the data were analyzed by digital imaging software (Scion Image).

### 3. Results and discussion

#### 3.1. Characterization of poly(3-thiopheneacetic acid), P3TAA and poly(3-thiopheneacetic acid)/acrylonitrile-butadiene rubber, P3TAA/NBR, blends

The peak in the FT-IR spectrum of P3TAA at 3000–2800 cm<sup>-1</sup> can be assigned to the stretching vibration of the C–H band on the thiophene ring. The absorption band at 1735–1750 cm<sup>-1</sup> is due to the C=O stretching vibrations; the peak at 1432 cm<sup>-1</sup> is evidence for the thiophene ring stretching vibration, and the peak at 1300–1200 cm<sup>-1</sup> is due to the C–O stretching vibration. These peaks confirm the successful oxidative polymerization of 3-thiophene methyl acetate [15]. According to Senadeera [15], the characteristic peaks of P3TAA at 3200–3000 cm<sup>-1</sup> can be

assigned to the stretching vibration of the C–H bond on the thiophene ring. The peak at 3000–2800  $\text{cm}^{-1}$  represents the aliphatic C–H bonds; at 1700  $\text{cm}^{-1}$ , the C=O stretching vibration; at 1400  $\text{cm}^{-1}$ , the thiophene ring stretching vibration; and at 1300–1200  $\text{cm}^{-1}$ , the C–O stretching vibration [15]. The most characteristic feature of the spectrum is the extremely broad O–H absorption occurring in the region from 3400 to 2400  $\text{cm}^{-1}$  [14].

The P3TAA/NBR blends were characterized by using an FT-IR spectrometer equipped with HATR. As P3TAA particles were added to the NBR matrix, the peak at 3400  $\text{cm}^{-1}$ , which represents the –OH group of poly(3-thiopheneacetic acid), can still be detected from the blend spectrum. It should be noted that the peak wavenumber is slightly higher for the blends having higher P3TAA amounts, indicating some interactions between P3TAA and NBR.

The structure of the P3TAA was characterized by  $^1\text{H-NMR}$  to verify the successful synthesis of poly(3-thiopheneacetic acid). The  $^1\text{H-NMR}$  spectra of the polymers provide data in agreement with the

expected structures: P3TMA  $\delta$  at 7.26–7.3 ppm (m, thiophene ring proton, 1H), 3.68 ppm (s, thiophene ring  $-\text{CH}_2-$ , 2H), and 3.66 ppm (s,  $-\text{CH}_3$ , 3H); and P3TAA (DMSO) at 12.60 ppm (s,  $-\text{COOH}$ , 1H), 7.55–7.28 ppm (m, thiophene ring proton, 1H), and 3.80–3.37 ppm (m, thiophene ring  $-\text{CH}_2-$ , 2H). The position at 12.6 ppm is the most important peak of poly(3-thiopheneacetic acid), identifying that the structure changes from poly(3-thiophene methyl acetate) to poly(3-thiopheneacetic acid), since this peak disappears with the presence of poly(3-thiophene methyl acetate) [14].

The TGA thermogram of the undoped P3TAA indicates three transitions: 30–120, 120–300, and 450–650 $^\circ\text{C}$ ; these refer to the loss of water and residue solvent, the side chain degradation, and the backbone degradation, respectively [16]. Acrylonitrile-butadiene rubber has a better thermal stability, whose main transition temperature starts at 415 $^\circ\text{C}$ . The P3TAA/NBR blends were characterized by using a thermogravimetric/differential thermal analyzer under nitrogen gas. The P3TAA/NBR thermogram shows the decomposition temperature at around 230 $^\circ\text{C}$ , the decomposition temperature of

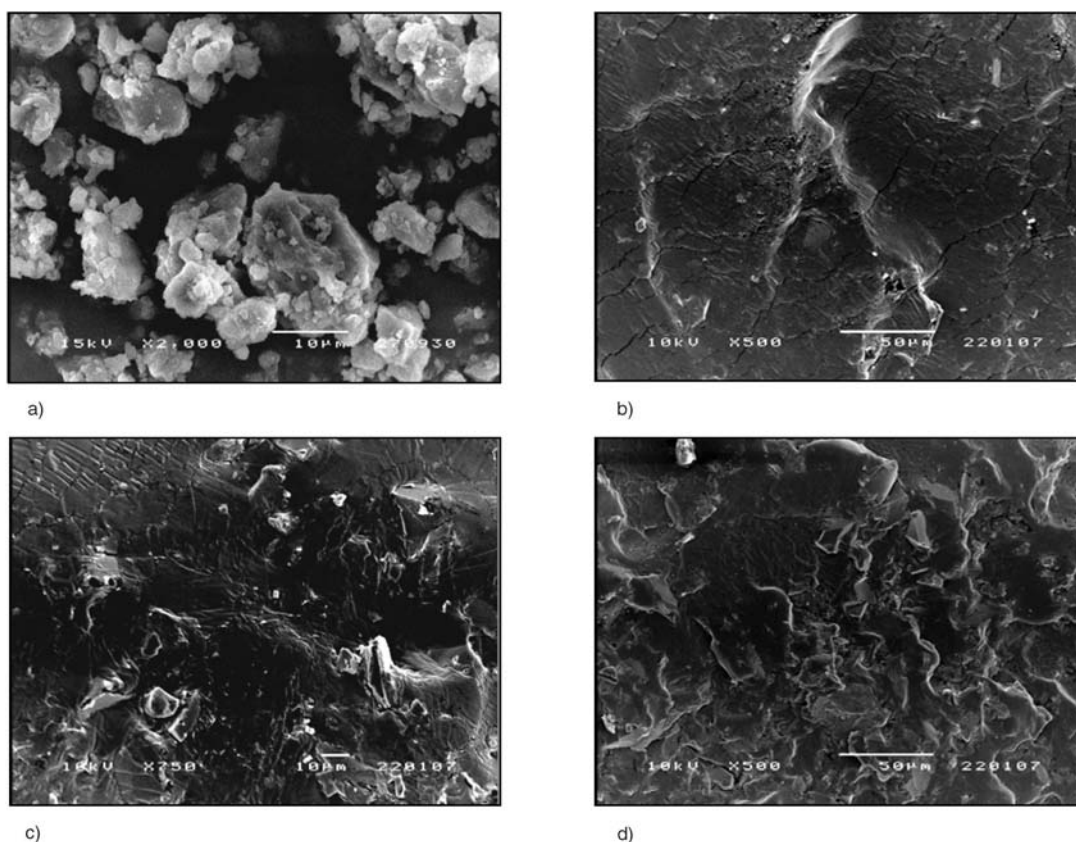


**Figure 1.** SEM photographs of: (a) undoped poly(3-thiopheneacetic acid) at 2000 $\times$ ; (b) P3TAA\_5/NBR1 at 500 $\times$  (c) P3TAA\_20/NBR1 at 500 $\times$ ; and (d) P3TAA\_30/NBR1 at 500 $\times$

the P3TAA side chain. As more P3TAA particles are added, the decomposition temperature varies between those of P3TAA and NBR. We infer therefore, that P3TAA enhances the thermal stability of the rubber.

The P3TAA particle size is 20  $\mu\text{m}$  with a standard deviation of 0.131, which is confirmed by SEM microphotographs (Figure 1a).

The morphology of the blend films was observed from SEM microphotographs to determine the dispersion of the particles. Figures 1b–1d show that the P3TAA particles are moderately dispersed in the NBR matrix.

The electrical conductivity of the undoped P3TAA is approximately  $5 \cdot 10^{-6}$  S/cm with a standard deviation of  $2.73 \cdot 10^{-6}$  S/cm. The electrical conductivities of pure NBR is  $3.31 \cdot 10^{-10}$  S/cm, with a standard deviation of  $7.71 \cdot 10^{-11}$  S/cm. As more P3TAA particles are added to the NBR matrix, the blend electrical conductivity increases; at the highest concentration (30% vol/vol) it is  $4.02 \cdot 10^{-9}$  S/cm, with a standard deviation of  $8.97 \cdot 10^{-10}$  S/cm.

### 3.2. Dielectric properties of pure acrylonitrile-butadiene rubber and poly(3-thiopheneacetic acid)/pure acrylonitrile-butadiene rubber, P3TAA/NBR, blends

#### 3.2.1. Effect of acrylonitrile (ACN) content

The effect of acrylonitrile (ACN) content on the dielectric properties of pure acrylonitrile-butadiene rubbers, NBR1, NBR2, NBR3, NBR4, and NBR5 (with acrylonitrile contents of 42.5, 33, 28, 18.5, and 26.5%, and the last containing the carboxylic group of 7%) was investigated in the frequency range of 20 Hz to 600 kHz at an applied voltage of 1 V and a fixed temperature of 27°C. Figure 2a shows that the dielectric constant ( $\epsilon'$ ) of the pure NBRs increases with increasing ACN content. The dielectric constant of NBR having the highest ACN content (NBR1) at a frequency of 20 Hz is 14, and the lowest ACN content (NBR4) is 7.8. With increasing frequency ( $>10^4$  Hz), the dielectric constants decrease; NBR1 shows a higher drop in  $\epsilon'$  relative to the others. The results suggest that the increase in  $\epsilon'$  is evidently due to the increase in the  $\text{C}\equiv\text{N}$  dipoles, leading to an increase in the orientation polarization, which diminishes when the frequency is above  $10^4$  Hz [5].

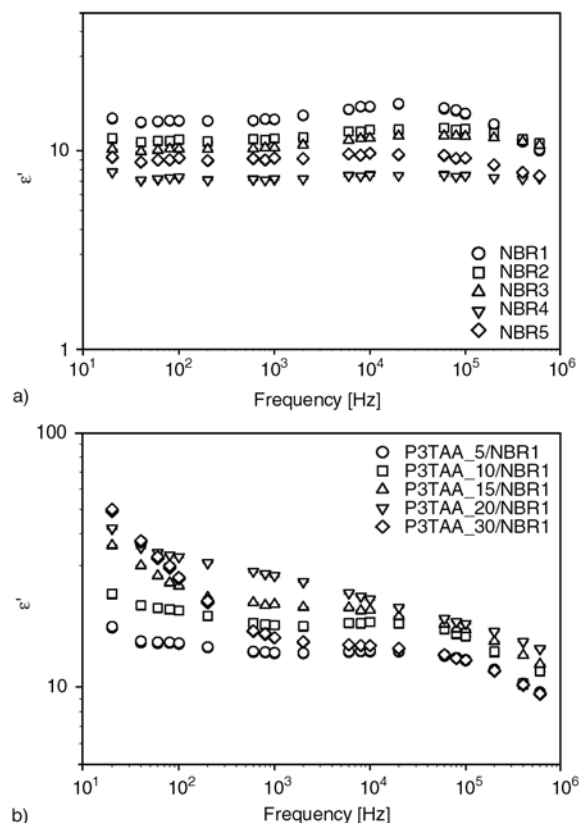


**Figure 2.** Comparison of the dielectric constants ( $\epsilon'$ ) of pure NBR and P3TAA/NBR1 vs. frequency at an applied voltage of 1.0 V, a temperature of  $27 \pm 0.5^\circ\text{C}$ , a gap range of 0.7–1.0 mm: (a) pure NBR; (b) P3TAA/NBR blends

#### 3.2.2. Effect of particle concentration

NBR1 is a matrix containing poly(3-thiopheneacetic acid) at various particle concentrations (5, 10, 15, 20, and 30% vol). In Figure 2b, the dielectric constant increases with increasing particle concentration when the frequency is lower than  $10^2$  Hz. The dielectric constant of the blend system having the highest concentration of 30% vol/vol is 48.92 at a frequency of 20 Hz. The increase in dielectric constant with particle concentration occurs as the conductive particles in NBR1 setup the interfacial polarization [17]. From Figure 2b, the dielectric constants of the blend systems monotonically decrease with increasing frequency. In particular, the dielectric constant of the 30% vol/vol system drops sharply, relative to the others, when the frequency is above  $10^2$  Hz. This indicates that for the high particle concentration system, the particles lose their ability to be polarized by an electric field due to a screening effect. In addition, the matrix of the 30% vol system has a smaller number of polar

sections (C≡N); hence the effect of orientation polarization of the 30% vol can be expected to be less than that of the 20% vol/vol system, which inherently contains more NBR sections.

### 3.3. Electrorheological properties of pure acrylonitrile-butadiene rubber and poly(3-thiopheneacetic acid)/pure acrylonitrile-butadiene rubber, P3TAA/NBR, blends

#### 3.3.1. Effect of acrylonitrile (ACN) content

Figures 3a and 3b show the storage modulus responses, defined as  $\Delta G' = G'_E - G'_0$ , where  $G'_E$  is the storage modulus under electric field, and  $G'_0$  is the storage modulus without electric field, vs. electric field strength. Figure 3a shows the storage modulus responses ( $\Delta G'$ ) of the pure rubbers increase with electric field strength ( $E$ ):  $\Delta G' \propto E^\alpha$ , where  $\alpha$  is the scaling exponent. The  $\alpha$  values of pure NBRs having various ACN contents (NBR1, NBR2, NBR3, NBR4, and NBR5) are 0.66, 0.66, 0.61, 0.60, and 0.79, respectively.

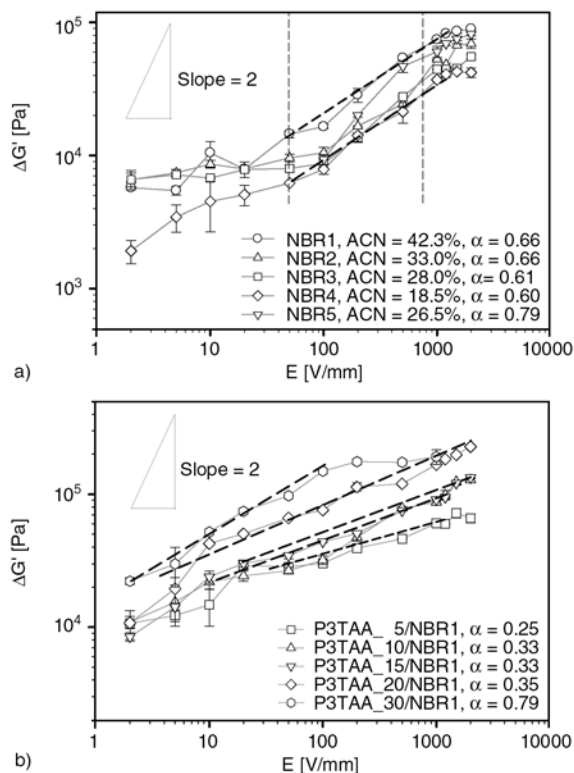


**Figure 3.** Comparison of the storage modulus responses ( $\Delta G'$ ) of pure NBR and P3TAA/NBR1 of various particle concentrations (5, 10, 15, 20, and 30% vol) vs. electric field strength, at a frequency of 1.0 rad/s, a strain of 0.1%, a temperature  $27 \pm 0.5^\circ\text{C}$ , and a gap range of 0.7 to 1.0 mm: (a) pure NBR; (b) P3TAA/NBR1 blends

0.61, 0.60, and 0.79, respectively, when  $0.05 \text{ kV/mm} < E < 1.2 \text{ kV/mm}$ . The electrostatic model of actuation pressure of Perline [2] predicts that the scaling exponent  $\alpha$  should be equal to 2. In our work,  $\Delta G'$  inherently depends on ACN content and  $\alpha$  varies slightly with ACN content. As an electric field is applied, electrical dipole moments are generated and electrostatic interactions between the elastomeric segments are induced, leading to an intermolecular interaction acting like an electrical network. The intermolecular interaction results in a loss of chain free movements, higher chain rigidity, and, as a result, higher  $G'(\omega)$  [18].

#### 3.3.2. Effect of particle concentration

P3TAA/NBR1 blends at various P3TAA particle concentrations (5, 10, 15, 20, and 30% vol/vol) were investigated at electric field strengths between 0 and 2 kV/mm. Figure 3b shows the storage modulus ( $\Delta G'$ ) of each polymer blend system, which generally increases with increasing electric field strength:  $\Delta G' \propto E^\alpha$ ,  $\alpha$  of each blend system is 0.25, 0.33, 0.33, 0.35, and 0.49 for the particle concentrations of 5, 10, 15, 20, and 30% vol/vol, respectively. The scaling behavior of the storage modulus responses on the electric field strength can be compared to the power law behavior of the Maxwell-Wagner model [19]:  $\Delta G' \propto E^\alpha$ , in which  $\alpha$  is predicted to be equal to 2. For our blend systems, the scaling exponent is less than two. The deviation from the quadratic dependence on electric field at low concentration is because the distances between particles are too large to create a significant particle interaction [21] and the fact that the model is based on the center-to-center distance between the adjacent spheres [19]. At high concentrations, the deviation might also result from the nonlinear conduction proposed by Atten *et al.* (1994) [20], and the steric hindrance [21]. They suggested that the electric field between particles can become so large that the dielectric breakdown strength of the continuous phase is exceeded.

Figure 4 shows the storage modulus response of P3TAA/NBR1 vs. particle concentration at low electric field strength (0.1 and 0.2 kV/mm) and at high electric field strengths (1.0 and 2.0 kV/mm). At low electric field strengths, the response is linear with respect to particle concentration up to 0.1% vol/vol; beyond this concentration, the

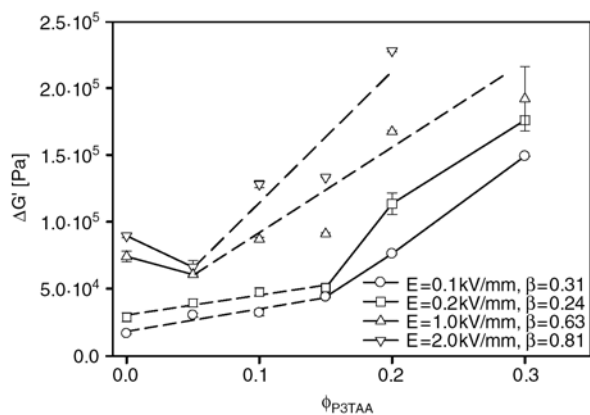


**Figure 4.** Comparison of the storage modulus responses ( $\Delta G'$ ) of pure NBR and P3TAA/NBR1 blends at various electric field strengths (0.1, 0.2, and 1 kV/mm) vs. particle concentration ( $\phi = 0, 5, 10, 15, 20,$  and  $30\%$  vol) at a frequency of 1.0 rad/s, a strain of 0.1%, a temperature of  $27 \pm 0.5^\circ\text{C}$ , and a gap range of 0.7 to 1.0 mm

response is clearly nonlinear. At high electric field strengths, the response first decreases to a minimum near a particle concentration of 0.5% vol/vol; beyond this concentration it appears to increase linearly. At the low electric field strengths, the linear increase in the modulus results from the P3TAA particles behaving as fillers in the matrix. As more P3TAA particles are added, above 15% vol/vol, the modulus response sharply increases due to the interparticle interaction. At the high electric field strengths (1.0, 2.0 kV/mm), the initial decrease in the storage modulus response may occur from the cancellation of dipoles of P3TAA particles, which try to align along an electric field, and the particles only act as fillers, which induce an additional free volume, instead of enhancing the storage modulus response [13].

Shiga *et al.* [8] found a similar effect for poly(*p*-phenylene) and silicone elastomer blends. The storage modulus response increased with increasing particle content; it was negligible below 8.4% vol. Chotpattananont *et al.* (2004) [16] found that the storage and loss moduli of a polymer blend between polythiophene and silicone oil increased with increasing polythiophene concentration. However, at high concentration, the storage modulus is not responsive to electric field due to the steric hindrance effect. Liu and Shaw (2001) showed that the enhancement of shear modulus of silicone/silica ER elastomers was negligible below 8.0% vol, but increased dramatically above threshold concentra-

tion [21]. At a volume fraction above 55% vol, the shear modulus decreased because the interparticle force decreased with the steric hindrance effect.

### 3.4. Electrorheological properties and dielectric properties of acrylonitrile-butadiene rubber (NBR) and poly(3-thiopheneacetic acid)/acrylonitrile-butadiene rubber (P3TAA/NBR) blends

#### 3.4.1. Pure NBR

In Figure 5a, the storage modulus responses ( $\Delta G'$ ) at a frequency of 1.0 rad/s and 0.1% strain of the pure rubbers increase linearly with increasing the dielectric constant  $\epsilon$  (20 Hz) or ACN content at both low (0.1 and 0.2 kV/mm) and high (1 kV/mm) electric field strengths. This result is consistent with the electrostatic model of actuation, in which the actuation pressure is proposed to be proportional to the dielectric constant [2].

#### 3.4.2. Poly(3-thiopheneacetic acid)/acrylonitrile-butadiene rubber

P3TAA/NBR blends were fabricated, in which the conductive polymer particles were added to the rubber (NBR1) at 5, 10, 15, 20, and 30% vol/vol, corresponding to P3TAA\_5/NBR1, P3TAA\_10/NBR1, P3TAA\_15/NBR1, P3TAA\_20/NBR1, and P3TAA\_30/NBR1, respectively. Figure 5b shows the storage modulus response ( $\Delta G'$ ) vs. the dielectric constant ( $\epsilon'$ ) at 20 Hz, which depends on particle concentration. The storage modulus response ( $\Delta G'$ ) increases nonlinearly with increasing dielectric constant, notably beyond the particle concentration of 15% vol/vol. This result suggests that the interfacial polarization is operative on the  $G'$  response, as previously shown by Hao *et al.* (1998) [22]. Referring to Figure 2b, it is evident that the  $\epsilon'$  of the blends in the Maxwell-Wagner region ( $<100$  Hz) increases with increasing conductive particle concentration [17]. As more P3TAA particles are added to the NBR, a greater mismatch between their conductivities occurs, resulting in the interfacial polarization. As the conductivity mismatch increases, the interaction between particles is amplified, leading to the greater increase in the storage modulus [22].

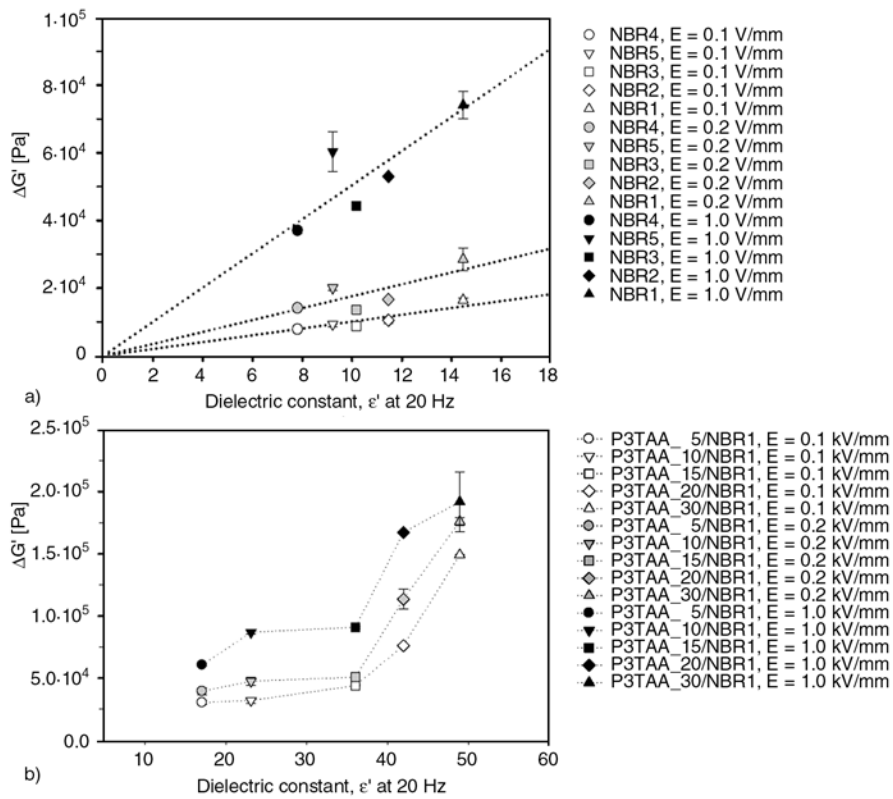


**Figure 5.** Storage modulus responses at a frequency of 1.0 rad/s, a strain of 0.1%, and at various electric field strengths (0.1, 0.2, and 1 kV/mm) of pure NBR and P3TAA/ vs. dielectric constant, at 20 Hz, an applied voltage of 1 volt, at  $27\pm 0.5^\circ\text{C}$ , and at a gap range of 0.7 to 1.0 mm: (a) pure NBR; (b) P3TAA/NBR1 blends of various particle concentrations (5, 10, 15, 20, and 30% vol)

### 3.5. Time dependence of the electrorheological response

The temporal characteristics (the storage modulus) of the pure NBR1 and the P3TAA\_20/NBR1 blend, at an electric field strength of 1.2 kV/mm, were investigated. The temporal characteristic of each sample was recorded in the linear viscoelastic regime at a strain of 0.1% and at a frequency of 1.0 rad/s. Table 1 shows the induction and recovery times of the two samples. They were detected during a time sweep test, in which an electric field was turned on and off alternately. The response of storage modulus,  $G'$ , of the pure NBR system can be divided into two regimes: the initial regime, in which  $G'$  rapidly overshoots to a large value ( $\Delta G'$  is 23470 Pa) on the first cycle, followed by an irreversible decay. The time required for  $G'$  to reach

the steady-state value under electric field is called the induction time,  $\tau_{ind}$ . For NBR1, the  $\tau_{ind}$  is 1000 s. The time required for  $G'$  to decay towards its steady-state value when the electric field is turned off is called the recovery time,  $\tau_{rec}$ . It takes longer time to decay to the steady-state ( $\tau_{rec}$  is 1500 s). However,  $G'$  does not recover its initial state. The response decreases only by 1460 Pa. As the electric field is turned on again, the response slightly increases until reaching its steady-state. As the electric field is applied to the rubber, the dipoles of the  $\text{C}\equiv\text{N}$  segment align themselves along the electric field. When the electric field is turned off, some dipole moments remain due to the interaction in the  $\text{C}\equiv\text{N}$ , leading to the irreversible storage modulus responses. Berlepsch *et al.* (1989) [23] studied a stretched copolymer of acrylonitrile and methy-

**Table 1.** Induction time and recovery time at an electric strength of 1.2 kV/mm of the pure NBR system and the P3TAA\_10/NBR1 blend

Sample	Induction time ( $\tau_{ind}$ ) [s]	Reduction time ( $\tau_{rec}$ ) [s]	$\Delta G_{ind}$ [Pa]	$\Delta G_{rec}$ [Pa]
NBR1	1000	1500	23470	1460
P3TAA_20/NBR1	1500	3000	209920	4010

lacrylate. They found that their samples showed appreciable piezoelectric activity [23]. Eid and El-Nashar (2006) investigated the relaxation time of polymer blend between NBR and EPDM, they found that the relaxation time increased slightly by the addition of NBR to the EPDM. The relaxation time could be associated with those orientations of small aggregates caused by the movement of the main chain [5].

P3TAA\_20/NBR1 is also an irreversible system. Table 1 shows that the modulus response and  $\tau_{ind}$  of the first cycle are 209 920 Pa and 1500 s, respectively; both values are larger than those of the pure NBR1 system. The blend system takes a longer time to decay to the steady-state when the electric field is turned off. This result suggests that there are some irreversible interactions between polythiophene particles, perhaps due to the hydrogen bonding between adjacent polythiophene particles, and to the residual dipole moments inducing permanent interparticle interactions [12].

### 3.6. Bending response

Pure NBR1 and P3TAA\_10/NBR1 blend bending was observed in response to electric field. The samples were clamped between copper plates and immersed in silicone oil. Different voltages were

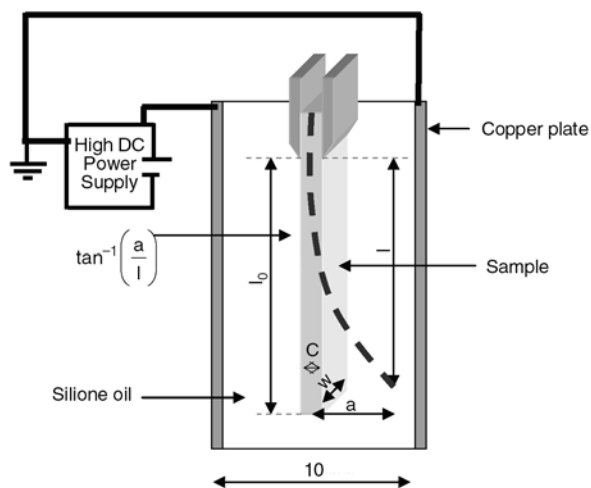


**Figure 6.** Schematic of the bending response measurement of pure NBR1 and P3TAA\_10/NBR1 films suspended vertically in a silicone oil bath and sandwiched between copper plates (30 mm long, 30 mm wide, and 1.0 mm thick, with a distance of 10 mm between the electrodes in an acrylic box. A DC electric field is applied horizontally at  $\pm 0.5^\circ\text{C}$  causing a deflection distance ( $a$ ) of the film from its original position to a new position (dashed line).

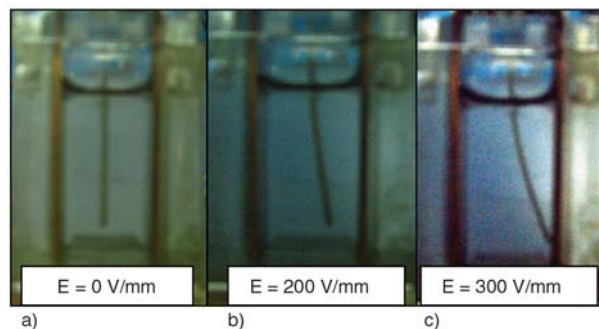


**Figure 7.** Bending response pictures of pure NBR1 at various applied voltages at  $27 \pm 0.5^\circ\text{C}$ : (a)  $E = 0$  V/mm; (b)  $E = 200$  V/mm; (c)  $E = 300$  V/mm. Size of pure NBR sample: 0.6 mm thick, 5.55 mm in wide, and a weight of 0.1515 g.

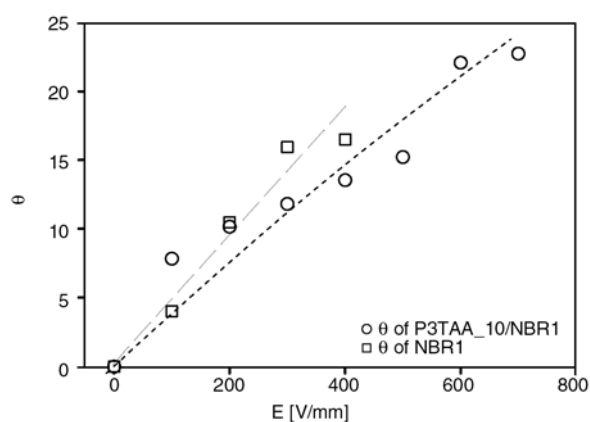


**Figure 8.** Bending angle of pure NBR1 and P3TAA\_10/NBR1 vs. electric field strength at  $27 \pm 0.5^\circ\text{C}$ . The thickness of the pure NBR sample is 0.6 mm with a weight of 0.1515 g; for the P3TAA\_10/NBR1, thickness is 0.5 mm, with a weight of 0.1356 g; both samples have a width of 5.55 mm.

applied to the copper plate (Figure 6). The deflection responses of the samples were recorded by a video camera, as shown in (Figure 7). The bending angle, theta, was calculated from the arctan(theta) obtained from the measured deflection distance ( $a$ ) and the sample length ( $l$ ). Figure 8 shows the bending angles of pure NBR1 and the P3TAA/NBR1 blend. For pure NBR1, the bending angle increases linearly with electric field up to  $E = 400$  V/mm. For the blend system (10% vol/vol P3TAA), the bending angle increases linearly at low electric field ( $< 500$  V/mm) and then nonlinearly beyond the electric field strength of 500 V/mm. However, the bending angle of the blend at low electric field strength ( $< 200$  V/mm) is comparable to that of the pure system. At higher electric field strength, the bending angle of the blend is clearly lower than that

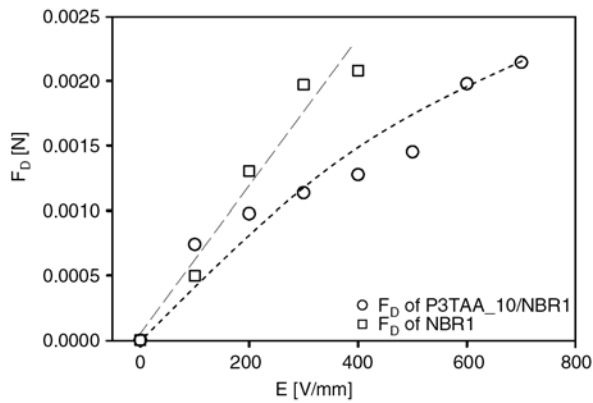


**Figure 9.** Electric force of pure NBR1 and P3TAA\_10/NBR1 vs. electric field strength at  $27 \pm 0.5^\circ\text{C}$ . The thickness of the pure NBR sample is 0.6 mm, with a weight of 0.1515 g; for the P3TAA\_10/NBR1, the thickness is 0.5 mm, the weight is 0.1356 g; both samples have a width of 5.55 mm.

of the pure rubber system. It may be noted that both the pure rubber and the blend bend towards the neutral copper electrode.

Figure 9 shows the resultant dielectrophoresis forces ( $F_D$ ) calculated from the horizontal force balance Equation (1):

$$F_D = mgs \sin \theta + P_E(\theta) \quad (1)$$

where  $m$  is the sample mass [kg],  $g$  is the gravity ( $9.8 \text{ m/s}^2$ ),  $\theta$  is the bending angle, and  $P_E$  is the resisting elastic force [N] calculated from Equation (2) [24]:

$$P_E = \frac{3EIa}{l_0^3} \quad (2)$$

where  $E$  is Young's modulus which is equal to  $2G'(1+\nu)$ ,  $G'$  is the shear modulus at a particular electric field,  $\nu$  is Poisson's ratio equal to  $1/2$  (incompressible material), and  $I$  is the moment of inertia equal to  $2/3C^3W$ , where  $C$  is the sample thickness, and  $W$  is the sample width. In Equation (2),  $a$  is the deflection distance ( $a$ ), and  $l_0$  is the initial sample length.

From Figure 9, it can be seen that the dielectrophoresis force of the pure NBR1 system increases linearly with electric field. For the blend system, the resultant dielectrophoresis force varies nonlinearly with applied electric field and it is lower than that of the pure rubber system at any electric field strength. For the pure acrylonitrile-butadiene system, as the electric field is applied,

positive dipole moments are generated in the direction of the anode, resulting in a repulsive interaction between the pure rubber and the copper anode. On the other hand, for the blend system, negative dipole moments are generated from the P3TAA particles counteracting the matrix dipole moments, resulting in a smaller dielectrophoresis force at a given electric field strength. Thus, the presence of the conductive polymer filler, P3TAA, can serve to control the overall magnitude of the resultant dielectrophoresis force.

#### 4. Conclusions

In this study, the electrorheological properties and dielectric properties of acrylonitrile-butadiene rubber (NBR) and poly(3-thiopheneacetic acid)/acrylonitrile-butadiene rubber blends, P3TAA/NBR, were investigated at electric field strengths varying from 0 to 2 kV/mm. Poly(3-thiopheneacetic acid) particles were synthesized via oxidative polymerization.

For the pure NBR system, the storage modulus responses ( $\Delta G'$ ) increase with increasing electric field strength to nearly one order of magnitude. With increasing ACN content,  $\Delta G'$  slightly increases. The storage modulus ( $\Delta G'$ ) in the pure rubber system increases linearly with dielectric constant ( $\epsilon'$ ).

For the P3TAA/NBR blend systems, at P3TAA particle concentrations of 5, 10, 15, 20, and 30% vol, the storage modulus responses ( $\Delta G'$ ) increase with particle concentration due to the particle-particle interacting under electric field. The storage modulus response becomes saturated at an electric field strength of 1 kV/mm. Unlike the pure rubber systems,  $\Delta G'$  is nonlinearly correlated with  $\epsilon'$ . The storage modulus of the blends increases nonlinearly at high particle concentrations above 15% vol.

For the temporal response, both systems are irreversible since they have residual dipole moments remaining in the systems when the electric field is turned off.

The bending responses of the pure rubber and the blend systems were observed from a vertical cantilever fixture, and the bending angle and electric force were calculated. In the pure rubber system (NBR1), the response and force increase linearly with electric field. For the blend system, the

response and the force are nonlinearly correlated with electric field. The P3TAA particles set up dipole moments in the opposite direction to those of the rubber matrix, resulting in smaller dielectrophoresis forces.

## Acknowledgements

The authors would like to acknowledge the Conductive & Electroactive Polymers Research Unit and KFAS, both of Chulalongkorn University, the Thailand Research Fund (TRF, BRG), the Petroleum Petrochemicals and Advanced Materials Consortium, the Royal Thai Government (Fiscal Year 2551), Zeon Advance Polymix (ZAP), and Lanxess of Thailand.

## References

- [1] Bar-Cohen Y.: Electroactive polymer (EAP) actuators as artificial muscles: Reality, potential and challenges. SPIE Press, Bellingham (2004).
- [2] Perline R., Kornbluh R., Joseph J., Heydt R., Pei Q., Chiba S.: High-field deformation of elastomeric dielectrics for actuators. *Materials Science and Engineering: C*, **11**, 89–100 (2000).
- [3] Yong K. C., Foot P. J. S., Morgan H., Cook S., Tinker A. J.: Conductive poly(butadiene-co-acrylonitrile)-polyaniline dodecylbenzenesulfonate [NBR-PAni. DBSA] blends prepared in solution. *European Polymer Journal*, **42**, 1716–1727 (2006).
- [4] Li Y., Vamvounis G., Holdcroft S.: Facile functionalization of poly(3-alkylthiophene)s via electrophilic substitution. *Macromolecules*, **34**, 141–143 (2001).
- [5] Eid M. A. M., El-Nashar D. E.: Filling effect of silica on electrical and mechanical properties of EPDM/NBR blends. *Polymer-Plastics Technology*, **45**, 675–684 (2006).
- [6] Vallim M. R., Felisberti M. I., De Paoli M-A.: Blends of polyaniline with nitrilic rubber. *Journal of Applied Polymer Science*, **75**, 677–684 (2000).
- [7] Lokander M., Stenberg B.: Performance of isotropic magnetorheological rubber materials. *Polymer Testing*, **22**, 245–251 (2003).
- [8] Shiga T., Okada A., Kurauchi T.: Electroviscoelastic effect of polymer blends consisting of silicone elastomer and semiconducting polymer particles. *Macromolecules*, **26**, 6958–6963 (1993).
- [9] Shiga T.: Deformation and viscoelastic behavior of polymer gels in electric fields. *Advanced in Polymer Science*, **134**, 133–163 (1997).
- [10] Hiamtup P., Sirivat A., Jamieson A. M.: Electromechanical response of a soft and flexible actuator based on polyaniline particles embedded in a cross-linked poly(dimethyl siloxane) network. *Materials Science and Engineering: C*, **28**, 1044–1051 (2008).
- [11] Naimlang S., Sirivat A.: Dielectrophoresis force and deflection of electroactive poly(*p*-phenylene-vinylene)/polydimethylsiloxane blends. *Smart Materials and Structures*, **17**, 035036 p8 (2008).
- [12] Puvanattvattana T., Chotpattananont D., Hiamtup P., Naimlang S., Sirivat A., Jamieson A. M.: Electric field induced stress moduli in polythiophene/polyisoprene elastomer blends. *Reactive and Functional Polymers*, **66**, 1575–1588 (2006).
- [13] Khunanuruksaphong R., Sirivat A.: Poly(*p*-phenylene) and acrylic elastomer blends for electroactive application. *Materials Science and Engineering, A: Structural Materials*, **454–455**, 453–460 (2007).
- [14] Kim B., Chen L., Gong J., Osada Y.: Titration behavior and spectral transitions of water-soluble polythiophene carboxylic acids. *Macromolecules*, **32**, 3964–3969 (1999).
- [15] Senadeera G. K. R.: Microwave-assisted steps in the synthesis of poly(3-thiophenylacetic acid). *Current Science*, **88**, 145–148 (2005).
- [16] Chotpattananont D., Sirivat A., Jamieson A. M.: Electrorheological properties of perchloric acid-doped polythiophene suspensions. *Colloid and Polymer Science*, **282**, 357–365 (2004).
- [17] George S., Varughese K. T., Thomas S.: Dielectric properties of isotactic polypropylene/nitrile rubber blends: Effects of blend ratio, filler addition, and dynamic vulcanization. *Journal of Applied Polymer Science*, **73**, 255–270 (1999).
- [18] Krause S., Bohon K.: Electromechanical response of electrorheological fluids and poly(dimethylsiloxane) networks. *Macromolecules*, **34**, 7179–7189 (2000).
- [19] Parthasarathy M., Klingenberg D. J.: Electrorheology: Mechanisms and models. *Materials Science and Engineering: R: Reports*, **17**, 57–103 (1996).
- [20] Atten P., Foulc J-N., Felici N.: A conduction model of the electrorheological effect. *International Journal of Modern Physics B*, **8**, 2731–2745 (1994).
- [21] Liu B., Shaw T. M.: Electrorheology of filled silicone elastomers. *Journal of Rheology*, **45**, 64–657 (2001).
- [22] Hao T., Kawai A., Ikazaki F.: Mechanism of the electrorheological effect: Evidence from the conductive, dielectric, and surface characteristics of water-free electrorheological fluids. *Langmuir*, **14**, 1256–1262 (1998).
- [23] Berlepsch H., K unstler W., Wedel A., Danz R., Gei D.: Piezoelectric activity in a copolymer of acrylonitrile and methylacrylate. *IEEE Transactions on Electrical Insulation*, **24**, 357–362 (1989).
- [24] Timoshenko S. P., Goodier J. N.: *Theory of elasticity*. McGraw-Hill, Auckland (1970).

# The effect of bimodality on tensile properties of filled silicone networks

G. B. Shah\*

Applied chemistry Laboratories (ACL), Pakistan Institute of Nuclear Science and Technology (PINSTECH), P.O. Nilore, Islamabad, Pakistan

Received 22 September 2008; accepted in revised form 10 November 2008

**Abstract.** The effect of blending short and long chains (bimodality) silicone prepolymer, in the presence of a filler (17.2 and 30.2% w/w) on tensile properties such as ultimate tensile strength (UTS), percent elongation at break (% Eb), 100% modulus and elastic modulus has been investigated. The content of short chain prepolymer was varied from 0–69% and 0–58% for 17.2 and 30.2% filled silicones respectively. It was found out that the tensile properties were enhanced for the low filled (17.2%) silicone networks while in the case of highly filled (30.2%) silicone networks; the bimodality adversely affected the tensile properties such as UTS, % Eb. It is also observed that the optimum in these properties was recorded at 95 mol% as compared to 70 mol% of short chain prepolymer for unfilled silicone system. The phenomenon of improvement in mechanical properties due to bimodality in this system has been discussed.

**Keywords:** material testing, bimodal polymer networks, monomodal polymer networks, mixing, crosslinking

## 1. Introduction

The blending of long and short chains of the same polymer which results in bimodal molecular weight distribution is known as bimodality and the resulting polymer networks prepared from such blends are known as bimodal networks. The interest in studies of these bimodal networks initiated due to the fact that these bimodal networks exhibits a combination of good mechanical properties, such as tear energy, tensile behaviour, resilience [1–3], non-linear stress-optic response [4–6] and a proportional orientation–stretch response with respect to molar concentration of short chains HOPDMS (hydroxy functional polydimethylsiloxane) in the bimodal network [7, 8].

The mechanism of enhancement in these properties due to bimodality is not clear [2], but the accepted view to date is that the introduction of short chains prepolymers creates high crosslink density domains

with in the otherwise uniform polymer networks. This results in the low incidence of chain irregularities (i.e. the presence of polymer ends that do not form part of the load bearing networks) and limited extensibility to the polymer networks hence gives rise to the non-Gaussian effects which are reported to be responsible for the enhancement [1, 9]. The domains of high crosslink density within the bimodal networks support the applied stress, thus hiding the imperfections which are otherwise more exposed in monomodal networks. The longer prepolymers chains which have potentials for high extension, on the other hand provide high tear energy in the unfilled and filled state, tensile properties, in accordance with the Lake-Thomas equation [10]. These effects coupled together, make bimodal polymer networks superior to monomodal ones in respect of tear properties. Tensile and shear properties have also been reported to be improved

\*Corresponding author, e-mail: [gbshah.gul@gmail.com](mailto:gbshah.gul@gmail.com)  
© BME-PT and GTE

due to bimodality for unfilled silicone networks [11, 12].

A great deal of work has been done by other researchers [13–19] to prepare such tough elastomers by using this technique. The concept of bimodality is not only limited to silicone networks for enhancement in mechanical properties but, has also been reported for enhancement in system such as polyisoprene [20]. Grobler and McGill observed improvement in tear and tensile properties for polyisoprene via different curing condition and have attributed these improvements to the polymer network heterogeneity.

Apart from the economical reasons, fillers are being used as reinforcing agents in various polymer systems. It is this example of reinforcement of properties of expensive polymer by cheap particulate fillers that is the root of the commercial exploitation of these materials [21].

Coupling the concept of bimodality with reinforcement due to filler seemed to be a novel way of achieving enhancement in the properties of silicone networks. For this purpose, the effect of bimodality on tensile properties of the bimodal silicone networks in the presence of pyrogenic silica HDK type 2000-4 as a filler has been studied. In this respect two concentrations i.e. 17.2 and 30.2% w/w HDK, in conjunction with variation of concentration of short chain silicone prepolymer have been used for silicone networks preparation. These networks have been studied for their tensile properties.

## 2. Experimental

### 2.1. Materials

The liquid hydroxyfunctional polydimethylsiloxanes (HOPDMS) prepolymers (Silopren), long chain (C50, M.Wt = 88 000) and a short chain silicone prepolymer of viscosity 100 mPa·s (P100) used were supplied by Bayer Ltd. and Petrarch Ltd. respectively. The catalyst, dioctyltinmaleate (DOTM) (LT195, M.W 459), was supplied by Lankro Ltd. and a trifunctional crosslinker vinyltris(ethoxymethoxy)silane VTEMS (A172, M.W 280.4) was procured from Union Carbide Ltd. The filler employed in this study, supplied by Wacker Ltd was pyrogenic silica HDK type H 2000-4.

### 2.2. Methods

Two series of compositions having different concentrations i.e. 17.2 and 30.2% w/w of the filler (HDK) based on the total weight were mixed with C50 separately. The amount of short chain prepolymer i.e. P100, to be mixed with the above compositions was varied from 0 to 69% and 0 to 58% for the 17.2 and 30.2% filled HOPDMS respectively. The concentrations of crosslinker and catalyst for these compositions were kept constant i.e. 13.79 and 0.7% respectively. Each of the compositions, after mixing to a homogeneous paste, was cast onto a polyethylene plate separately and spread to a uniform film of approximately 1.4 mm thickness. These films were left in an open air at room temperature (25°C) for seven days to complete the crosslinking (curing) reaction. Dumbbell shaped specimens were cut from the films according to BS 903 Part A2 1956 Die C. Instran Model 4301 High Wycombe (England) was used for measuring tensile properties i.e. tensile strength (TS) and percent elongation at break (% Eb) at a strain rate of 50 mm/min. An average of the three modal values out of that of five specimens tested has been used for presentation.

## 3. Results and discussions

As reported [3] previously, the amount of crosslinker necessary to cure the mixture has a positive effect on the mechanical properties such as % Eb, and UTS and 100% modulus. In the present studies for the filled bimodal silicone network preparation, the amount of crosslinker necessary to cure the whole series of each of the two compositions separately, was selected on the basis of trial and error experiments.

The polymer networks prepared from the two series of filled bimodal prepolymer compositions prepared were tested for tensile properties such as % Eb, ultimate tensile strength (UTS), 100% modulus. The 17.2% filled silicone networks showed an increase in these tensile properties with the increases in concentration of short chain prepolymer (bimodality). However, surprisingly, when this silicone system is filled to 30.2% w/w level, the ultimate tensile property suffers continuous decrease

**Table 1.** Variation of tensile properties of filled C50 networks with bimodality

P100 concentration		17.2% filled network				P100 concentration		32.2% filled networks			
Wt%	Mol%	% Eb	UTS [MN·m <sup>-2</sup> ]	100% modulus [MN·m <sup>-2</sup> ]	E [MN·m <sup>-2</sup> ]	Wt%	Mol%	%Eb	UTS [MN·m <sup>-2</sup> ]	100% modulus [MN·m <sup>-2</sup> ]	E [MN·m <sup>-2</sup> ]
0	0.0	215	1.520	1.121	1.12	0	0.0	280	4.75	2.97	5.28
20	64.0	214	1.631	1.301	1.17	11	52.1	195	4.17	3.25	4.76
40	84.2	250	2.516	1.384	1.94	21	71.8	132	4.23	3.47	4.76
50	89.9	251	2.760	1.567	2.01	31	82.9	120	3.94	–	5.55
60	94.1	267	2.841	1.646	2.13	41	90.1	126	4.23	–	5.01
64	95.5	300	3.152	1.722	2.41	51	95.5	78	3.24	–	5.34
72	97.9	350	2.817	1.197	2.22	55	96.7	78	3.21	–	6.05
76	99.0	298	2.513	1.173	2.22	59	98.1	80	2.87	–	5.01
80	100.0	276	2.417	1.090	1.79	61	98.8	96	3.56	–	7.54
						71	100.0	68	3.64	–	6.84

Crosslinker (A172) = 13.8% w/w; Catalyst (LT195) = 0.07% w/w.

The calculation of mole% of P100 is based on the limiting values of prepolymer networks (Mc P100 = 2250 and Mc C50 = 12000) while the concentration of filler has been ignored.

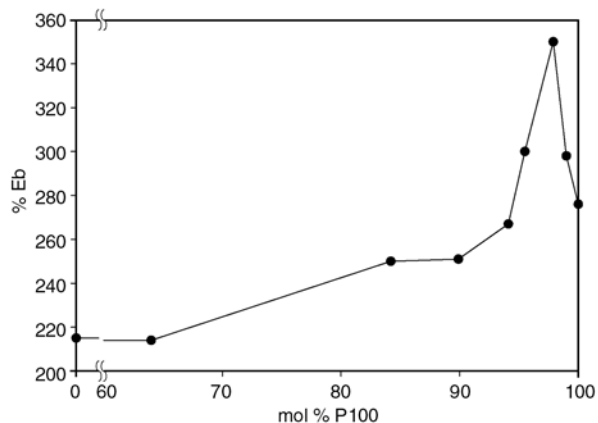


**Figure 1.** Effect of variation of bimodality on % Eb for 17.2% filled silicone networks

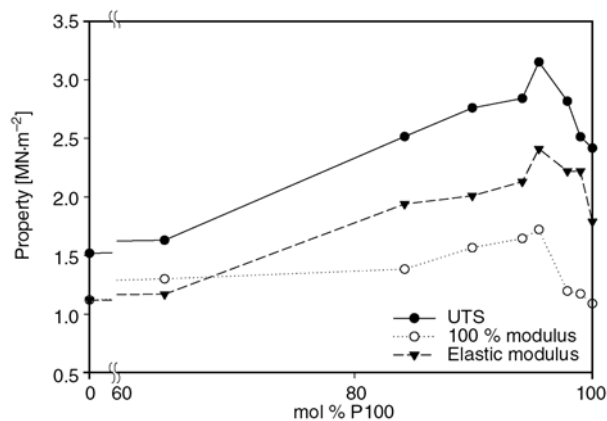


**Figure 2.** Effect of variation of bimodality on UTS, 100% and elastic moduli

with increase in concentration of short chain prepolymer (Table 1). Previously, the enhancement of tensile properties due to bimodality has been reported [1, 15, 16, 22, 23] but invariably for only unfilled system.

Looking at Figure 1 it is shown that the effect of bimodality on % Eb in presence of the 17.2% filler can be divided into three stages. In the first stage (0–90 mol% P100), % Eb gradually increases with increase of P100 to about 90 mole. In the second stage, the % Eb exhibits a dramatic increase with increase in P100 concentration up to 97 mol%. In the third stage, there is a drastic decrease with onward increase in P100 concentration.

The increase in UTS, 100% and elastic moduli with increase bimodality in the case of 17.2% filled network is shown as Figure 2. It is evident from this

figure that the increase in all these three cases is almost linear and becomes optimum at about 95 mol% short chain prepolymer. It is interesting that the optimum values of these properties in the case of unfilled bimodal silicone networks were observed and reported [3, 24] at 70 mol% short chain prepolymer. This indicates that the incorporation of filler to bimodal silicone network shift the optimum for these mechanical properties to a higher limits of the short chain prepolymers. It is clear that the increase in UTS due to bimodality in the filled silicone system at about 95 mol% short chain prepolymer as compared to the correspondingly filled monomodal network is about 2 fold. Similarly, in the case of 100% modulus as well as that of elastic modulus, an optimum increase of about 55 and 115% respectively can be noted due to

bimodality. The incorporation of more than 95 mol% short chain prepolymer with in the network, makes these properties inferior and a drastic decrease in these properties is observed. The effect of bimodality on the tensile properties of silicone networks in the presence of filler has not previously been reported.

The about 2 fold increase in UTS due to bimodality for the 17.2% filled C50/P100 system can be attributed to the increase in the number of effective crosslinks with increase in short chain prepolymer up to 95 mol%. These crosslinks, whether chemical or physical, originate both from the short chain prepolymer and filler and tighten the chain network. The longer HOPDMS chains present in the bimodal networks at the same time retain the flexibility of the polymer chains. Unfortunately, in the case of highly filled (30.2%) networks the contribution of effective crosslinks from the filler coupled with successive increases in short chain prepolymer tips the balance between chain tightening due to crosslinking and chain flexibility. As a result, the increase in concentration of short chain prepolymer decreases the elongation and reduces the UTS. As shown in Figure 3, the % Eb shows a linear decrease with the increase in concentration of short chain HOPDMS. In the case of UTS, a gradual decrease is first recorded with increase in mol% of P100 as shown in Figure 4 and then a drastic drop in the property occurs. The inferior %Eb and UTS of the 30.2% filled bimodal networks for all the compositions as compared to that of 17% filled one networks are due to the inability of the network to absorb the applied load reversibly. However in contrast, the elastic modulus for the 30.2% filled bimodal networks experiences a slow increase up

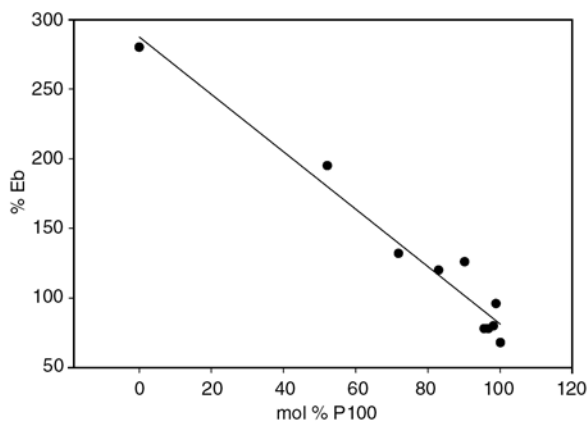


Figure 3. Effect of variation of bimodality on % Eb for 30.2% filled silicone networks

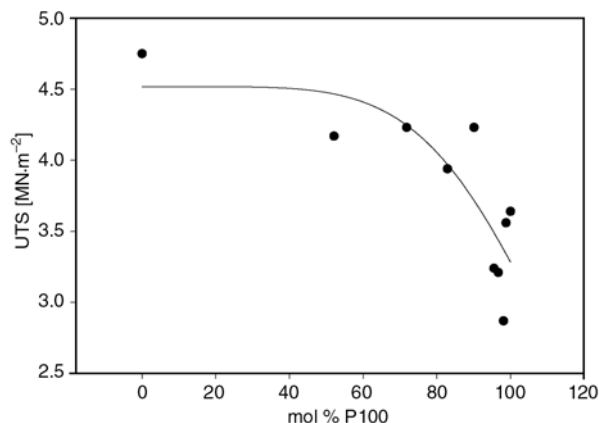


Figure 4. Effect of variation of UTS with mol% P100 for 30.2% filled silicone networks

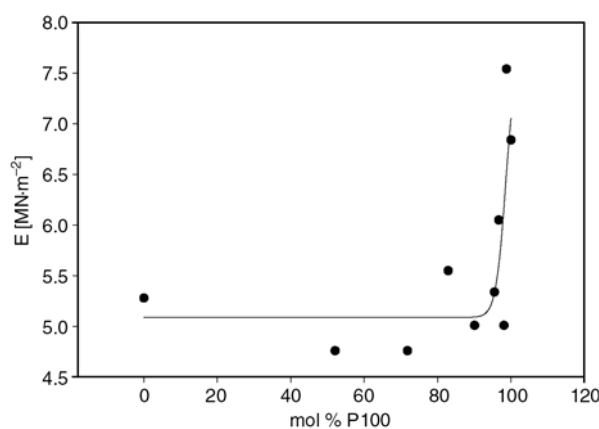


Figure 5. Effect of variation elastic modulus with mol% P100 for 30.2% filled silicone networks

to about 80 mol% P100 followed by an exponential increase (Figure 5) with concentration of short chain HOPDMS. In this highly loaded (30.2% filled) system the OH groups on the filler (2.5 to 3.5/nm<sup>2</sup>, surface area of filler 125–400 m<sup>2</sup>/g) are more than sufficient to react via crosslinker with short chain prepolymer available and results in a network having inactive filler. In presence of sufficient fillers anchoring along the polymer chain at frequent interval, the further successive increments of short chain decrease the degree of freedom of orientation of polymer in the resulting networks. This employ that the excessive amounts of filler (30.2%) coupled with the increase in amount of short chains some how undermines the role of the long chain prepolymer in the silicone network in reference to these mechanical properties. These inactive points may act as stress centers and hence responsible for the inferior tensile properties.

The enhancement in the tear, tensile and tensile-optic behaviour due to bimodality in the unfilled

state of polydimethylsiloxanes has been dealt in detail in literature [7, 25–30]. A number of studies including experimental, numerical and analytical ones have been carried out to predict the said enhancement and ascertain its relationship with the various parameters of the structure of the bimodal polymer network.

For example von Lockette and Arruda [29] set a crosslinking algorithm, which apart from predicting the enhancement in mechanical properties, show correlation between the molar short chain concentration at which enhancement in the toughness occurs and the magnitude of certain short chain topologies peak, namely the density of loops in the gel and the percentage of doubled connections in the gel.

Von Lockette *et al.* [30] also developed a micromechanics-based constitutive model for the non-linear large deformation stress and birefringence responses of bimodal networks. This law is claimed to have capability of comparatively straightforward implementation to tensile test and tensile-optic behaviour of bimodal networks compared to the previous theories and moreover is predictive over a wide range of composition.

However, the above mentioned crosslinking algorithm and the micromechanics-based constitutive models are designed for unfilled bimodal polydimethylsiloxanes and unfortunately no such model exists presently for application to the present system.

The effect of filler on monomodal networks is also generally well documented [31–37]. The reinforcement of polymer network is related to the concentration of filler. The size and nature of the filler particle within the polymer network determine the effective crosslinks which in turn are responsible for improvement in the mechanical properties [38]. For example, Bueche [39] reported an increase up to about 6 fold in effective crosslinks in polydimethylsiloxane on addition of 50 phr silica. Polmanteer and Helmer [38] realizing the presence of this interaction have enumerated the various kinds of linkages that can be present in the filler vulcanisate. It is all these crosslinks which can be used to explain the increasing physical properties such as tensile strength with increase in concentration of filler.

Bueche suggests that the interaction between polymer and filler whether chemical or physical

between the Si–O of the resin with the hydrogen of the filler promotes reinforcement. It is well established [40, 41] that this reinforcement depends upon the chemical nature as well as on the size of the particles. A ten time increase in UTS and 100% modulus and 2.5–5 times increase in %Eb for silicone networks on incorporation of HDK (filler) has also been attributed to the small particle size of the filler (5–30 nm) and high concentration of surface silanol groups (2–3.5 SiOH/nm).

The mechanical property of elastomers depends upon the number of effective linkages in the polymer network. These linkages are of different kinds and their identification becomes difficult after incorporation of filler into the polymer network. However, the addition of filler considerably increases the effective crosslinks. The unexpected improvement in tensile properties due to bimodality in 17.3% filled silicone system is difficult to explain. In unfilled polymer system the effective crosslinks consist of: i) crosslink joining polymer with polymer and ii) polymer entanglement.

In the case of filled monomodal polymer system, the effective crosslinks constitute from the:

- 1) filler to polymer covalent linkage,
- 2) filler to polymer linkage resulting from polar or Van der Waals forces between filler and polymer,
- 3) effective filler to polymer linkage from entanglement influenced by filler structure,
- 4) effective filler to polymer linkage resulting from simple wetting of the filler surface by polymer.

In fact it is difficult to separate all these kinds of linkage from one another, analyse it and then attribute each one with a separate explanation. Then furthermore, explanation for improvement in the mechanical properties of filled (17.5%) silicone system due to bimodality, becomes even more difficult.

In the case of highly filled (32.2%) silicone networks, the 100% modulus records increase in its values up to about 84 mole% of P100. Further increase in mole% of P100 results in polymer networks which fails prematurely during the test and hence this property can not be recorded. For modulus of elasticity, there is an increase in its values up to incorporation of about 98 mole% P100 after which a decrease is observed. The data is given in Table 1.

#### 4. Conclusions

Like the tear property of unfilled and filled silicone network, the tensile behaviour of the filled silicone polymer network is sensitive to bimodality. The effect of bimodality on the tensile properties was also found to be beneficial for the 17.2% filled silicone network. The optimum in tensile properties was observed at 95 mol% of short chain prepolymer. In the case of highly filled (32.2%) networks bimodality brought adverse effect on the tensile properties such as UTS, % Eb. In the light of the results of the present studies, the slightly higher physical properties of the high molecular weight prepolymer network reported earlier in the literature can be sacrificed in favour of the easy processing of low molecular silicone prepolymers in the low filled (17.2%) bimodal networks.

#### References

- [1] Andrady A. L., Llorente M. A., Mark J. E.: Model networks of end-linked polydimethylsiloxane chains. VII. Networks designed to demonstrate non-Gaussian effects related to limited chain extensibility. *Journal of Chemical Physics*, **72**, 2282–2290 (1980).
- [2] Bhowmick A. K., Stephens H. L.: *Handbook of elastomers. New Developments and Technology*. Marcel Dekker, New York (1988).
- [3] Shah G. B., Winter R. W.: Effect of bimodality on tear properties of silicone networks. *Macromolecular Chemistry and Physics*, **197**, 2201–2208 (1996).
- [4] Galiatsatos V., Mark J. E.: Non-Gaussian optical properties of bimodal elastomeric networks. *Macromolecules*, **20**, 2631–2632 (1987).
- [5] Zeigler J. M., Fearon F. W. G.: *Silicone base polymer science: A comprehensive resource*. American Chemical Society, Washington (1990).
- [6] Galiatsatos V., Subramanian P.R.: Stress-optical properties of bimodal networks. *Macromolecular Symposia*, **76**, 233–240 (1993).
- [7] Monnerie L., Besbes S., Ceremelli I., Bokobza L.: Molecular orientation in deformed bimodal networks 2. Fourier transform infrared measurements on polydimethylsiloxane networks and comparison with theory. *Macromolecules*, **28**, 231–235 (1995).
- [8] Bahar I., Erman B., Bokobza L., Monnerie L.: Molecular orientation in deformed bimodal networks. 1. theory. *Macromolecules*, **28**, 225–231 (1995).
- [9] Zhang Z-M., Mark J. E.: Model networks of end-linked polydimethylsiloxane chains. XIV. Stress-strain, thermoelastic, and birefringence measurements on the bimodal networks at very low temperatures. *Journal of Polymer Science: Polymer Physics Edition*, **20**, 473–480 (1982).
- [10] Lake G. J., Thomas A. G.: The strength of highly elastic materials. *Proceedings of the Royal Society of London, A*, **300**, 108–119 (1967).
- [11] Shah G. B.: Aspects of the polycondensation of hydroxyfunctional polydimethylsiloxanes. PhD Thesis, University of Wales, College of Cardiff, UK (1990).
- [12] Wen J., Mark J. E.: Torsion studies of thermoelasticity and stress-strain isotherms of unimodal, bimodal, and filled networks of poly(dimethylsiloxane). *Polymer Journal*, **26**, 151–157 (1994).
- [13] Wada T., Ito K.: Heat-curable elastomeric silicones compositions. U.S. Patent 3652475, USA (1972).
- [14] Bobear W. J.: Organopolysiloxane elastomer. U.S. Patent 3660345, USA (1972).
- [15] Andrady A. L., Llorente M. A., Mark J. E.: Model networks of end-linked polydimethylsiloxane chains. IX. Gaussian, non-Gaussian, and ultimate properties of the trifunctional networks. *Journal of Chemical Physics*, **73**, 1439–1445 (1980).
- [16] Llorente M. A., Andrady A. L., Mark J. E.: Model networks of end-linked polydimethylsiloxane chains. XI. Use of very short network chains to improve ultimate properties. *Journal of Polymer Science: Polymer Physics Edition*, **19**, 621–630 (1981).
- [17] Patel S. K., Malone S., Cohen C., Gillmor J. R., Colby R. H.: Elastic modulus and equilibrium swelling of poly(dimethylsiloxane) networks. *Macromolecules*, **25**, 5241–5251 (1992).
- [18] Mark J. E., Andrady A. L.: Model networks of end-linked polydimethylsiloxane chains. X. Bimodal networks prepared in two-stage reactions designed to give high special heterogeneity. *Rubber Chemistry and Technology*, **54**, 366–373 (1981).
- [19] Yanyo L. C., Kelley F. N.: Effect of chain length distribution on the tearing energy of silicones elastomers. *Rubber Chemistry and Technology*, **60**, 78–88 (1987).
- [20] Grobler J. H. A., McGill W. J.: Effect of network heterogeneity on tensile and tear strengths of radiation, peroxide, efficient and conventional cured polyisoprene. *Journal of Polymer Science Part A: Polymer Chemistry*, **32**, 287–295 (1994).
- [21] Murphy J.: *Additives of plastics handbook*. Elsevier Advanced Technology, Oxford, UK (2001).
- [22] Mark J. E.: The effect of strain-induced crystallization on the ultimate properties of an elastomeric polymer network. *Polymer Engineering and Science*, **19**, 409–413 (1979).
- [23] Erich F. R.: *Rheology*, vol 5., Academic Press, New York (1969).
- [24] Shah G. B.: The effect of bimodality on the tear properties of filled silicone networks. *Journal of Applied Polymer Science*, **94**, 1719–1722 (2004).
- [25] Mark J. E., Tang M-Y.: Dependence of the elastomeric properties of bimodal networks on the length and amount of short chains. *Journal of Polymer Science: Polymer Physics Edition*, **22**, 1849–1855 (1984).

- [26] Arruda E. M., Boyce M. C.: A three-dimensional constitutive model for the large stress behaviour of rubber elastic material. *Journal of the Mechanics and Physics of Solids*, **41**, 389–412 (1993).
- [27] Mark J. E.: The use of model polymer networks to elucidate molecular aspects of rubberlike elasticity. *Advances in Polymer Science*, **44**, 1–26 (1982).
- [28] Leung Y-K., Eichinger B. E.: Computer simulation of end linked elastomers 1. Trifunctional network cured in the bulk. *Journal of Chemical Physics*, **80**, 3877–3884 (1984).
- [29] von Lockette P. R., Arruda E. M.: Topological studies of bimodal networks. *Macromolecules*, **32**, 1990–1999 (1999).
- [30] von Lockette P. R., Arruda E. M., Wang Y.: Mesoscale modeling of bimodal elastomer networks: Constitutive and optical theories and results. *Macromolecules*, **35**, 7100–7109 (2002).
- [31] Boonstara B. B., Cochrane H., Dannenberg E. M.: Reinforcement of silicone rubber by particulate silica. *Rubber Chemistry and Technology*, **48**, 558–576 (1975).
- [32] Smallwood W. M.: Limiting law of the reinforcement of rubber. *Journal of Applied Physics*, **15**, 758–766 (1944).
- [33] Bueche F.: Mullins effect and rubber-filler interaction. *Journal of Applied Polymer Science*, **5**, 271–281 (1961).
- [34] Kraus G.: Reinforcement of elastomers. Wiley, New York (1965).
- [35] Sudár A., Móczó J., Vörös Gy., Pukánszky B.: The mechanism and kinetics of void formation and growth in particulate filled PE composites. *Express Polymer Letters*, **1**, 763–772 (2007).
- [36] Li Z. H., Zhang J., Chen S. J.: Effects of carbon blacks with various structures on vulcanization and reinforcement of filled ethylene-propylene-diene rubber. *Express Polymer Letters*, **2**, 695–704 (2008).
- [37] Kolesov I. S., Radusch H-J.: Multiple shape-memory behavior and thermal-mechanical properties of peroxide cross-linked blends of linear and short-chain branched polyethylenes. *Express Polymer Letters*, **2**, 461–473 (2008).
- [38] Polmanteer K. E., Helmer J. D.: Complexities of crosslink density in filled elastomers. *Rubber Chemistry and Technology*, **38**, 123–133 (1965).
- [39] Bueche A. M.: The curing of silicone rubber with benzoyl peroxide. *Journal of Polymer Science*, **15**, 105–120 (1955).
- [40] Mark J. E.: Elastic properties of model polymer networks. *Pure and Applied Chemistry*, **53**, 1495–1504 (1981).
- [41] Gessler A.: Evidence for chemical interaction in carbon and polymer associations. Butyl and acidic oxy blacks. The possible role of carboxylic acid groups on the black. *Rubber Chemistry and Technology*, **42**, 850–857 (1969).

# Preparation and characterization of regenerated *Bombyx mori* silk fibroin fiber with high strength

Z. H. Zhu, K. Ohgo, T. Asakura\*

Department of Biotechnology, Tokyo University of Agriculture and Technology, Koganei, Tokyo 184-8588, Japan

Received 1 October 2008; accepted in revised form 10 November 2008

**Abstract.** Regenerated *Bombyx mori* silk fibers were spun from hexafluoro-iso-propanol solution of silk fibroin sponge in methanol used as a coagulant solvent and then elongated in water. The stress-strain curves of the regenerated fibers changed dramatically depending on the draw ratio and the structure was studied by  $^{13}\text{C}$  CP/MAS NMR and X-ray diffraction methods. The patterns of  $^{13}\text{C}$  CP/MAS NMR spectra of two regenerated fibers with different draw ratios (1 $\times$  and 3 $\times$ ) and native silk fiber are all  $\beta$ -sheet structure although the fraction of random coil/distorted  $\beta$ -turn decreases in the order of 1 $\times$ , 3 $\times$  and native fiber gradually. On the other hand, azimuthal scans of their X-ray fiber patterns changed remarkably with increasing the draw ratio. This indicates that long-range orientation of the fibroin chain changes remarkably during the drawing process, but the short-range local structure does not change significantly. Regenerated silk fiber with a draw ratio of 3 $\times$  is a fiber with high strength which is comparable with that of natural silk fiber. The regenerated fiber is also more degradable than natural silk fiber in enzyme solution *in vitro*.

**Keywords:** biopolymers, regenerated silk fiber, hexafluoro-iso-propanol

## 1. Introduction

Silk proteins are of practical interest because of their excellent intrinsic properties utilizable in biotechnological and biomedical fields [1]. It is advantageous to focus on the regeneration of natural silks and their structural information in the spinning process because these can be used as a benchmark for evaluating the success of the spinning process. Hexafluoro-iso-propanol (HFIP) [2–7], hexafluoroacetone hydrate [8] and formic acid [9] have been used as useful solvents for the regeneration of the silk fibroins. Since the mechanical properties of the regenerated silk fiber depend on the condition of the preparation strongly, the nature of the solvent and the post-spinning treatments applied to the fibers may be important factors, affecting the overall quality and properties of the fibers produced.

One of the requirements for scaffolds for tissue engineering is degradability to be metabolized by the host once its repair function has been completed. Silk fiber is well-known as a hardly degradable material *in vivo*, but the regenerated silk fiber might be a candidate of biodegradable fiber. The regenerated silk fiber with high strength and high degradability will undoubtedly lead the development of new biocompatible scaffolds made of silk. In this paper, we attempt to show that HFIP may be a solvent of choice for the preparation of regenerated silk fibroin fibers. A process for the artificial spinning of *Bombyx mori* silk fibroin solution in HFIP will be confirmed. Solid-state  $^{13}\text{C}$  nuclear magnetic resonance (NMR) and wide-angle X-ray diffraction (WAXD) will be used for characterization of the regenerated silk fibers obtained here. The biodegradation of the regenerated fibers will

\*Corresponding author, e-mail: [asakura@cc.tuat.ac.jp](mailto:asakura@cc.tuat.ac.jp)  
© BME-PT and GTE

be examined by immersing the fibers in enzyme solution.

## 2. Materials and methods

### 2.1. Preparation of regenerated *Bombyx mori* silk fibroin fiber

*Bombyx mori* cocoons were degummed according to the method reported previously [8] and then the degummed silk fiber was dissolved in 9M LiBr solution to a concentration of 10% w/v at 40°C for 1 hour and then dialyzed against deionized water for 4 days at 4°C. HFIP was of analytical grade (Wako Pure Chemical Industries Ltd., Japan) and used for the solvent of the silk fibroin. The lyophilized silk sponge was dissolved in HFIP for 2 days, yielding a 12 w/v% solution. The HFIP solution was extruded through a stainless steel spinneret with 0.45 mm inner diameter using syringe pump into the methanol coagulation bath at room temperature. The extruded filament was soaked in the methanol bath over 3 h to allow the HFIP to diffuse from the fiber before drawing. The drawing process of as-spun silk fiber was performed in distilled water bath using a manual drawing method at 40°C. Draw ratios of 2.0 and 3.0 to its original length were used to examine the drawing effect on the structure and properties of the regenerated fibers. The fibers after the post-spinning treatments were immobilized on the bobbins to prevent recoil and dried overnight at room temperature. The surface morphology of samples was observed with VE-7800 scanning electron microscope (KEYENCE, Japan).

### 2.2. Characterization of regenerated silk fibers

The <sup>13</sup>C solid-state CP/MAS NMR spectra of the silk fibers were obtained on a Chemagnetics CMX 400 MHz spectrometer using a cross-polarization pulse sequence and with magic-angle spinning at 9 kHz. The experimental conditions were as follows: contact time of 1 ms, pulse delay of 3 s. The X-ray diffraction analyses of the fibers were performed using WAXD experiments on the ultra X 18 Rigaku rotating anode generator with graphite monochromatized CuK<sub>α</sub> radiation and cylindrical IP (R-AXIS Rapid). The voltage and current of the X-ray source were 50 kV and 250 mA, respec-

tively. Well-aligned fiber bundles of *Bombyx mori* native fibroin fibers or the regenerated fibroin fibers from HFIP system were mounted vertically at the exit of the collimator. The mechanical properties of the native and the regenerated silk fibers were measured using an EZ-Graph tensile testing machine (SHIMADZU Co. Ltd.) at room temperature with 5 N load cell. The rate of crosshead was 10 mm/min on samples of 25 mm length. Each value was the average of 10 measurements.

### 2.3. In vitro enzymatic degradation

The degradation of the regenerated silk fibroin fibers was evaluated using protease XIV (EC 3.4.24.31, Sigma-Aldrich) with an activity of 4 U/mg. The fibers were immersed in phosphate buffer saline (PBS, pH 7.4) containing protease (8 U/ml) at 37°C. After the specific time, the fibers were washed with PBS and distilled water. The enzyme solution was replaced with newly prepared solution every 24 h. For control, the silk fibers were immersed in PBS without enzyme. The degree of degradation was estimated by SEM pictures.

## 3. Results and discussion

### 3.1. Morphology and mechanical properties

The silk sponge obtained from 2 w/v% aqueous solution of silk fibroin was completely dissolved in HFIP for 2 days. Since the silk sponge used here takes random coil form and there are many holes within the sponge, it is relatively easy to resolve it in the solvent. The regenerated fibers exhibited a uniform and circular cross-sectional shape as well as a dense morphology. The fiber diameter could be varied from 50 μm (1×) to 30 μm (3×) with increasing the draw ratio although the circular shape remains during drawing. The mechanical properties of the regenerated silk fibers were improved by increasing the draw ratio. Figure 1 shows a comparison between the stress-strain curves of the regenerated silk fibers with different draw ratios (1×–3×) together with the native *Bombyx mori* silk fiber. The as-spun fiber (1×) shows the curve with low tensile strength and high elongation at break. The tensile strength of the fiber increases dramatically with increasing draw ratio. Namely, for as-spun fiber, the tensile strength [MPa] was 140±18, but the strength increased up to 162±25 at a draw

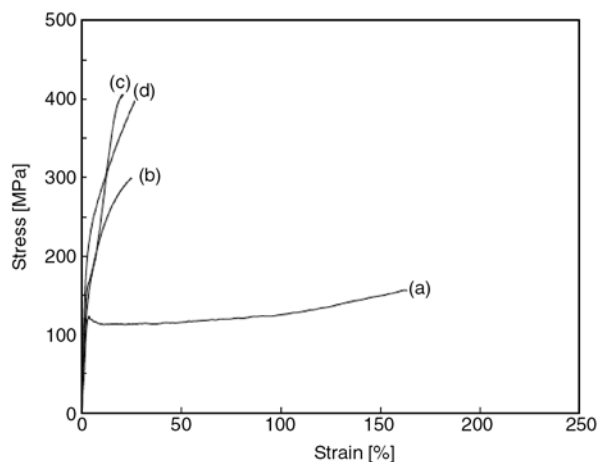


**Figure 1.** Stress-strain curves of wet-spun regenerated silk fibers with various draw ratios: (a) as-spun, (b) 2 $\times$ , (c) 3 $\times$  and (d) native silk fiber. All curves are the average of 10 measurements.

ratio of 3 $\times$ . The latter value is almost the same or slightly higher compared with the strength of native silk,  $398 \pm 51$ . The value of tensile strength of native *Bombyx mori* fiber is slightly lower than the value reported previously. One of the reasons is due to the native fiber with silk sericin used here which is slightly lower than the value of silk fiber without sericin [10]. In addition, difference of the race of silkworm and part of the fiber taken from the cocoon might be the origin of the difference. However, we can compare the values of tensile strength between native and regenerated silk fibers because the experimental condition is the same between them. The elongation at break [%] changes from  $162 \pm 25$  (1 $\times$ ) to  $21 \pm 3$  (3 $\times$ ), where the latter value is similar to the value of the native fiber,  $27 \pm 0.8$ . The initial modulus [GPa] changes from  $5.6 \pm 1.8$  (1 $\times$ ) to  $7.3 \pm 0.2$  (3 $\times$ ), and the latter is smaller than the corresponding value of the native fiber,  $9.8 \pm 0.6$ .

### 3.2. Solid state NMR analysis

The conformation-dependent  $^{13}\text{C}$  NMR chemical shift and also the line-width have been successfully used to distinguish the secondary structure among Silk I, Silk II,  $\alpha$ -helix,  $3_1$ -helix and random coil [11]. Figure 2 shows  $^{13}\text{C}$  CP/MAS NMR spectra of the regenerated silk fibers prepared from the HFIP solution together with that of native *Bombyx mori* silk fiber. The peak assignments have been reported previously [4]. The peak positions of the C $\alpha$  and C $\beta$  carbons from Ala and Ser residues indicate clearly that these samples take  $\beta$ -sheet structure. In

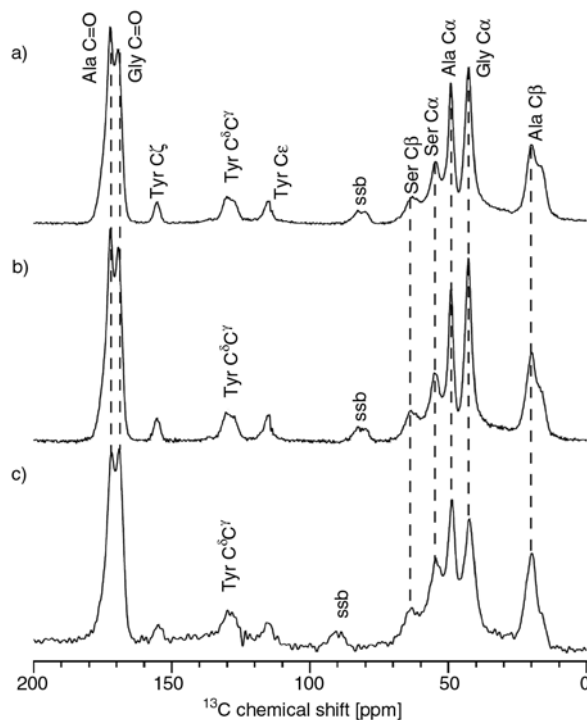


**Figure 2.**  $^{13}\text{C}$  CP/MAS NMR spectra of wet-spun regenerated silk fibers with various draw ratios: (a) as-spun, (b) 3 $\times$  and (c) native silk. Spinning sidebands are indicated by ssb.

addition, gradual decrease in the fraction of random coil/distorted  $\beta$ -turn peak observed as shoulder at 16.8 ppm [4], was observed for the Ala C $\beta$  peak in the order of 1 $\times$ , 3 $\times$  and native fiber.

Methanol is known as a coagulant and an inducer of  $\beta$ -sheet for the silk solutions such as aqueous, formic acid, and HFA solutions. In this study, methanol also induced  $\beta$ -sheet of silk fibroin chain for the HFIP solution. Simultaneously HFIP is dispersed in the methanol bath during wet-spinning process. Namely, no trace of the HFIP peaks was observed in the  $^{13}\text{C}$  CPMAS NMR spectrum of as spun fiber (Figure 2 (a)).

### 3.3. WAXD analysis

WAXD fiber patterns of the regenerated silk fibroin fibers are shown in Figure 3, along with that of native silk fiber. As the draw ratio increased from 1 $\times$  to 3 $\times$ , the fiber shows an increase of the preferential orientation along the fiber axis (Figure 3a and 3b). The native silk fiber shows a highly orientated diffraction pattern with characteristic arcs having some degree of diffraction intensity (Figure 3c). In order to determine the crystalline characteristics and molecular orientation of the

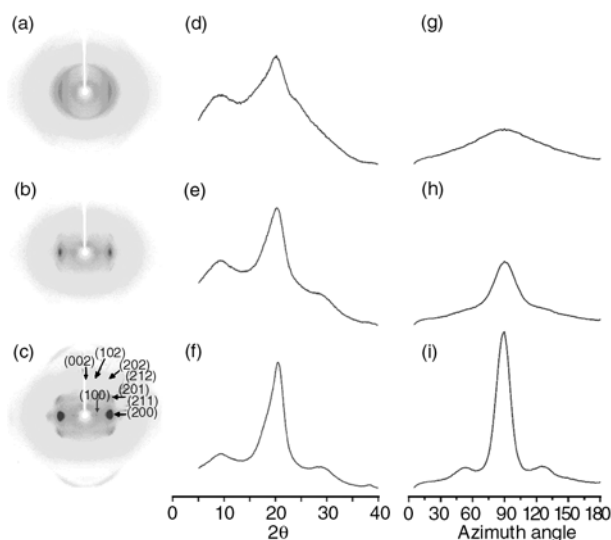


**Figure 3.** X-ray fiber patterns (a–c), diffractograms (d–f) and azimuthal scans (g–i) of the regenerated silk fibers: (a, d, g) as-spun, (b, e, h) 3 $\times$  and (c, f, i) native silk fibers.

regenerated fibers more precisely,  $2\theta$  and an azimuthal scan were performed. Figure 3d–3f shows the X-ray diffractograms of the fibers with different draw ratios. Regardless of the draw ratio, the regenerated fibers showed characteristic  $\beta$ -sheet crystalline spacings which are identical to those of the native silk. This is consistent with the result from  $^{13}\text{C}$  CP/MAS NMR spectra that the short-range local structure in the regenerated silk fiber does not change if the drawing ratio changes. To investigate the long-range molecular orientation in crystalline region, an azimuthal scan was performed on XRD fiber patterns (Figure 3g–3i). The crystalline orientation was examined at  $2\theta = 19\text{--}21^\circ$ , which well reflects a  $\beta$ -sheet crystalline. The full width at half-maximum (fwhm) of the peaks taken from the azimuthal intensity scan was  $15^\circ$  for the native fibers, and  $70$  and  $30^\circ$  for the regenerated fibers of  $1\times$  and  $3\times$ , respectively. Thus the degree of the long-range orientation is ordered as; native fiber > the regenerated fiber with a draw ratio of  $3\times \gg$  as-spun fiber[KO1] ( $1\times$ ).

### 3.4. Enzymatic degradation

*In vitro* degradation of the regenerated fibers incubated in protease was observed. Figure 4 shows change in the mechanical property before and after degradation (5 days after degradation) together with SEM pictures of the regenerated silk fibers

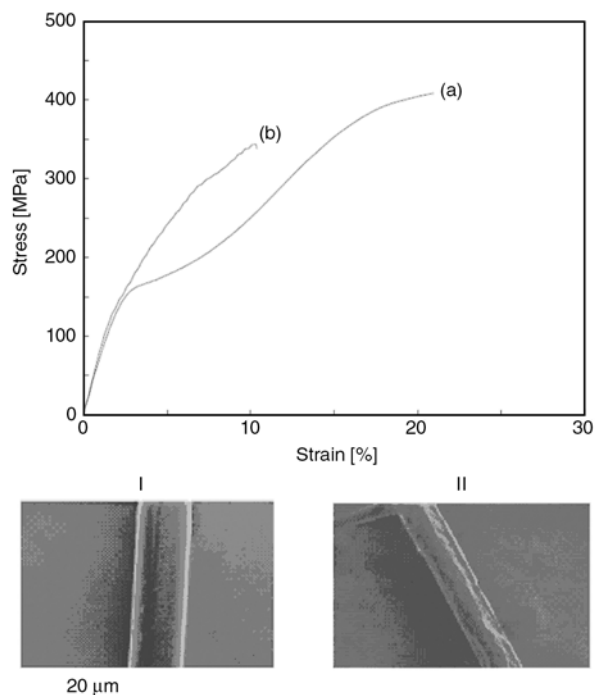


**Figure 4.** Stress-strain curves of wet-spun regenerated silk fibers with draw ratio (3 $\times$ ) before (a) and after degradation (5days) (b). All curves are the average of 10 measurements. The SEM pictures of the fibers before (I) and after degradation (5days) (II) are also shown.

(3 $\times$ ). The roughness of the surface was started on 5 days in the case of 3 $\times$  drawn fiber as shown in Figure 4 II. The tensile strength [MPa] and elongation at break [%] decrease by degradation by protease;  $333\pm 51$  and  $11\pm 4$  compared with the corresponding values (a) before degradation,  $408\pm 80$  and  $21\pm 3$ , respectively. The initial modulus [GPa] is almost the same,  $7.3\pm 0.2$  and  $7.4\pm 0.4$  for before and after degradation, respectively.

On the other hand, there are no changes in the surface morphology for native fiber in enzyme solution even after 9 days.

The difference of enzymatic degradation between the regenerated silk and the native silk fibers likely reflects differences in the long-range molecular orientation in crystalline region. This may be attributed to the mechanism that low molecular orientation allows the penetration of water molecules and protease into the crystalline domain and then the degradation is accelerated [12]. The degradation rate of scaffolds is an important parameter for sutures and scaffolds for tissue engineering to match new tissue in growth.

#### 4. Conclusions

The regenerated silk fibroin fibers with a comparable strength with natural silk fibers were obtained with HFIP as a spinning solvent and methanol as a coagulant solvent. The combination with the useful mechanical properties and biocompatibility of the regenerated fibers offer new options such as suture, artificial blood vessels with bladed fibers and other scaffolds made of fibers.

#### Acknowledgements

The authors thank Dr. Keichi Noguchi at Tokyo University of Agriculture and Technology for assistance with the X-ray diffraction measurements. T. A. acknowledges support from Grants-in-Aid for Scientific Research (S) (No. 18105007), Japan.

#### References

- [1] Asakura T., Kaplan D. L.: Silk production and processing. in 'Encyclopedia of agricultural science' (ed.: Arutzen C. J.) Academic Press, New York, Vol 4, 1–11 (1994).
- [2] Trabbic K. A., Yager P.: Comparative structural characterization of naturally- and synthetically-spun fibers of *Bombyx mori* fibroin. *Macromolecules*, **31**, 462–471 (1998).
- [3] Liivak O., Blye A., Shah N., Jelinski L. W.: A micro-fabricated wet-spinning apparatus to spin fibers of silk proteins. Structure-property correlations. *Macromolecules*, **31**, 2947–2951 (1998).
- [4] Zhao C. H., Yao J. M., Masuda H., Kishore R., Asakura T.: Structural characterization and artificial fiber formation of *Bombyx mori* silk fibroin in hexafluoro-iso-propanol solvent system. *Biopolymers*, **69**, 253–259 (2003).
- [5] Kim H. J., Kim U.-J., Gordana V.-N., Min B.-H., Kaplan D. L.: Influence of macroporous protein scaffolds on bone tissue engineering from bone marrow stem cells. *Biomaterials*, **25**, 4442–4452 (2005).
- [6] Drummy L. F., Phillips D. M., Stone M. O., Farmer B. L., Naik R. R.: Thermally induced alpha-helix to beta-sheet transition in regenerated silk fibers and films. *Biomacromolecules*, **6**, 3328–3333 (2005).
- [7] Ha S. W., Asakura T., Kishore R.: Distinctive influence of two hexafluoro solvents on the structural stabilization of *Bombyx mori* silk fibroin protein and its derived peptides: C-13 NMR and CD studies. *Biomacromolecules*, **7**, 18–23 (2006).
- [8] Yao J. M., Masuda H., Zhao C. H., Asakura T.: Artificial spinning and characterization of silk fiber from *Bombyx mori* silk fibroin in hexafluoroacetone hydrate. *Macromolecules*, **35**, 6–9 (2002).
- [9] Um I. C., Kweon H., Lee K. G., Ihm D. W., Lee J. H., Park Y. H.: Wet spinning of silk polymer – I. Effect of coagulation conditions on the morphological feature of filament. *International Journal of Biological Macromolecules*, **34**, 89–105 (2004).
- [10] Altman H. G., Diaz F., Jakuba C., Calabro T., Horan R. L., Chen J., Lu H., Richmond J., Kaplan D. L.: Silk-based biomaterials. *Biomaterials*, **24**, 401–416 (2003).
- [11] Asakura T., Yao J. M., Yamane T., Umemura K., Ulrich A. S.: Heterogeneous structure of silk fibers from *Bombyx mori* resolved by C-13 solid-state NMR spectroscopy. *Journal of the American Chemical Society*, **30**, 8794–8795 (2002).
- [12] Plaza G. R., Corsini P., Perez-Rigueiro J., Marsano E., Guinea G. V.: Effect of water on *Bombyx mori* regenerated silk fibers and its application in modifying their mechanical properties. *Journal of Applied Polymer Science*, **109**, 1793–1801 (2008).

# Study of the strength and erosive behavior of CaCO<sub>3</sub>/glass fiber reinforced polyester composite

M. G. Yilmaz<sup>1</sup>, H. Unal<sup>1</sup>, A. Mimaroglu<sup>2\*</sup>

<sup>1</sup>University of Sakarya, Faculty of Technical Education, Esentepe Kampusu, Adapazari, Turkey

<sup>2</sup>University of Sakarya, Faculty of Engineering, Esentepe Kampusu, Adapazari, Turkey

Received 3 September 2008; accepted in revised form 12 November 2008

**Abstract.** In this study, the strength and erosive characteristics of CaCO<sub>3</sub> filled unsaturated polyester/glass fiber (UPR/GFR) composite are evaluated. Samples of UPR with 40, 50 and 60 wt% content of CaCO<sub>3</sub> and different CaCO<sub>3</sub> particle sizes of 1, 2, 3, 5 and 10 micron were prepared and tested under tensile loading, indentation and erosion conditions. The tensile strength, hardness and erosion wear rate of unsaturated polyester/glass fiber (UPR composite)/CaCO<sub>3</sub> composite were obtained and evaluated. The results showed that the higher is the percentage of CaCO<sub>3</sub> in the composite and the smaller is the CaCO<sub>3</sub> particle size, the higher is the strength and the erosive resistance of the glass fiber reinforced/unsaturated polyester composite (UPR-GFR). Furthermore, the highest erosion wear rate is at 90° impingement angle. Finally the results show that the erosive wear of CaCO<sub>3</sub> content UPR/GFR composite in a brittle manner.

**Keywords:** polymer composites, CaCO<sub>3</sub>, strength, erosion

## 1. Introduction

Unsaturated polyester (UPR) is one of the most important thermoset resins in use in applications due to its ease of handling, molding characteristics and cured properties [1, 2]. Having said that in composites technology, in which particulate fillers such as CaCO<sub>3</sub>, glass fiber and carbon black are added into the polymers, may provide a good method to improve their stiffness, modulus and to reduce costs [3–5]. Fillers affect the tensile properties according to their packing characteristics, size and interfacial bonding [6]. The maximum volumetric packing fraction of filler reflects the size distribution and shapes of the particles. Srivastava and Shembekar [7] showed that the fracture toughness of epoxy resin could be improved by addition of fly ash particles as filler. Polymer composites are increasingly used in engineering applications such as gears, pump impellers where the components

undergo erosive wear. Having said that the composite materials present a rather poor erosion resistance [8, 9]. Hence, it is essential to evaluate their strength as well as their erosive behavior. Generally, variables influencing the erosive wear of composite materials are, mechanical properties of the composites, fiber content, eroding particle size, impingement angle and velocity. In viewing past work on erosive wear of composites, most efforts were focused on the study of the influence of the material properties rather than the operating parameters [10–13]. Srivastava and Pawar [14] studied the effect of additives and impingement angle and eroding particle velocity on erosive wear of neat E-glass fiber reinforced epoxy resin composite materials and composites with 2 and 4 g fly ash additive particles. They concluded that the erosive wear rate of GFRP composite with 4 g fly ash is the lowest and that the maximum erosion occurs at 60°

\*Corresponding author, e-mail: [mimarog@sakarya.edu.tr](mailto:mimarog@sakarya.edu.tr)  
© BME-PT and GTE

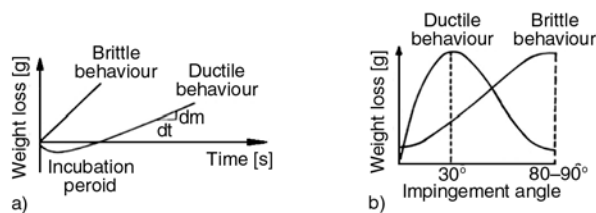


**Figure 1.** Schematic representation of brittle and ductile type of erosive wear [4]

impingement angle. Finnie [15] and Barkoula and Karger-Kocsis [16] studied the influences of operating condition such as impingement angle and speed on the erosion of polymer composites under small particle erodes. Barkoula and Karger-Kocsis [16] summarized the behavior of polymer composite materials under erosion conditions in schematic diagram see Figure 1. This figure shows and state the typical erosion diagram as a function of impingement angle and time. The erosion mechanisms can be grouped into ductile and brittle. In ductile type initially due to entrapment there is a gain in weight then a linear weight loss. In case of brittle type a linear weight loss is observed with higher loss at 90° degree angle. The ductile materials are characterized by maximum erosion at low impingement angles (15–30°). Having said that this grouping is not definitive [17]. Hutchings [18] observed that material behavior can vary with the variation of erosion conditions. Häger *et al.* [19] carried out erosion test for several thermoset and thermoplastics composites and observed a semi-ductile behavior. Maximum erosion is observed at 60° impingement angle for most of the tested composites. A different observation was made by Tsiang [20] as using Al<sub>2</sub>O<sub>3</sub> particles erosion sand. He concluded that in GF/EP and some other thermoset matrices, the erosion occurred in a brittle manner, while in thermoplastic matrices a semi-ductile erosion was dominant. Rajesh *et al.* [21] studied erosive wear of five different polyamides and observed that all polyamides showed maximum erosion wear at 30° impingement angle indicating a ductile failure behavior. Tilly and Sage [22] have investigated the influence of velocity, impingement angle, eroding particle size and weight on the erosion wear of nylon, carbon fiber reinforced nylon, and epoxy resin, polypropylene and glass fiber reinforced plastics. Their results show that these particulate filled materials behave in an ideal brittle fashion and E-glass fiber rein-

forced epoxy composite exhibits erosion rates less than those of the other composites by a factor of 5. The E-glass epoxy composite exhibits semi-ductile erosion at 45 and 60° impingement angle while others eroded in brittle manner with a maximum weight loss occurring at 75–90° impinging angles. Zahavi and Schmitt [23] and Miyazaki and Takeda [24] also studied the erosive behavior of fiber reinforced polymer composites and concluded that the maximum erosion rate is at 90° impingement angle. Bitter [25, 26] in his study on erosion phenomenon, stated that ductile behavior shows a peak erosion rate around 30° impingement angle because the cutting mechanism is the dominant in erosion. Past work shows some uncertainty in this respect, because most of studies concentrated on erosive and strength behaviors of polymer composites separately. To reach more clear conclusions there is a need to investigate both strength and erosive behavior of polymer composites in parallel.

In composite technology additives have been used in composite materials to minimize the overall material cost. This is also the case for the addition of CaCO<sub>3</sub> to GFR unsaturated polyester (UPR). It is believed that the additive is influencing the strength and the erosive wear behavior of GFR-UPR composites. In this study, the tensile strength, the hardness and the erosive wear behaviors of CaCO<sub>3</sub>/GFR filled unsaturated polyester (UPR) composites were examined. The variation of the strength, the hardness and the erosion resistance with CaCO<sub>3</sub> weight fraction, CaCO<sub>3</sub> particle size and impingement angle were studied and evaluated. Samples of UPR with 40, 50 and 60 wt% content of CaCO<sub>3</sub> and different CaCO<sub>3</sub> particle sizes of 1, 2, 3, 5 and 10 micron were prepared and tested under tensile loading and erosion conditions. The results indicated the effect of filler content, filler size and test conditions on the strength and erosive behavior of UPR/GFR/CaCO<sub>3</sub> composite.

## 2. Experimental procedures

### 2.1. Materials and preparation of composite material

In this work the compound under investigation is UPR/GFR/CaCO<sub>3</sub> composite consisting of unsaturated polyester resin (UPR), fiber glass (GF) and CaCO<sub>3</sub> powder. For materials details see Table 1. In the sample preparation process the unsaturated

**Table 1.** Materials

Materials	Supplier	Size
Unsaturated polyester (UPR)	From Poliya Polyester Inc.	13 micron in diameter, 12mm in length
Fiber glass(GF)	From locally available Turkish Glass Fiber Inc.	
The BC500 inhibitor	Akzo Nobel, Turkey	1, 2, 3, 5 and 10 micron
CaCO <sub>3</sub> powder	Omya Mining, Turkey	

polyester and the styrene were mixed in a ratio 100:25 parts by weight respectively. Additionally methyl ethyl ketone peroxide was used as a catalyst, BC500 as an inhibitor; zinc stearate as stabilizer; magnesium oxide as a thickening paste; viscosity reducer and pigment were added and all were mixed for 10 min. Then the paste was transferred to a Z-mixer and surface modifier and CaCO<sub>3</sub> were added and were mixed for 0.5 hr. Afterwards 25 wt% glass fibers were added to the paste and mixed for another 15 min. Afterwards the mixture was conditioned for one week before samples preparation. Finally, samples (tensile, hardness and erosion) were prepared from the mix by molding using a hydraulic press at 1500 MPa pressure. The samples were then cured at a temperature of 150°C for about 60 second within the mold.

**2.2. Tensile strength, hardness and erosive tests**

Tensile tests were carried out at a cross head speed of 5 mm/min and temperature of 23°C. The tensile strength and elongation at break were recorded. Indentation test was carried out using Barcol hardness measurement. On each sample several tests were carried out and average values were recorded. The erosion tests were carried out using in-house made erosion rig, see Figure 2. This rig consists of a compressed air-supply system, a sand-supply system and a sample holder unit. During the test the holder was held at selected angles of 30, 60 and 90° with respect to the flow of the impingement sand particles. Al<sub>2</sub>O<sub>3</sub> impingement sand particles of

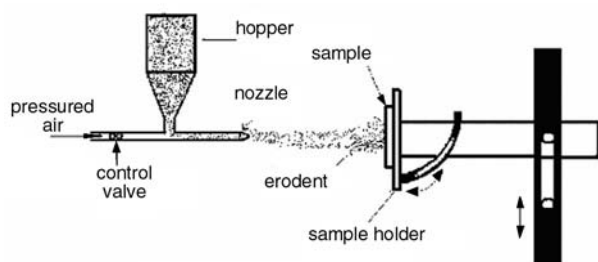


**Figure 2.** Schematic erosion wear test rig

400–500 micron size were used as eroding elements. Before and after each test, composite samples were cleaned with acetone and a brush was used to remove Al<sub>2</sub>O<sub>3</sub> particles attached to the surface and their weights were recorded. All tests were carried out at a 40 m/sec impingement speed. Erosion wear was measured by the weight loss. The normalized erosion rate ( $W_s$ ) was expressed in terms of Equation (1):

$$W_s = W_c / W_{Er} \tag{1}$$

Where  $W_c$  is the loss in weight of the composite material and  $W_{Er}$  is the total weight of erodent (Al<sub>2</sub>O<sub>3</sub>) used ( $W_{Er} = 2360$  g).  $W_c$  is determined by weighing the sample before and after the erosive wear test using a balance with an accuracy of  $1 \cdot 10^{-4}$  g. Each erosive wear tests was performed twice and average wear values were calculated.

**3. Results and discussions**

Figures 3–5 illustrate the influences of CaCO<sub>3</sub> content (by weight) and CaCO<sub>3</sub> particle size on the mechanical properties of UPR/GFR/CaCO<sub>3</sub> composites. Figure 3 presents the influence of CaCO<sub>3</sub> content on the tensile strength of 10 micron CaCO<sub>3</sub> particle size UPR/GFR/CaCO<sub>3</sub> composite. It is clear from this figure that the tensile strength is increasing with the increase in CaCO<sub>3</sub> content. As the investigation is mainly focused on filler content rather than neat composite, taking the 40% CaCO<sub>3</sub>

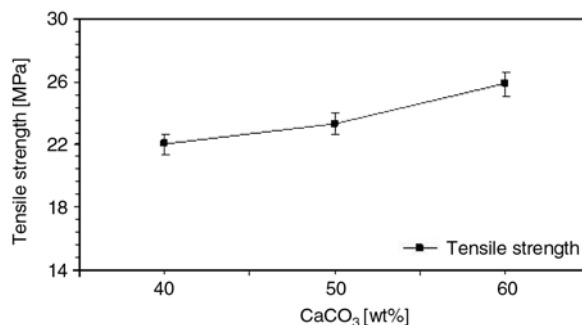


**Figure 3.** Influence of CaCO<sub>3</sub> content on the tensile strength of composite material (particle size 10 μm )

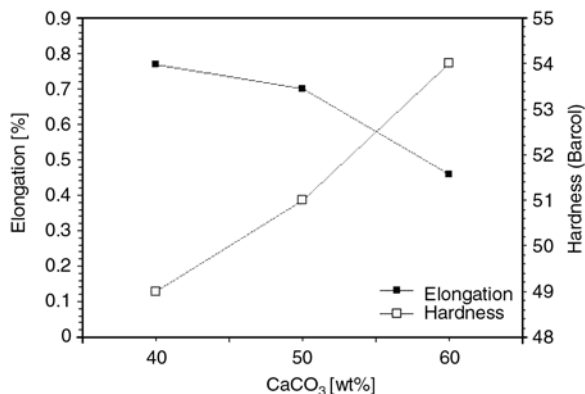


**Figure 4.** Influence of CaCO<sub>3</sub> content on the elongation at break and hardness of composite material

content composite the baseline there is about 18% increase in tensile strength for a 50% increase in CaCO<sub>3</sub> content. Because all added component materials are brittle in nature in comparison to UPR therefore this is reflected by the mechanical properties of the composite as a whole compound. Thus there is an increase in tensile strength of UPR/GFR/CaCO<sub>3</sub> composite with the increase in CaCO<sub>3</sub> content. Figure 4 presents the influence of CaCO<sub>3</sub> content on the elongation at break and on the Barcol hardness. In this particular case CaCO<sub>3</sub> of 10 micron particle size UPR/GFR/CaCO<sub>3</sub> composite were tested. It is clear from this figure that the elongation at break is decreasing while the hardness is increasing with the increase in CaCO<sub>3</sub> content. This figure shows that for a 50% increase in CaCO<sub>3</sub> content there is a 40% decrease in percentage of elongation at break and 10% increase in hardness. The increase in CaCO<sub>3</sub> content result to increase in brittleness of the composite. Hence this results in a decrease of the percentage of elongation at break and in an increase in hardness value of the compos-

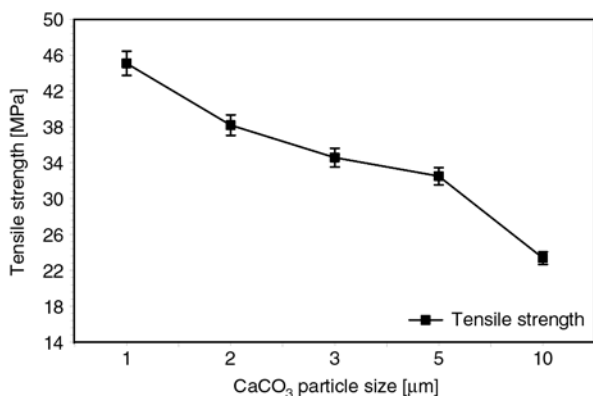
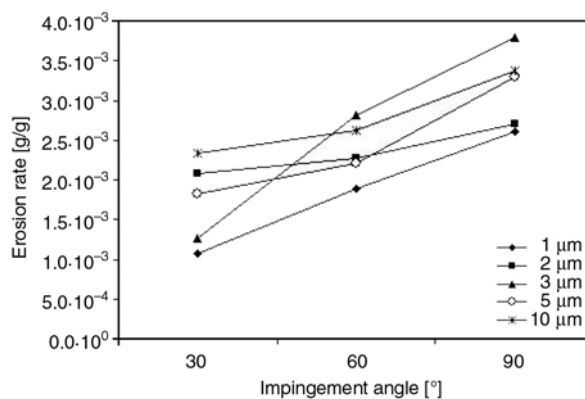


**Figure 5.** Influence of CaCO<sub>3</sub> particle size on the tensile strength of composite material (50wt% content CaCO<sub>3</sub>)

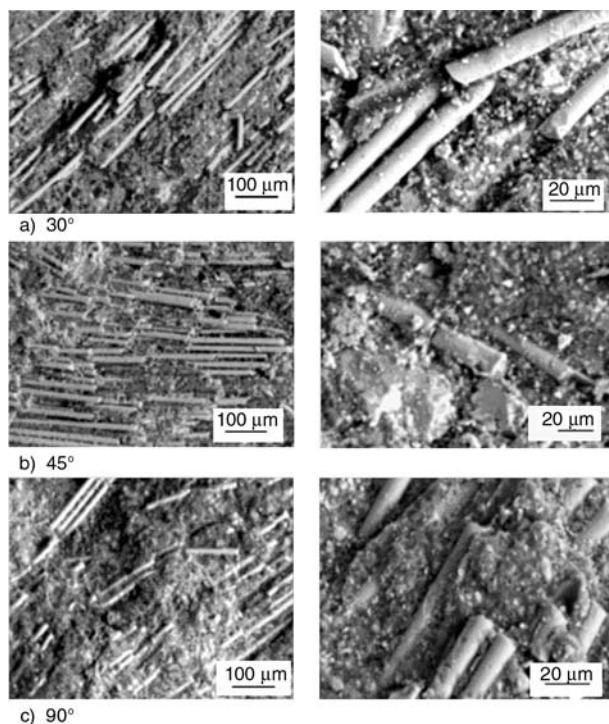
ite. On the other hand more brittle the material, the larger is the fraction of volume that is removed and hence the erosion rate is higher. The results from Figures 3 and 4 suggested that 50% content CaCO<sub>3</sub> composite has a balanced properties (tensile strength, hardness and elongation at break). Therefore further studies were carried out on 50% CaCO<sub>3</sub> content compound only. Figure 5 presents the influence of the CaCO<sub>3</sub> particle size on the tensile strength of UPR/GFR/CaCO<sub>3</sub> composite. It is clear from this figure that the tensile strength decreases with the increase in CaCO<sub>3</sub> particle size. This is related to the fact that for a particular CaCO<sub>3</sub> content the contact surface between the matrix and CaCO<sub>3</sub> particles decreases with increasing particle size resulting in a weaker bonding with the matrix, hence in a drop of the strength of the composite.

Figure 6 presents the influence of the impingement angle and CaCO<sub>3</sub> particle size on the erosion wear rate of UPR composite. It is clear from this figure that the larger is the impingement angle and the larger is the CaCO<sub>3</sub> particle size, the higher is the erosive wear rate of UPR/GFR/CaCO<sub>3</sub> composite. This could be explained so that in case of impingement of hard particles on a brittle material, plastic indentation takes place along with generation of long cracks extending from plastic zone. As these cracks do not stop and reach the surface leading to material removal. Impingement at 90° leads to greater depth in plastic zone hence to larger removal of material and maximum erosion rate.

Figure 7 present scanning microscopy of o 50 wt% and 1 μm particle size CaCO<sub>3</sub> content UPR/GFR/CaCO<sub>3</sub> composite surface eroded at different impingement angles: (a) 30°, (b) 60° and (c) 90°.



**Figure 6.** The influence of impingement angle on erosion rate of 50wt% CaCO<sub>3</sub> filled unsaturated polyester composites, erodent: Al<sub>2</sub>O<sub>3</sub>, velocity: 40 ms<sup>-1</sup>



**Figure 7.** Scanning electron micrographs showing erosion features of unsaturated polyester 50 wt% CaCO<sub>3</sub> (particle size 1 μm) /UPR composites at different angles of impingement: a – 30°, b – 60° and c – 90°

The figure illustrates that the higher is the impingement angle, the more glass fibers are exposed. This means higher erosion in the matrix and filler materials and embedding of the GFR fiber. This shows the brittle behavior of UPR/GFR/CaCO<sub>3</sub> composite. Therefore the erosion is mainly caused by damage mechanisms as cracking due to the impact of Al<sub>2</sub>O<sub>3</sub> particles.

#### 4. Conclusions

It could be concluded that:

- The higher percentage of CaCO<sub>3</sub> content in UPR/GFR/CaCO<sub>3</sub> composite results to higher tensile strength, hardness and a less percentage of elongation at break.
- The larger the size of CaCO<sub>3</sub> particles, the higher is the decrease in tensile strength of UPR/GFR/CaCO<sub>3</sub> composite. A composite with 50% content with 1 micron CaCO<sub>3</sub> particle size has balanced erosive resistance with reliable tensile strength, elongation at break and hardness values.
- The maximum erosive wear rate is observed at 90° impingement angle.

- The SEM microscopy for UPR/GFR/CaCO<sub>3</sub> composite showed the brittle behavior and the cracking mechanism under erosive conditions.
- Although the addition of CaCO<sub>3</sub> to the composite has the advantage of minimizing the material cost there is a limitation in its percentage in the compound from point of view of strength and erosive resistance.

#### References

- [1] Katz H. S., Milewskin J. V.: Handbook of fillers and reinforcements for plastics. van Nostrand Reinhold, New York (1978).
- [2] Nalwa H. S.: Handbook of advanced functional molecules and polymers. Gordon and Breach, London (2000).
- [3] Sare I. R., Mardel J. I., Hill A. J.: Wear-resistant metallic and elastomeric materials in the mining and mineral processing industries – an overview, *Wear*, **250**, 1–10 (2001).
- [4] Zhou S. S., Wu L. M., Sun J., Shen W.: The change of the properties of acrylic-based polyurethane via addition of nano-silica. *Progress in Organic Coatings*, **45**, 33–42 (2002).
- [5] Baral D., De P. P., Nando G. B.: Thermal characterization of mica-filled thermoplastic polyurethane. *Polymer Degradation and Stability*, **65**, 47–51 (1999).
- [6] Srivastava V. K., Prakash R., Shembekar P. S.: Fracture behavior of fly ash filled FRP composites. *Composite Structures*, **10**, 271–279 (1988).
- [7] Srivastava V. K., Shembekar P. S.: Tensile and fracture properties of epoxy resin filled with fly ash particles. *Journal of Materials Science*, **25**, 3513–3516 (1990).
- [8] Tilly G. P.: Sand erosion of metals and plastics: A brief review. *Wear*, **14**, 241–248 (1969).
- [9] Pool K. V., Dharan C. K. H., Finnie I.: Erosive wear of composite materials. *Wear*, **107**, 1–12 (1986).
- [10] Kulkarni S. M., Kishore: Influence of matrix modification on the solid particle erosion of glass/epoxy composites. *Polymer and Polymer Composites*, **9**, 25–30 (2001).
- [11] Miyazaki N., Hamao T.: Solid particle erosion of thermoplastic resins reinforced by short fibers, *Journal of Composite Materials*, **28**, 871–883 (1994).
- [12] Bijwe J., Rattan R., Fahim M., Tiwari S.: Erosive wear of carbon fabric reinforced polyetherimide composites: Role of amount of fabric and processing technique. *Polymer composites*, **29**, 337–344 (2008).
- [13] Rattan R., Bijwe J.: Carbon fabric reinforced polyetherimide composites: Influence of weave of fabric and processing parameters on performance properties and erosive wear. *Materials Science and Engineering: A*, **420**, 342–350 (2006).

- [14] Srivastava V. K., Pawar A. G.: Solid particle erosion of glass fiber reinforced flyash filled epoxy resin composites. *Composites Science and Technology*, **66**, 3021–3028 (2006).
- [15] Finnie I.: Some reflections on the past and future of erosion. *Wear*, **186–187**, 1–10 (1995).
- [16] Barkoula N. M., Karger-Kocsis J.: Solid particle erosion of unidirectional GF reinforced EP composites with different fiber/matrix adhesion. *Journal of Reinforced Plastics and Composites*, **21**, 1377–1388 (2002).
- [17] Barkoula N-M., Karger-Kocsis J.: Effects of fiber content and relative fiber-orientation on solid particle erosion of GF/PP composites. *Wear*, **252**, 80–87 (2002).
- [18] Hutchings I. M.: *Tribology: Friction and wear of engineering materials*. Edward Arnold, London (1992).
- [19] Häger A., Friedrich K., Dzenis Y. D., Paipetis S. A.: Study of erosion wear of advanced polymer composites. in: 'ICCM-10 Conference Proceedings, British Columbia, Canada' 155–162 (1995).
- [20] Tsiang T-H.: Sand erosion of fiber composites: Testing and evaluation. in 'Test Methods and Design Allowables for Fibrous Composites, vol 2.' (ed.: Chamis C. C.) ASTM, Philadelphia, 55–74 (1989).
- [21] Rajesh J. J., Bijwe J., Tewari U. S., Venkataraman B.: Erosive wear behavior of various polyamides. *Wear*, **249**, 702–714 (2001).
- [22] Tilly G. P., Sage W.: The interaction of particle and material behavior in erosion process. *Wear*, **16**, 447–465 (1970).
- [23] Zahavi J., Schmitt G. F.: Solid particle erosion of reinforced composite materials. *Wear*, **71**, 179–190 (1981).
- [24] Miyazaki N., Takeda T.: Solid particle erosion of fiber reinforced plastics. *Journal of Composite Materials*, **27**, 21–31 (1993).
- [25] Bitter J. G. A.: A study of erosion phenomena part I. *Wear*, **13**, 5–21 (1963).
- [26] Bitter J. G. A.: A study of erosion phenomena part II. *Wear*, **13**, 169–190 (1963).